Ministerie van Verkeer en Waterstaat

Directoraat-Generaal Rijkswaterstaat

Dienst Weg- en Waterbouwkunde

BOUNDARY CONDITIONS FOR A SEICHE MODEL

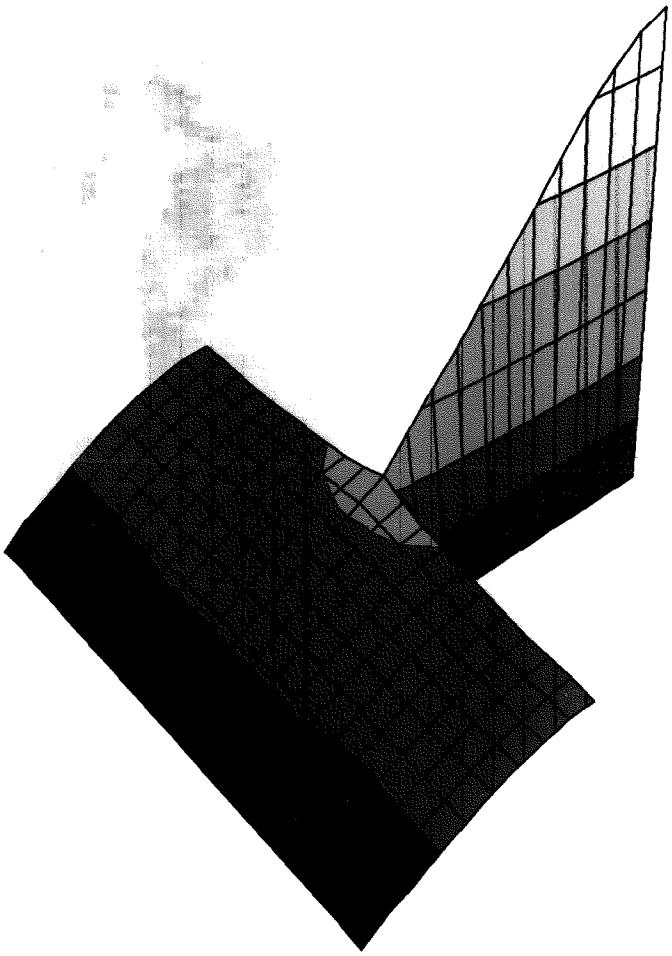

Erik de Haas
November 1998

Boundary Conditions for a Seiche model

Thesis report for:

The faculty of Civil Engineering
TU Delft
Section fluid mechanics

In cooperation with:

Dienst Weg- en Waterbouwkunde, Rijkswaterstaat.

Student:

E. de Haas
295122

Commission:

Prof. dr. ir. G.S. Stelling
Prof. dr. ir. J.A. Battjes
Ir. A.B. Méndez Lorenzo
Ir. H.W.J. Kernkamp
Ir. A. van Dongeren

Preface

This is the final report of my thesis project carried out at the Dienst Weg- en Waterbouwkunde, Rijkswaterstaat. From January 1998 to December 1998 I have studied two alternatives for a boundary condition that is capable of correctly modeling the seiche phenomenon. I wish to thank the members of my commission and professor G.S. Stelling in particular for their support and encouragement to go the extra mile. Many thanks also go to A.B. Méndez Lorenzo for her patience and guidance. The DWW I thank for their hospitality and for giving me the opportunity contribute to the project.

Delft, December 1998

E. de Haas

Summary

The Storm Surge Barrier in the New Waterway was built to protect the city and port of Rotterdam and the area of the lower Rhine against flooding during extreme conditions. This construction, consisting of two gigantic arc shaped barriers, is to be pivoted into the New Waterway and then lowered in case of an impeding emergency. The arc shape makes it a very efficient design against forces from the seaside, but if the level on the riverside surpasses the level on the seaside, a negative force will be exerted on the construction. Seiches contribute to this effect. The barrier only has a relatively small capacity to withstand a negative head difference. To accurately predict the maximum expected head difference a numerical model that handles seiches correctly is needed. In this thesis, the boundary conditions for such a numerical model are investigated.

The program currently used to calculate the effects of seiches, RAS/FLOW predicts a head difference that exceeds the design specifications of the construction. However, the calculations done with Rasflow are not accurate with respect to the amplification of the seiches. The amplitude is overestimated significantly due to the use of an inaccurate boundary condition at the sea boundary of the model.

The boundary condition at the channel entrance is very complex. Méndez Lorenzo (1997) studied a new boundary condition: the epsilon boundary. This boundary is a combination of a water level and a Riemann invariant with a factor epsilon. In the analytical case the results of this boundary condition match the analytical solution exactly. The step from the analytical boundary condition to a numerical boundary condition involves a set of derivations and simplifications that fixate the value for Epsilon. With a fixed value for epsilon, the amplification function obtained will only match one of the peaks in the spectrum: the peak for which the value of epsilon is set. In this thesis the addition of non-linear terms to the epsilon model can be found. The non-linear terms did not resolve the problem of the fixed epsilon.

To reduce the complexity of the boundary condition a different approach to the problem is taken, namely a combination of a one and two-dimensional approach. In this model a two-dimensional sea area is attached to the one-dimensional channel. Thus moving the complex boundary condition at the channel entrance to a simpler boundary condition on the open sea boundary. With this model it is possible to correctly model the amplification for more than one peak. The results obtained with this model are satisfactory and are recommended for a future implementation.

1. Introduction

1.1 Introduction

The Storm Surge Barrier in the New Waterway was built to protect the area of the lower Rhine against flooding, from the sea, during extreme conditions. This structure, consisting of two gigantic arc shaped barriers, is to be pivoted into the New Waterway and then lowered in case of an impeding emergency. The arc shape makes it a very efficient design against forces from the seaside, but if the level on the riverside surpasses the level on the seaside, a negative force will be exerted on the structure. Seiches can contribute to this effect. The barrier only has a relatively small capacity to withstand a negative head difference. To accurately predict the maximum expected head difference a numerical model that handles seiches correctly is needed. In this thesis, the boundary conditions for such a numerical model will be investigated.

1.2 Problem definition

Seiches are resonating standing waves in a (semi-) closed basin. Closure of the Storm Surge Barrier creates a basin in which, under certain circumstances, standing waves can resonate. Their contribution to a positive head difference over the barrier is relatively small (0.5m, contract BD001, 1989), because during these extreme conditions there is a flooding of the neighboring harbor areas at the seaside of the barrier. This has a damping effect on the amplitude of the seiches. A negative head difference can occur during the opening of the barrier. This is the result of the delayed opening operation and the lowering of the outside water level. In this case, the amplitude of the seiche can be larger because there is no flooding of the harbor areas. At the closing operation, there is also a chance of a negative head difference due to seiches if the water level on the seaside does not rise fast enough.

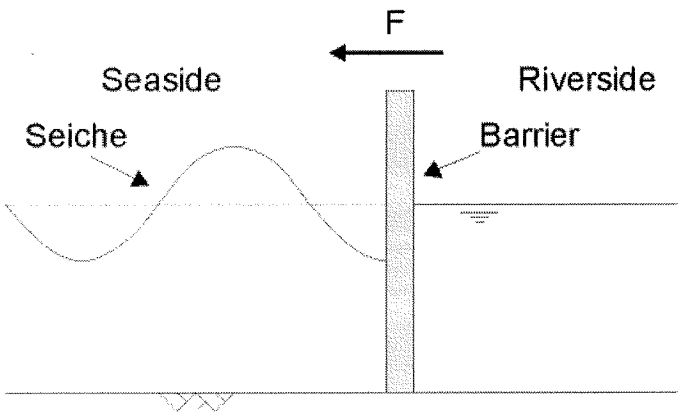

Figure 1 Effect of a seiche on the barrier

The design the barrier allows for a negative head difference of 1.5 meters. Recent calculations (BMK, 1996), show a maximum negative head difference of 1.7 meters. However, the model used to calculate this head difference, RAS/FLOW, cannot accurately handle seiches. The boundary condition on the sea boundary, used in RAS/FLOW is a highly reflective water level boundary condition. This leads to insufficient damping in the system, causing the amplitude of the seiches in the model to be overestimated.

It is expected that the negative head difference caused by seiches can be reduced by an interactive response from the barrier to the water levels. This requires modifications to the present decision support system. To investigate this further a numerical model is required which can properly model the seiches phenomenon.
Two-dimensional models such as PHAROS and TRISULA are capable of accurately modeling seiches. The largest drawback of the two-dimensional models is that their calculation time is relatively long compared to that of a one-dimensional model. Probabilistic calculations have to be executed with this model, therefore a one-dimensional approach is preferred.

Due to finite computational resources, numerical models are always restricted to a limited space domain. This leads to areas being enclosed by open boundaries. These open boundaries are by definition artificial; they are only meaningful for the mathematical model. On open boundaries, boundary conditions are needed that are defined in such way they approximate the calculated solution obtained in the case that the model would not be limited. In the case of a one-dimensional numerical model of the Europort area, there is an open boundary at the outlet of the New Waterway into the North Sea. The imposed boundary condition at this boundary replaces the entire sea area, which makes it very complex.

One approach for this boundary condition has been studied by Méndez Lorenzo (1997). It is based on modeling the radiation of energy in the seaward direction. However, due to restrictions in the numerical modeling this boundary condition needs to be investigated further.

1.3 Scope and Aim

Scope

The scope of this study is limited to the amplification factor of waves with a wavelength in the order of the length of the channel itself. The amplitude of the waves is assumed very small so that the behavior can be considered as being linear. This implies that the loss of energy at the entrance of the channel due to the in and outflow is negligible and will not be dealt with. In the channel itself, a one-dimensional network will be used.

Aim

Development of a practical solution for the seaward boundary condition for a numerical model which describes the amplification effect of seiches in a channel as correct as possible.

1.4 Outline

Introductory part

After the introduction in chapter 1, chapter 2 gives a description of the seiche phenomenon and its damping mechanisms. In chapter 3 the test problem is presented (see figure 1) together with the analytical solution of the test problem as derived by Mei (1984). In the linear analytical solution, only the damping caused by radiation to the sea is accounted for. The test problem will serve as a reference point to compare all relevant numerical results.

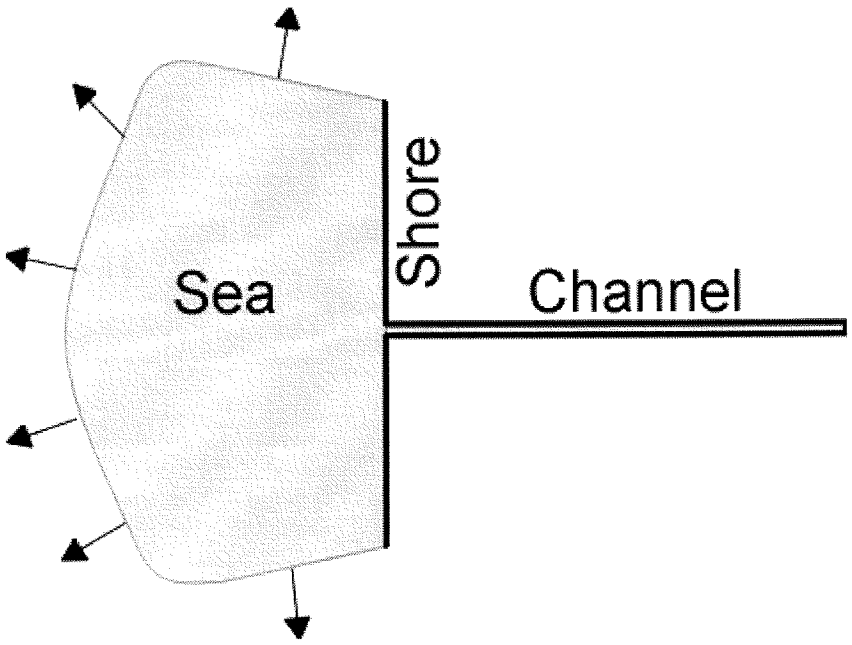

Figure 2 Schematic layout of the Test problem

One-dimensional approach

A one-dimensional numerical approach to the problem is described in chapter 4 (see figure 2). In this part, an attempt is made to make a numerical seiches model consisting of only a one-dimensional network for the channel. In this approach the open boundary is located at the entrance of the channel. The boundary condition imposed on the open boundary virtually represents the entire sea area. A summary will be given of the approach to this problem used by Méndez Lorenzo (1997). This approach will then be investigated in further detail by the addition of non-linear terms to the model.

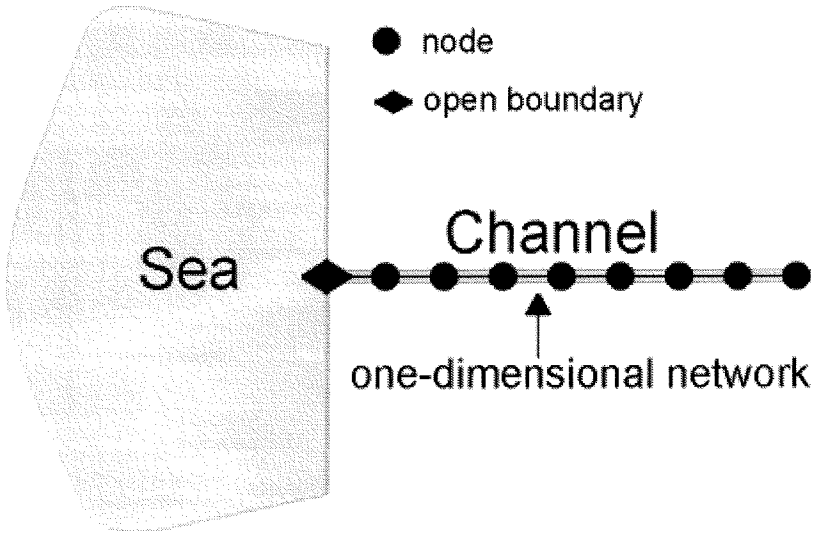

Figure 3 One-dimensional approach

One-dimensional / two-dimensional approach

In chapter 5, a description can be found of the combined one-dimensional and two-dimensional approach to the problem (see figure 3). In this chapter an attempt is made to construct a numerical seiches model by connecting a one-dimensional network, representing the channel, to a two-dimensional sea area. The open boundary of the numerical model is thus moved from the entrance of the channel, used in the previous approach, to a region further at sea. This simplifies the required boundary condition.

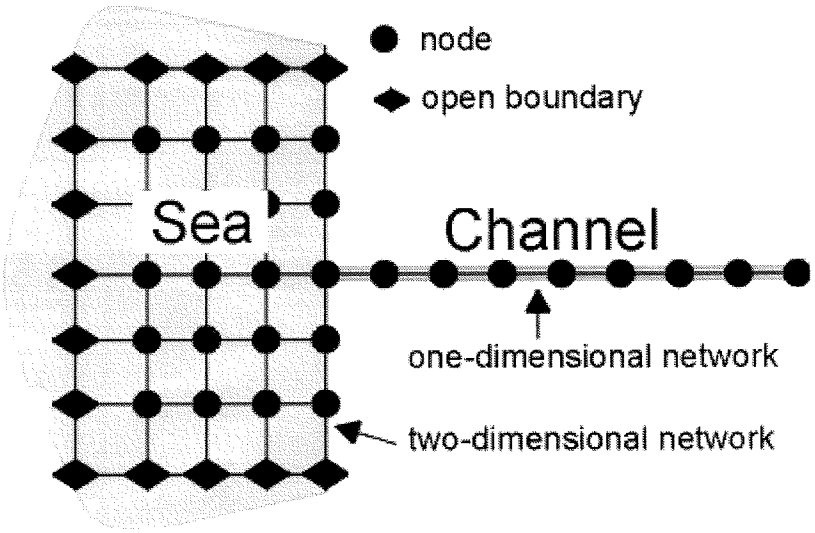

Figure 4 One-dimensional / two-dimensional approach

Results

Chapter 6 compares the results obtained with both approaches to the results of the two-dimensional programs Pharos and Trisula. The conclusion and recommendations for a further study are presented in Chapter 7 together with recommendations for a future implementation of the model.

2. Seiches

2.1 Introduction

Free oscillations of a free water surface, seiches, can be observed in harbors, bays, lakes, etc. Earthquakes, moving storm depressions, tidal currents and ocean waves, can trigger seiches. Seiches are a resonance phenomenon. To understand roughly the physical mechanism of these oscillations, consider a harbor with the entrance in line with a long and straight coastline. Incoming waves are partly reflected and partly absorbed along the coast. A small portion is, however, diffracted through the entrance into the harbor and reflected repeatedly by the interior boundaries. Some of the reflected wave energy escapes the harbor and radiates into the ocean again., while some stays inside. If the incoming wavetrain is of long duration and the incident wave frequency is close to a natural frequency in the basin, resonance will occur in the basin so that a relatively weak incident wave can induce a large response in the harbor.
If one would just keep sending long waves into the channel these would go on reflecting between the sea transition and the channel's end. If the frequency of these waves coincides with the resonant frequency, this results in more and more wave energy trapped in the channel, and consequently an increasing wave height. Without any energy dissipative mechanisms, the amount of energy inside the system would increase with time and so would the amplitude of the waves.

2.2 Damping mechanisms

Without damping mechanisms, no energy dissipated. This results in an ever-increasing wave height for waves with a resonant frequency. This is not possible, in reality the attainable amplitude is restricted. For a growing wave height, the energy dissipating process will become increasingly important until equilibrium is reached, when the incoming energy equals the outgoing energy plus dissipated energy. For short waves, breaking is an important dissipative factor. However, for the long wavelengths of seiches, the shores and banks can be considered vertical so no breaking will occur. Seiches will be restricted in their amplitude through several mechanisms:

- Radiation of energy to the sea
- Bottom friction
- Non-linear terms other than bottom friction

These damping mechanisms are described below.

Radiation

Waves that encounter the open boundary on the seaside partially radiate their energy outward to the sea through diffraction. When the reflected wave encounters the transition between the harbor and the sea, part of it will be reflected back into the channel and the other part will be transmitted outwards to the sea. The ratio of the amplitudes of these waves depends on the wavelength relative to the width of the channel. Relatively short waves barely notice the transition and will travel into the ocean. However, relatively long waves are reflected by the sudden transition. The waves with a wavelength between these two extremities will be partially reflected and partially transmitted, depending on the wavelength. In the next graph, the factor for reflection and transmission is plotted against ka, which is a measure of the wavelength to the width of the channel.

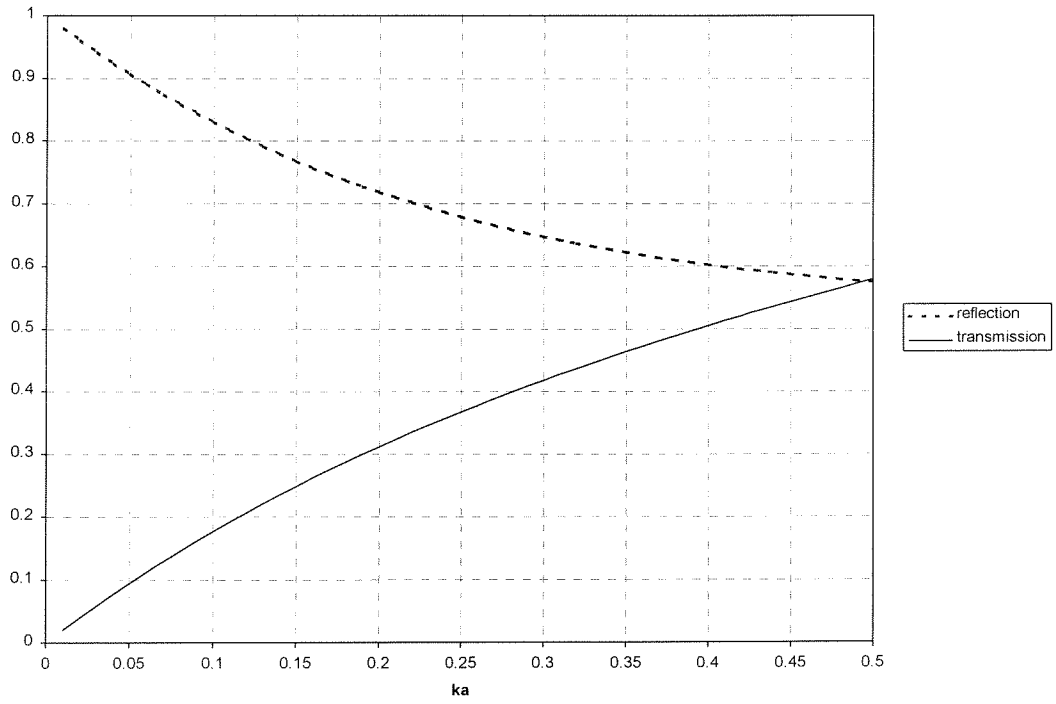

Graph 1 Factor for transmission and reflection.

With:

$$ka = \pi \frac{2a}{\lambda}$$

2a = width of the channel
λ = wavelength

It can be clearly seen from this graph that the longer waves, with a lower ka, are reflected more. The reflection factor i.e. for the shorter waves, with increasing ka, decreases and it can be seen that these waves are transmitted more.

Friction

Energy is lost due to friction forces on the bottom of the channel. The effect of friction mainly depends on the amplitude and wavelength of the wave. For small waves, the effect is barely noticeable, but as the wave amplitude increases in height the effect of bottom friction increases.

Non-linear terms other than friction

Advection causes wave energy to be transferred from the base tone to the higher harmonics. The distortion of the wave, caused by its higher celerity in deeper water, transfers the waves base tone energy to its higher harmonics. These in turn again create higher harmonics. This process cascades until at the highest frequency the energy is dissipated into heat and turbulence. On a larger scale, advection is also responsible for the head losses at the channel entrance due to the energy loss resulting from a sudden widening.

3. Test problem and linearized solution by Mei

3.1 Introduction

To evaluate and to compare the various approaches to the seiches problem described in this thesis a test problem will be used, Mei (1984). The test problem consists of a straight and narrow channel connected to an infinite sea. The seashore and the banks of the channel are assumed vertical. Waves coming in from the ocean at an angle, are reflected on the shore. Parts of these waves enter the channel, causing seiches in the resonant case. At the channel entrance waves are emitted radially. This situation is depicted in Figure 5. In this chapter the analytical solution for the test problem will be presented.

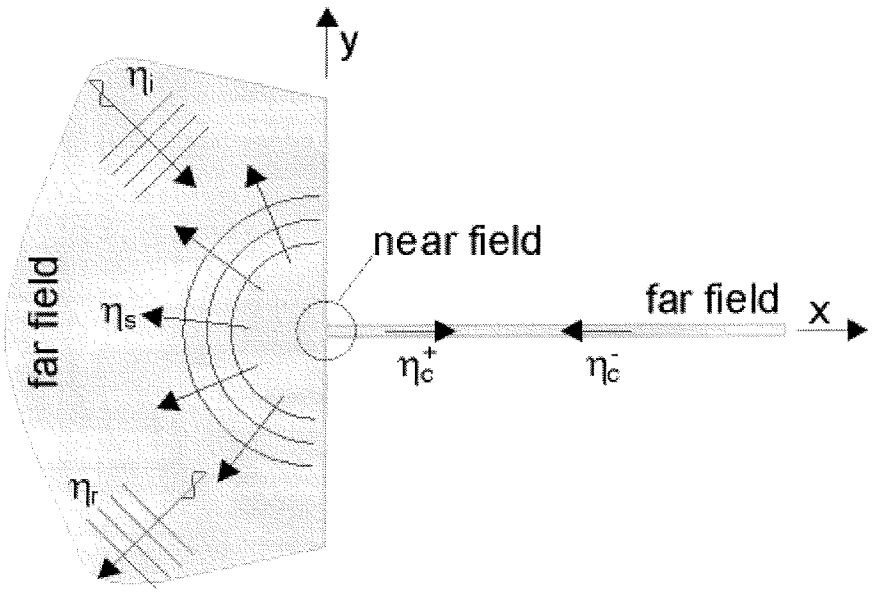

Figure 5 Test Problem

With:

η_c^-	Wave in the channel moving towards the end of the channel.
η_c^+	Wave in the channel moving towards the entrance of the channel.
η_i	Incoming wave with a straight crest.
η_r	Wave reflected on the straight shore.
η_s	Scattered wave with a radially expanding crest.

3.2 Linearized solution of the test problem by Mei

The two-dimensional shallow water equations will be used in the modeling of the sea and channel section of the test problem. They can be derived from the Navier Stokes equations by a number of simplifications.

Equation of continuity

The continuity equation is based on the basic principle of conservation of mass, which for an incompressible fluid reduces to:

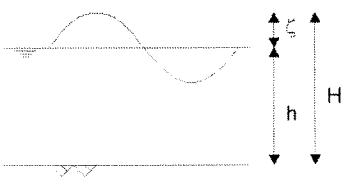

$$\frac{\partial \zeta}{\partial t} + \frac{\partial uh}{\partial x} + \frac{\partial vh}{\partial y} = 0 \qquad (1)$$

With:

ζ = Deviation of the water level from the still water level
u = Velocity in x direction averaged over the depth
v = Velocity in y direction averaged over the depth
h = still water depth

Equation of motion
The equation of motion is based on the conservation of momentum. For this scale the effects of Coriolis are negligible so the equations are reduced to:

$$\frac{\partial u}{\partial t} + u\frac{\partial u}{\partial x} + v\frac{\partial u}{\partial y} + g\frac{\partial \zeta}{\partial x} + g\frac{u\sqrt{u^2+v^2}}{C^2 h} - \upsilon_H \frac{\partial^2 u}{\partial x^2} - \upsilon_H \frac{\partial^2 u}{\partial y^2} = 0 \qquad (2)$$

$$\frac{\partial v}{\partial t} + u\frac{\partial v}{\partial x} + v\frac{\partial v}{\partial y} + g\frac{\partial \zeta}{\partial y} + g\frac{v\sqrt{u^2+v^2}}{C^2 h} - \upsilon_H \frac{\partial^2 v}{\partial x^2} - \upsilon_H \frac{\partial^2 v}{\partial y^2} = 0 \qquad (3)$$

With:
C = Chézy constant of friction
ν_H = Viscosity constant

For the linear case, the response has been solved analytically by Mei (1984). The linear case implies that all damping mechanisms for seiches, except for the radiation of energy to the sea have been omitted. For the radiation of energy to the sea the Sommerfeld radiation condition is used. This condition states that a wave emitted from a channel entrance will move in a radially expanding fashion; far away from the channel entrance its amplitude will be reduced to zero.

In the linear case the equations for motion and continuity can be reduced to:
Equation of continuity:

$$\frac{\partial \zeta}{\partial t} + \nabla \cdot h\bar{u} = 0 \qquad (4)$$

Equation of motion:

$$\frac{\partial \bar{u}}{\partial t} = -g\nabla\zeta \qquad (5)$$

Eliminating u for a constant depth yields:

$$g\nabla \cdot (h\nabla\zeta) - \frac{\partial^2 \zeta}{\partial t^2} = 0 \qquad (6)$$

For waves sinusoidal in time with radian frequency ω the space and time dependency may be separated by:

$$\zeta = \eta(x,y)e^{-i\omega t} \qquad (7)$$

For a constant depth h this reduces the previous equation to the Helmholtz equation:

$$\nabla^2\eta + k^2\eta = 0 \qquad (8)$$

with:

$$k = \frac{\omega}{\sqrt{gh}}$$

The Helmholtz equation is used for the entire model, but the solution cannot be found right away due to large differences in scale.

The general solution can be found by a method of matched asymptotic expansions, which is very convenient for a problem which is governed by different scales. The equations and boundary conditions are approximated according to local scales with solutions valid for these regions. Then the solutions are required to smoothly match in the intermediate region. To solve the test problem, Mei divides the problem into four regions, each with their own solution. In the following figure the different regions are depicted together with all the possible waves:

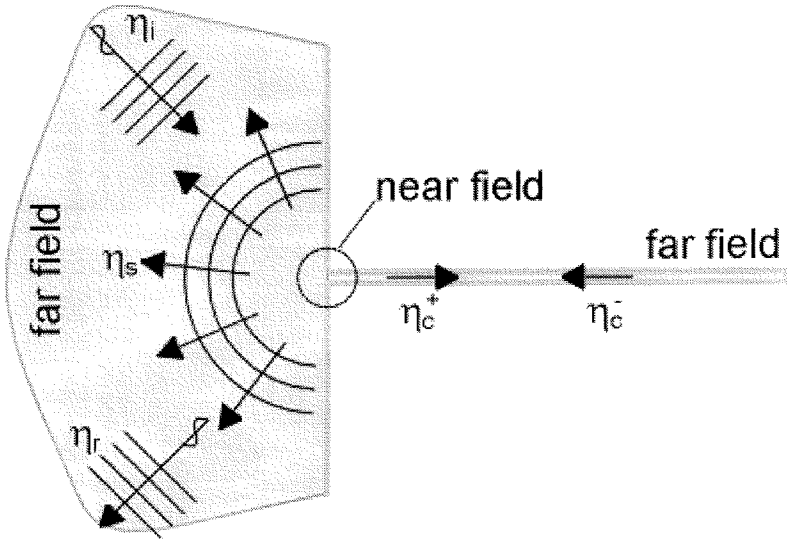

Figure 6 Definition of the far and near fields for the problem

For this problem the situation can be divided in four different regions:

1. Far field for the channel
2. Near field for the channel
3. Near field in the ocean
4. Far field in the ocean

As can be seen in Figure 6 the near field is used to match the solutions from the channel to those in the ocean.

Far field channel

In the far field section of the channel, the Helmholtz equation can be reduced to a one-dimensional equation The waves in the channel should satisfy the following 1D solution:

$$\eta_c = \eta_c^- + \eta_c^+ = Be^{-ikx} + De^{ikx} \qquad (9)$$

In the previous equation, both components can be distinguished clearly. The first term represents a wave travelling in the negative direction and the second a wave travelling in the positive direction. With B and D the amplitudes of the respective waves.

Far field ocean

In the ocean, far away from the channel, the system can be split into three different components.

$$\eta_o = \eta_i + \eta_r + \eta_s \qquad (10)$$

With:
The incoming wave, with a straight crest line:

$$\eta_i = Ae^{ik(x\cos\Theta + y\sin\Theta)} \tag{11}$$

This wave is reflected at the shoreline (x=0) creating the second wave.

$$\eta_r = Ae^{ik(-x\cos\Theta + y\sin\Theta)} \tag{12}$$

Third is the outgoing wave, which moves in a radially expanding fashion away from the origin. The latter waves correspond to the Sommerfeld radiation condition; a Hankel function is used to describe them in terms of the radius r from the origin at the channel entrance.

$$\eta_s \cong \frac{\omega Q}{2g} H_0^1(kr) \tag{13}$$

The Sommerfeld condition states that a wave emitted from a channel or narrow gap into the sea will expand radially with a decreasing wave height. Far away from the gap, the wave height will approach zero. At r = ∞ only incoming waves will be present.

Combining these three components, the solution for the far field in the ocean becomes:

$$\eta_o = 2A\cos kx + \frac{\omega Q}{2g} H_o^1(kr) \tag{14}$$

Near field

The near field is a problem of potential flow past a right-angled estuary. In this region, the ratio of r to half the width of the channel is in the order of one. This leads to the flow being essentially governed by the Laplace equation:

$$\nabla^2\eta = 0 \tag{15}$$

With a harmonic η may be taken as the real part of an analytic function W of the complex plane z.

$$\eta = \mathrm{Re}_j\, W(z) \tag{16}$$

To solve this problem the physical region in the complex z plane is mapped onto the upper half of the τ plane by using a Schwarz-Christoffel transformation.

$$\eta = \mathrm{Re}_j\, W\tau = \mathrm{Re}_j(M\ln\tau + C) \tag{17}$$

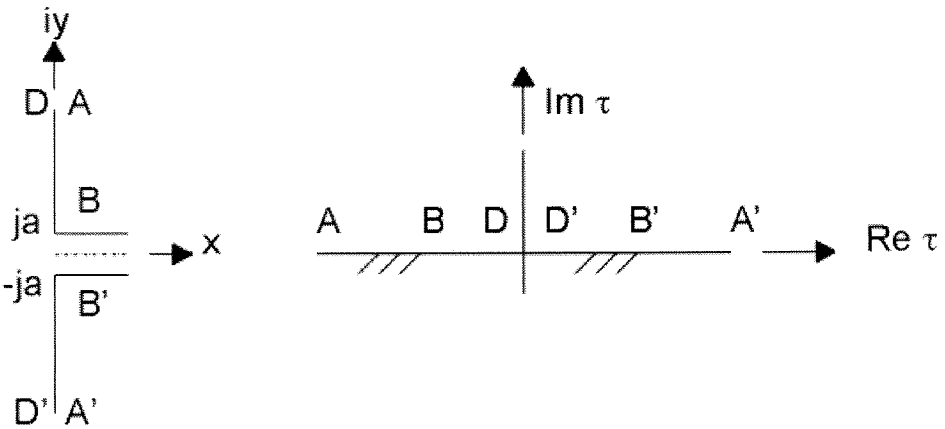

Figure 7 Mapping of the near field from the physical z plane to the τ plane.

To find the solution for the outer expansion the near field must be divided in two sections, one for the ocean side x>0 and one for the channel x<0. For the ocean side the solution is:

$$\eta \cong M \ln \frac{\pi r}{2a} + C \qquad (18)$$

For the near field in the channel the solution is reduced to:

$$\eta \cong M \frac{\pi x}{2a} - M \ln \frac{e}{2} + C \qquad (19)$$

Boundary condition

To find the solution to equation 10 a boundary condition is needed. For the end of the channel, this is a fixed highly reflective wall. Therefore at x=-L the flow is zero, which results in this boundary condition:

$$\frac{\partial \eta_c}{\partial x} = 0 \qquad \textit{(at x=-L)} \qquad (20)$$

Solution

The unknowns in the formulae can be solved by matching the solution from both the far (10) and near (20) field in the channel and the far (15) and near (19) field in the ocean. The found unknowns can then be used to provide the response of the channel:

$$\eta_c = \frac{2A\cos k(x+L)}{\cos(kL) + \frac{2ka}{\pi}\sin(kL)\ln\left(\frac{2\gamma ka}{\pi e}\right) - ika\sin(kL)} \qquad (21)$$

With:
γ: Euler's constant 0.577215

The amplification factor is defined as being the response of the bay to the incoming wave. The incoming wave for the channel is:

$$\eta_c = 2A\cos k(x+L) \qquad (22)$$

Amplification function

The amplification function at a certain point is defined as the ratio of the amplitude of the water level deviation at that point to the amplitude of the incoming wave. The amplification function for the analytical solution can thus be found by dividing the harbors response (22) by incoming wave (23) at the channel entrance. This results in the amplification factor, R:

$$\Re = \frac{1}{\cos(kL) + \frac{2ka}{\pi}\sin(kL)\ln\left(\frac{2\gamma ka}{\pi e}\right) - ika\sin(kL)} \qquad (23)$$

In this formula it can be clearly seen that the amplification depends only on the width to length ratio of the channel and the wavelength of the incoming wave. This is also found in the Miles and Munk harbor paradox (Miles and Munk, 1961).

Plotting this function for a length to width ratio of the channel of 12 gives the following graph:

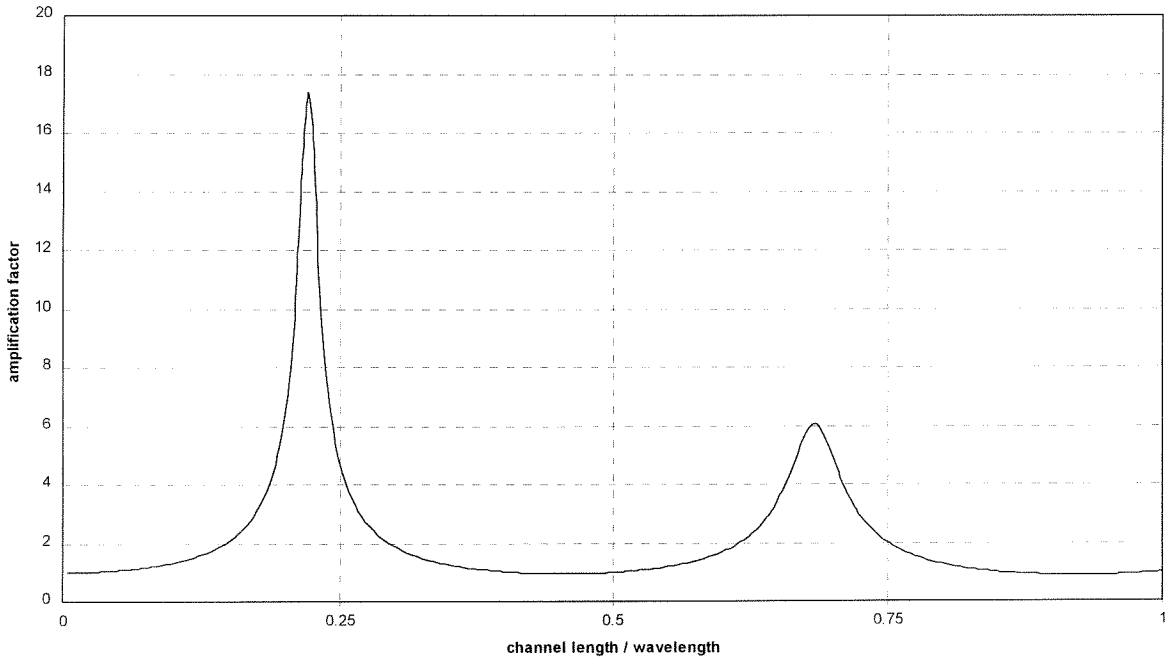

Graph 2 Analytical linear amplification function according to Mei (1984).

The first peak is the highest. It occurs at a channel length over wavelength ratio slightly less than one quarter. The second and subsequent peaks will be lower, because for higher frequencies more energy is radiated back to the sea.

4. One-dimensional approach

4.1 Introduction.

In this chapter, a one-dimensional approach is described. It is based on a one-dimensional network representing the channel with a boundary condition at the end node representing the sea area as shown in Figure 8. Méndez Lorenzo (1997) studied a boundary condition that is a combination of a water level and a Riemann invariant. Analytically this boundary condition models the radiation of energy to the sea exactly according to the Sommerfeld radiation condition, resulting in an exact match with the test problem. However, due to approximations required for a numerical model this boundary condition can only match a single peak in the amplification function correctly. The non-linear terms are added to the one-dimensional model in an attempt to overcome this problem.

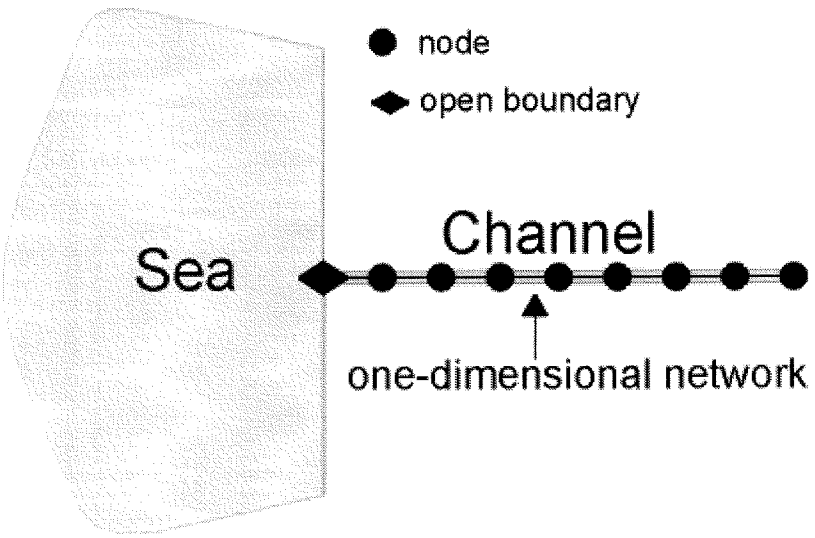

Figure 8 Schematic representation of a one-dimensional approach

4.2 Boundary condition types

4.2.1 Riemann boundary

The Riemann boundary condition is characterized by its non-reflective nature. A wave that encounters a Riemann boundary will travel onwards without reflection. Using a Riemann boundary condition the incoming and outgoing waves remain separated and do not affect each other. It is possible to impose an incoming Riemann invariant for the boundary condition, which sends a wave into the system. The Riemann boundary condition will be used throughout this thesis, and therefore its full derivation will be given.
The derivation of the Riemann boundary condition starts with the derivation of the Riemann invariants.
The linear shallow water equations are presented below.
Equation of continuity:

$$\frac{\partial \zeta}{\partial t} + h\frac{\partial u}{\partial x} = 0 \qquad (24)$$

Equation of motion:

$$\frac{\partial u}{\partial t} + g\frac{\partial \zeta}{\partial x} = 0 \qquad (25)$$

Multiplying the continuity equation with $(g/h)^{1/2}$ and rewriting the equation of motion leads to:

$$\frac{\partial \zeta \cdot \sqrt{\frac{g}{h}}}{\partial t} + \sqrt{gh}\frac{\partial u}{\partial x} = 0 \qquad (26)$$

$$\frac{\partial u}{\partial t} + \sqrt{gh}\frac{\partial \zeta \cdot \sqrt{\frac{g}{h}}}{\partial x} = 0 \qquad (27)$$

Adding both equations and subtracting them gives respectively:

$$\frac{\partial (u + \zeta \cdot \sqrt{\frac{g}{h}})}{\partial t} + \sqrt{gh}\frac{\partial (u + \zeta \cdot \sqrt{\frac{g}{h}})}{\partial x} = 0 \qquad (28)$$

$$\frac{\partial (u - \zeta \cdot \sqrt{\frac{g}{h}})}{\partial t} - \sqrt{gh}\frac{\partial (u - \zeta \cdot \sqrt{\frac{g}{h}})}{\partial x} = 0 \qquad (29)$$

The incoming and outgoing Riemann invariants are defined as follows:

Incoming Riemann invariant: $Z = u + \sqrt{\frac{g}{h}} \cdot \zeta$ *(30)*

Outgoing Riemann invariant: $Y = u - \sqrt{\frac{g}{h}} \cdot \zeta$ *(31)*

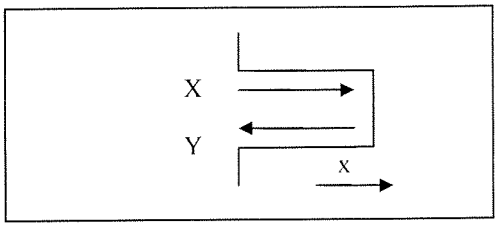

The Riemann invariants are constant along the lines:

$$\frac{\partial x}{\partial t} = \pm\sqrt{gh} \qquad (32)$$

(These are the characteristic directions)

At the boundary only the incoming Riemann invariant is imposed:

$$u + \sqrt{\frac{g}{H}}\zeta = \sqrt{\frac{g}{H}}e^{i\omega t} \qquad (33)$$

With:

$$\zeta = e^{i\omega t}$$

The resulting amplification factor in the case that this boundary condition is used is:

$$\Re = 1 \qquad (34)$$

When a Riemann boundary condition is used, no waves are reflected back into the channel. Therefore, no energy can be accumulated inside the channel to increase the wave amplitude, and no resonance occurs inside the channel.

4.2.2 Water level boundary condition

In the case of a water level boundary condition, the water level is imposed at the boundary.

$$\zeta = e^{i\omega t} \tag{35}$$

The amplification factor for a water level boundary can be calculated with:

$$\Re = \frac{1}{\cos(kL)} \tag{36}$$

It is clear that as the factor cos(kL) approaches zero the amplification factor increases to infinity. This happens for a channel length equal to an odd number of quarter wavelengths. (kL=π/2+nπ, n=0, ±1…)

4.2.3 Epsilon boundary condition

With a Riemann boundary condition there is no amplification in the channel and with a water level boundary condition there is too much amplification. A logical choice would therefore be to combine the two. This is the basis for the epsilon boundary condition. The epsilon boundary condition is a combination of the water level boundary condition and the Riemann boundary condition:

$$\sqrt{\frac{g}{H}}\zeta + \mu\left(u + \sqrt{\frac{g}{H}}\zeta\right) = \sqrt{\frac{g}{H}}\left(e^{i\omega t} + \mu e^{i\omega t}\right) \tag{37}$$

with:

$$\mu = \frac{ka + \frac{2ai}{\pi}\ln\left(\frac{2\gamma ka}{\pi e}\right)}{1 - ka - \frac{2ai}{\pi}\ln\left(\frac{2\gamma ka}{\pi e}\right)} \tag{38}$$

This boundary condition is derived from the analytical solution and in this form it will give the exact solution. However, there are two problems with μ:

1. It depends on the wavelength (ka)
2. It is a complex.

For the implementation of μ in a numerical model the complex operator has to be converted into a real operator. There are several methods by which this can be achieved, e.g. (Enquist, Majda, 1977) or (Taylor, 1975). In (Méndez Lorenzo, 1997) the μ is made real by rewriting it as:

$$\mu = i\omega\varepsilon \tag{39}$$

with:

$$\varepsilon = \sqrt{\frac{ka}{\omega^2\left(1 - 2ka + (ka)^2 + \frac{4(ka)^2}{\pi^2}\ln^2\left(\frac{2\gamma ka}{\pi e}\right)\right)}}$$

Now ωi can be approximated as $\partial/\partial t$ which yields a real operator for the boundary condition:

$$\sqrt{\frac{g}{H}}\zeta + \varepsilon \cdot \frac{\partial}{\partial t}\left(u + \sqrt{\frac{g}{H}}\zeta\right) = \sqrt{\frac{g}{H}}\left(e^{i\omega t} + i\omega\varepsilon e^{i\omega t}\right) \qquad (40)$$

However, ε is still dependent on the wavelength. A different way of converting the complex unit into a real operator might resolve this problem. The resultant amplification function for the epsilon boundary is given by the following formula:

$$\Re = \frac{2(1+\varepsilon\omega i)}{1+e^{-2ikL}+2\varepsilon\omega i} \qquad (41)$$

4.2.4 Comparison epsilon, water level and Riemann boundary conditions

Plotting the four amplification functions (24, 35, 37, 42) results in Graph 3.

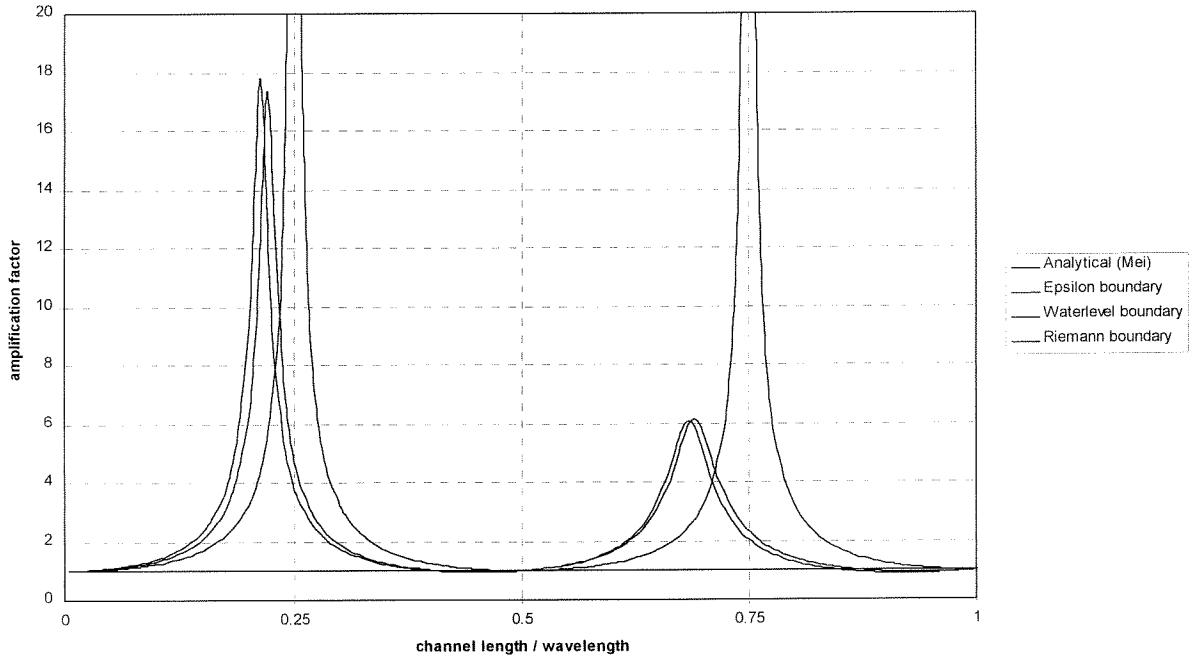

Graph 3 Amplification function of Epsilon, water level and Riemann boundary for a width/length ratio of 20.

This graph shows how the amplification function is equal to one for the whole wave spectrum when a Riemann boundary condition is imposed on the open boundary (there is no resonance). The water level boundary condition amplification function resonates to infinity at the resonant frequencies. The epsilon boundary condition comes closest to the analytical solution of the test problem. The peak is shifted just a bit for the epsilon boundary. This is caused by the approximations used to make ε a real operator.

A problem arises at the numerical implementation stage. For a numerical calculation, it is impossible to retain a variable epsilon in the formulae. The value for epsilon is therefore fixed. This value depends on the value of ka and has to be determined before the calculation is started. This is in contrast to the variable epsilon used in Graph 3. With a fixed value the epsilon can be tuned to either the first or the second peak. If it is tuned to the first peak, then for the higher frequencies the boundary condition will tend to Riemann boundary condition, resulting in insufficient reflections and consequently a lower amplification. If the value for epsilon is tuned for the second peak then, for the lower frequencies the boundary condition will tend too much to a water level boundary condition, reflecting too much energy. This results in an overestimation of the first peak. The following two graphs, in which a fixed value for epsilon is used to tune either the first peak or the second peak, clearly show this.

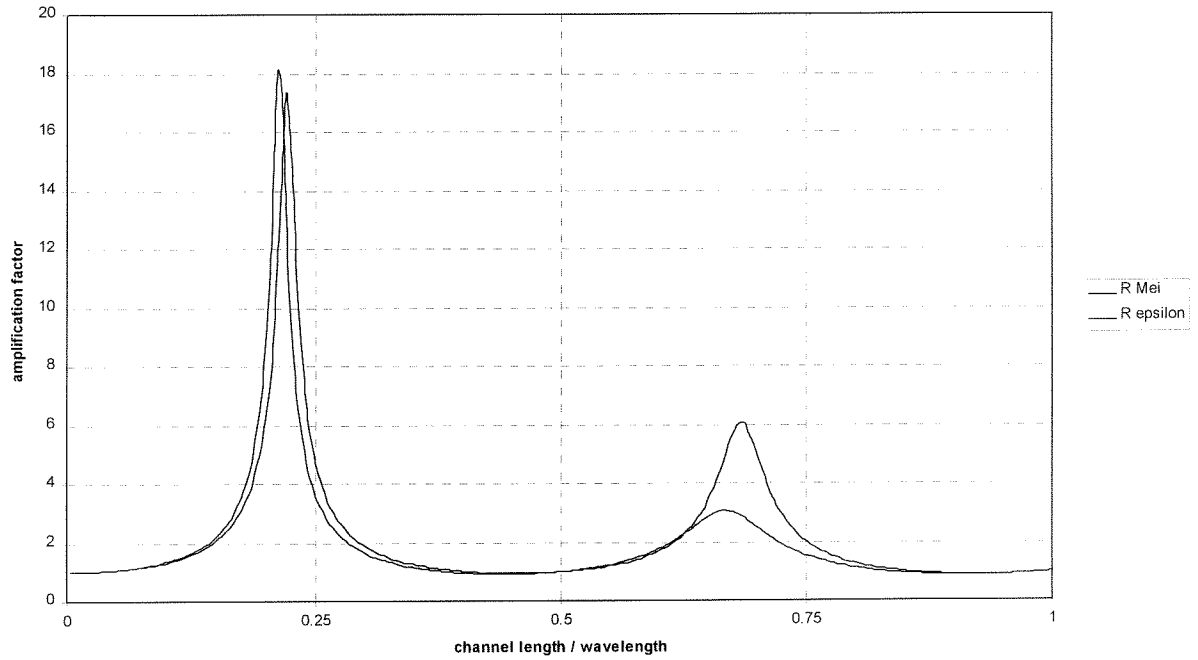

Graph 4 Amplification function for the Mei analytical solution and for the epsilon boundary condition. Length to width ratio of the channel set to 20. Value for fixed Epsilon tuned to the first peak.

With this value for Epsilon, the first peak is modeled correctly, but the second peak is too low. Now with a different value for Epsilon set to correctly model the second peak the amplification function plotted in Graph 5 is obtained.

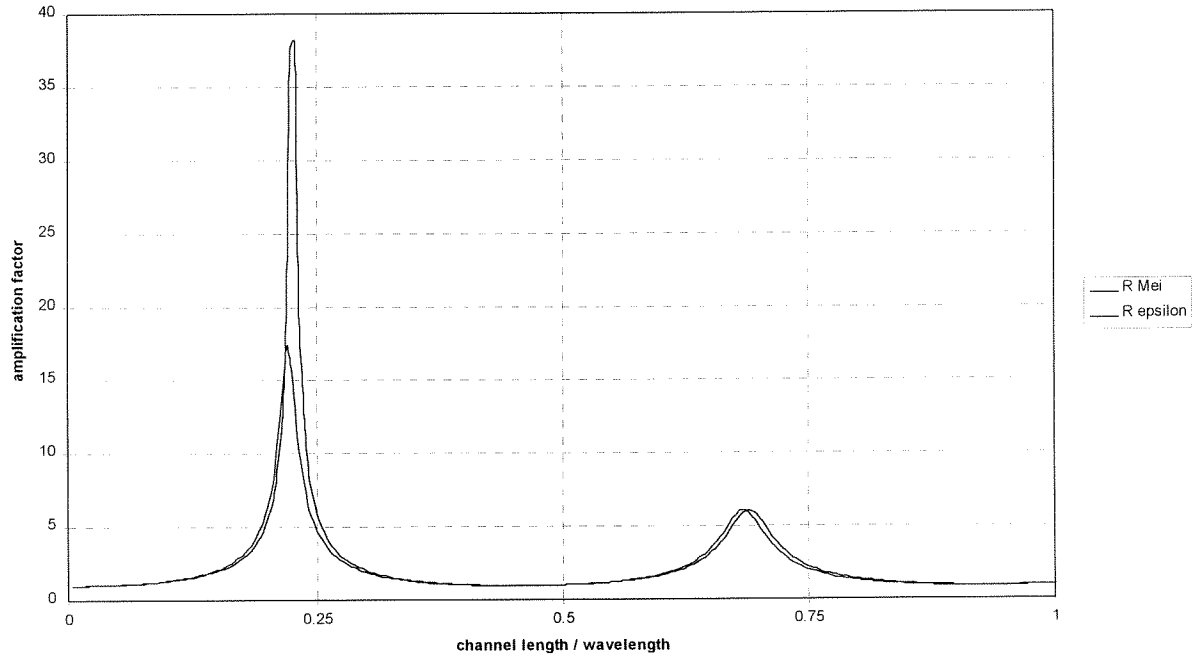

Graph 5 Amplification function for the Mei analytical solution and for the epsilon boundary condition. Length to width ratio of the channel 12. Value for fixed Epsilon tuned to the second peak. (Different scale)

With the fixed value for epsilon tuned to the second peak the second peak is modeled correctly. The first peak, however, is now a factor 2 too high.

This clearly illustrates the main drawback of using the epsilon boundary condition; a fixed value for epsilon has to be determined before the calculations can start. From the previous graphs it is clear that no matter what value

for epsilon is taken it is impossible to correctly model both peaks at the same time. For a simple prismatic and straight channel there are only two peaks one is interested in. It is not very difficult to determine the correct epsilon per peak and then do two runs on the system. In this manner, the amplification function can be determined. For a more complex geometry, determining the value for epsilon might prove to be very difficult. A system of channels has many resonant frequencies and if one wants to obtain correct results for the entire spectrum then the calculation has to be repeated for every peak and corresponding epsilon. This might prove to be an inefficient and impractical solution. Furthermore, for larger amplitudes, the non-linear terms start to play a role and the transfer of energy to higher harmonics cannot be modeled correctly if only one frequency is inserted in the model. Waves from the lower part of the spectrum will influence the ones in the higher region so a full spectrum run is required. Up to this point, there is a basis for a good boundary condition, but the results are not yet satisfactory.

4.3 Non-linear model (Seiches II) & numerical implementation

By adding non-linear terms to the system, the results from the epsilon boundary condition might be better, because the higher amplitudes are influenced more by them than the lower ones. Therefore, by tuning the system to the second peak, the first peak, which is presently overestimated, might be reduced to its proper proportion. This non-linear numerical model will be referred as Seiches II hereafter. With these non-linear terms, the first peak would be lower while the second peak should remain at almost the same height, resulting in an amplification function that resembles the analytical function more closely. It should be noted however that the analytical solution is linear. Therefore, a comparison between these two is not entirely valid.

4.4 Non-linear equations

The flow of the water in the channel can be modeled by using the long wave equations. The non-linear one-dimensional equations used in the model are:
Equation of motion:

$$\frac{\partial u}{\partial t} + u\frac{\partial u}{\partial x} + g\frac{\partial \zeta}{\partial x} + \frac{gu|u|}{C^2 h} = 0 \qquad (42)$$

The second term in this equation is the advective term, and the fourth term is the Chézy type friction.
Equation of continuity:

$$\frac{\partial \zeta}{\partial t} + \frac{\partial uh}{\partial x} = 0 \qquad (43)$$

Imposing a grid on the continuous time and space domain the grid size in the space direction is defined as Δx and numbered with the letter j, and the grid size in time is Δt numbered with the letter n. For every grid point (j,n) the water level and the velocity are calculated.

These partial differential equations are discretized using the Preissmann Box scheme:

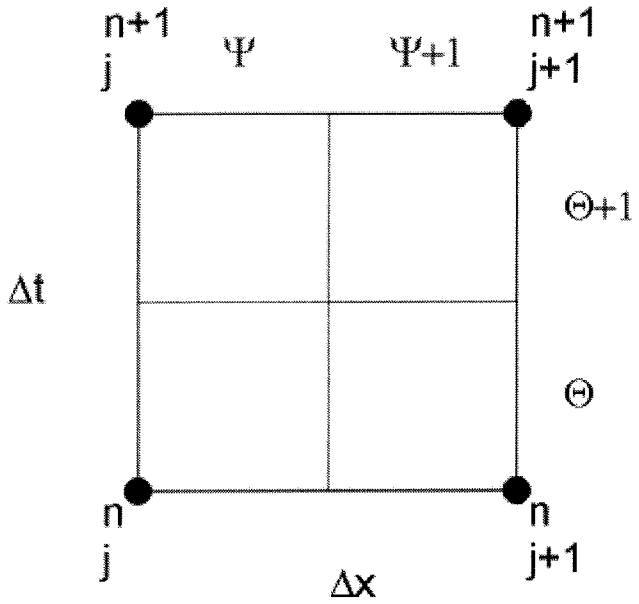

Figure 9 Preismann Box scheme

With $\psi = ½$ this results in the following form:

Motion:

$$\frac{u_j^{n+1}-u_j^n}{2\Delta t}+\frac{u_{j+1}^{n+1}-u_{j+1}^n}{2\Delta t}+g\left\{(1-\theta)\frac{\zeta_{j+1}^n-\zeta_j^n}{\Delta x}+\theta\frac{\zeta_{j+1}^{n+1}-\zeta_j^{n+1}}{\Delta x}\right\}+\left\{\frac{\frac{1}{2}u_{j+1}^n\cdot u_{j+1}^{n+1}-\frac{1}{2}u_j^n\cdot u_j^{n+1}}{\Delta x}\right\}+\frac{u_{j+1}^{n+1}+u_j^{n+1}}{2}\cdot g\frac{|u_{gem}|}{c^2\cdot H_{gem}}=0 \qquad (44)$$

Continuity:

$$\frac{\zeta_j^{n+1}-\zeta_j^n}{2\Delta t}+\frac{\zeta_{j+1}^{n+1}-\zeta_{j+1}^n}{2\Delta t}+\left\{\frac{u_{j+1}^{n+1}\cdot H_{j+1}^n-u_j^{n+1}\cdot H_j^n}{2\Delta x}+\frac{u_{j+1}^n\cdot H_{j+1}^{n+1}-u_j^n\cdot H_j^{n+1}}{2\Delta x}\right\}=0 \qquad (45)$$

H_{gem} is the water depth and u_{gem} is the velocity both averaged in space with $\psi = ½$. In the linearized case, the shallow water equations can be reduced by omitting the friction and advective terms (see equations 4 and 5)

4.5 Results

The biggest drawback of the epsilon boundary is the need to choose a fixed ka value. To show this the calculations in this section have been done with two ka values for each mode. One to get the first peak of the calculation right and a second to get the second peak of the amplification function right. If the second peak is right then the first peak will be too big. The graphs are done in two different scales to clearly show the details. For these numerical calculations, a ratio of 20 was used for the length and width of the channel because this provides blunter peaks than for higher ratios. With a blunter peak, the resolution of the number of frequency components of the numerical program will be sufficient to hit the peak value. For a sharper peak, this is more difficult.

4.5.1 Linear

The following results were obtained with the numerical program for a linear case. They are included here for comparison with the analytical solution as shown in graph 4 and 5. The graphs show how well the program works in the linear case.

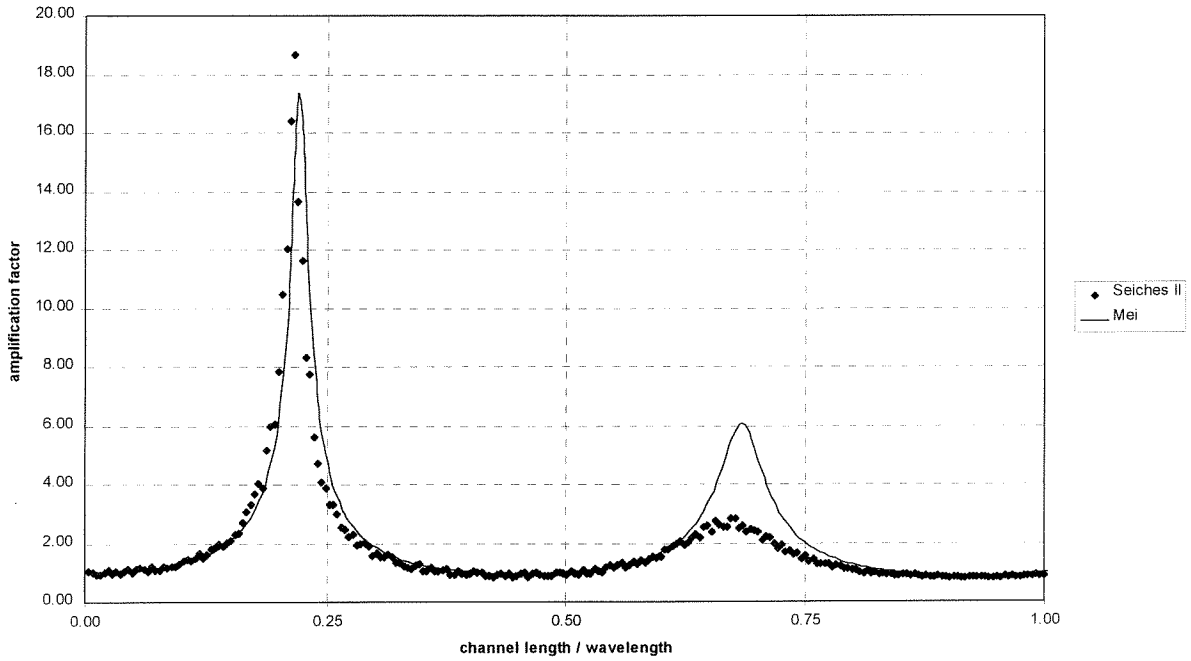

Graph 6 Amplification function Seiches II linear mode. Epsilon tuned to the first peak.

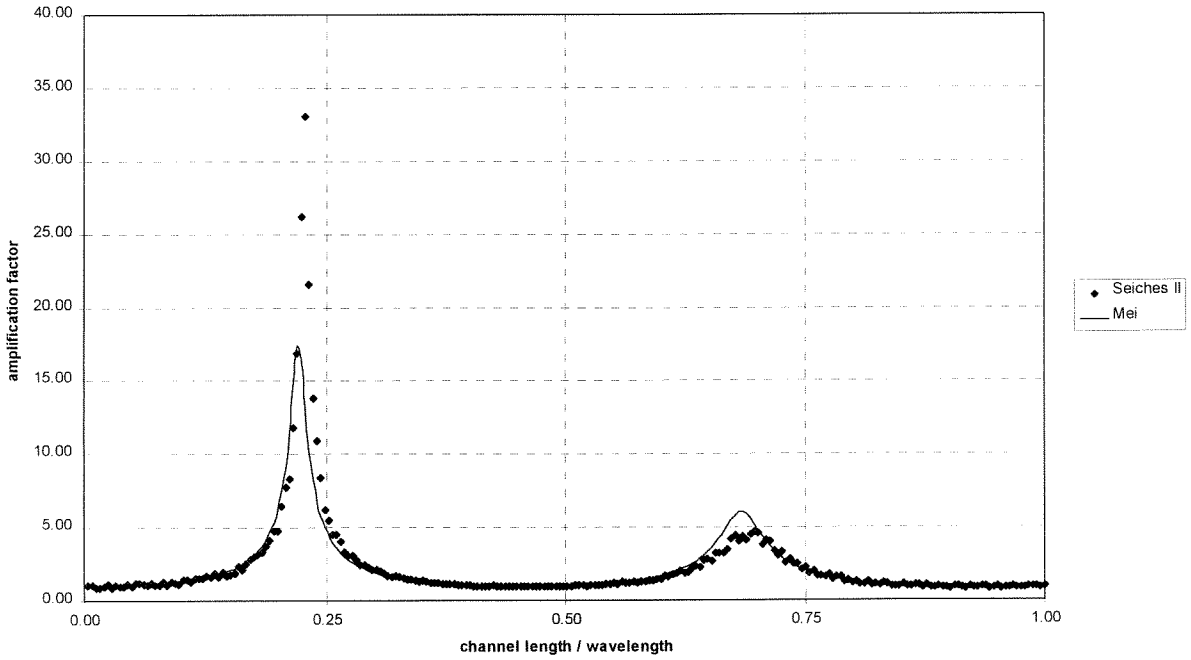

Graph 7 Amplification function Seiches II linear mode. Epsilon set on second peak. (Different Scale)

4.5.2 Advection

When adding the advection term to the model the height of the peak is not lowered. The advective term does not play a major role apparently. The transfer of energy to the higher harmonics is for these amplitudes small. (See appendix III for more details on the higher harmonics)

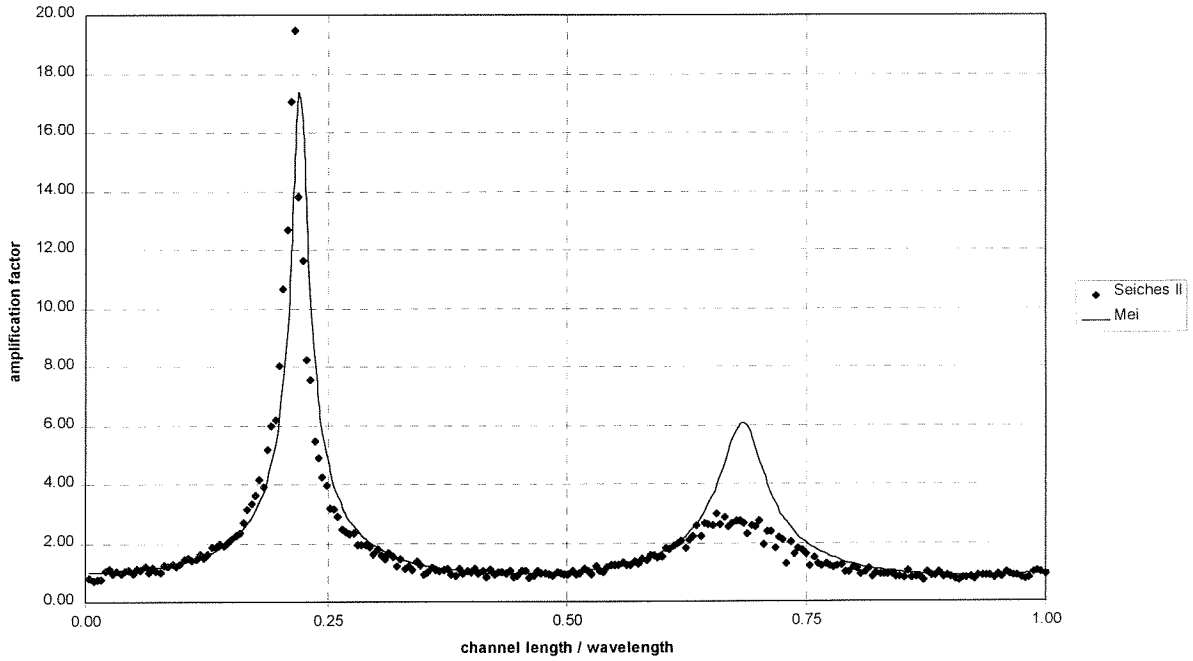

Graph 8 Amplification function Seiches II, non-linear mode. Advection term activated. Epsilon tuned to the first peak

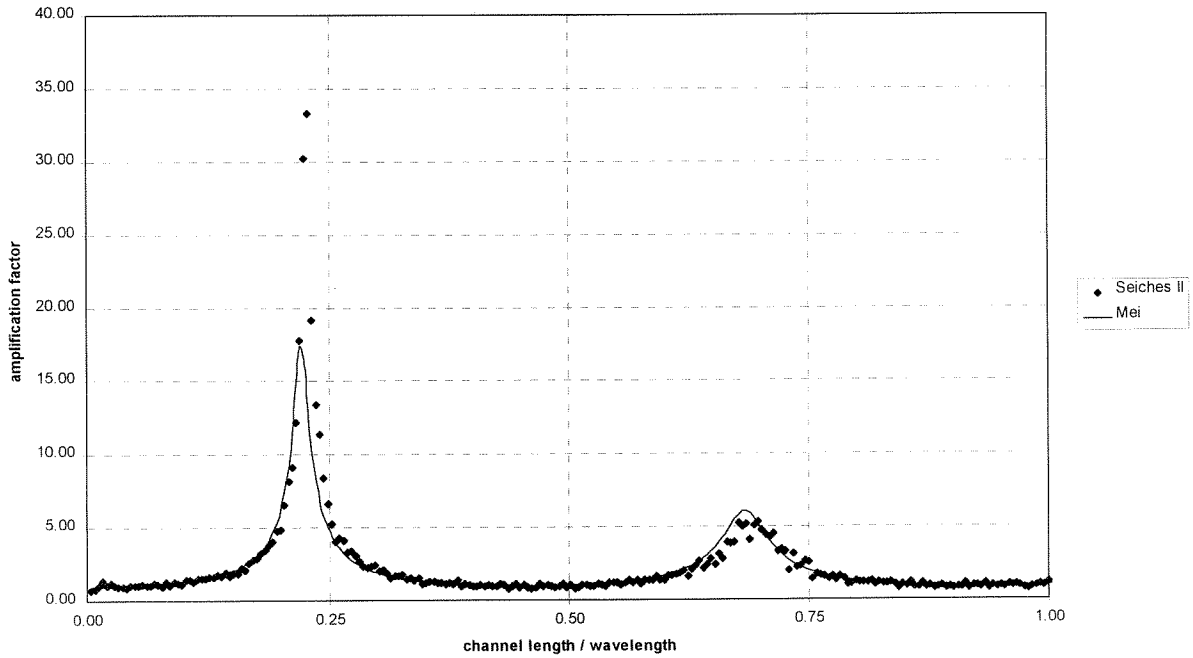

Graph 9 Amplification function Seiches II, non-linear mode. Advection term activated. Epsilon tuned to the second peak. (Different scale)

4.5.3 Friction

Adding the friction term has a much bigger effect than the advection term as can be seen on

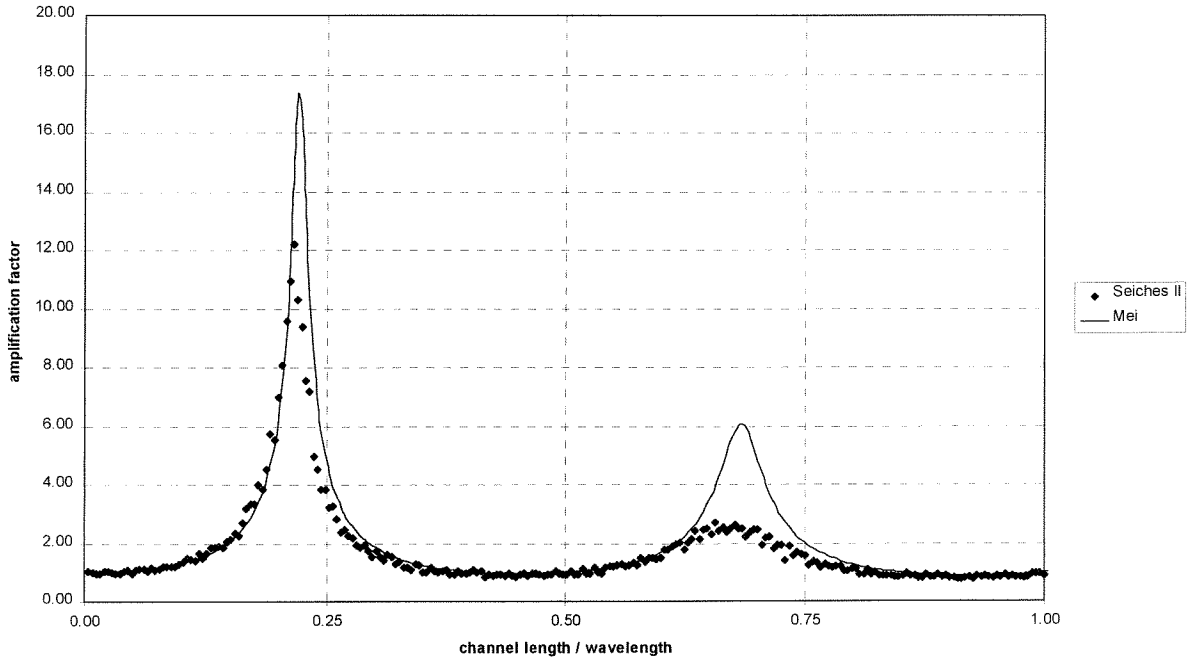

Graph 10 and Graph 11. Graphs 10 and 11 show how the highest peak is lowered significantly. This is because the friction term primarily reacts on the amplitude of the wave. At the first peak this amplitude has become so large that the bottom friction starts to play a mayor role. The results now match the analytical case closely as shown in graph 11.

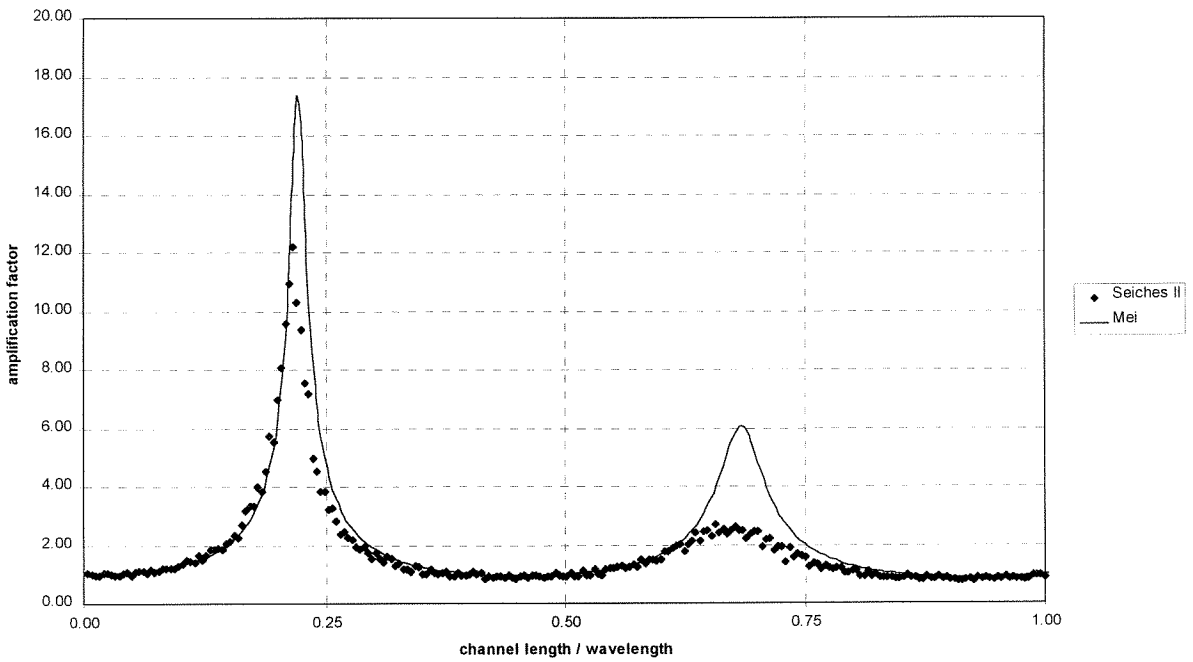

Graph 10 Amplification function Seiches II, non-linear mode. Friction term activated, advection term off. Epsilon tuned to the first peak.

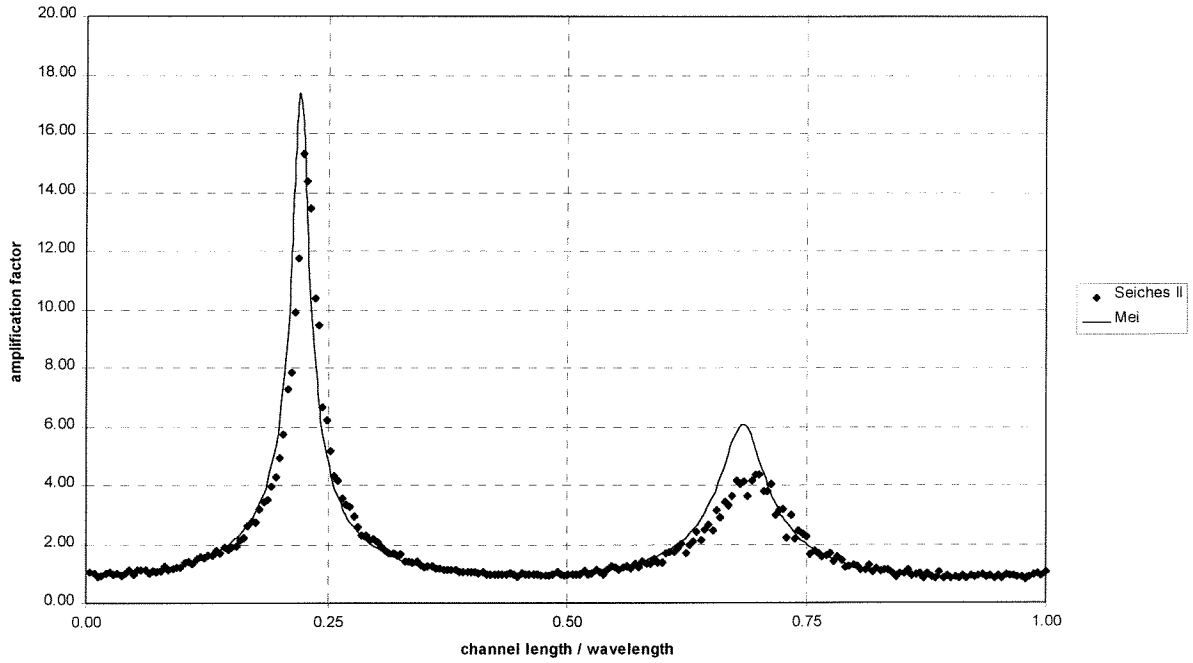

Graph 11 Amplification function Seiches II, non-linear mode. Friction term activated. Advection term off. Epsilon tuned to the second peak.

4.5.4 Advection & Friction

Graph 12 and 13 confirm that the friction term has the greatest damping effect, this in contrast to the noise created by the advection term. Just as in graph 11 the results of graph 13 coincide well with the analytical solution.

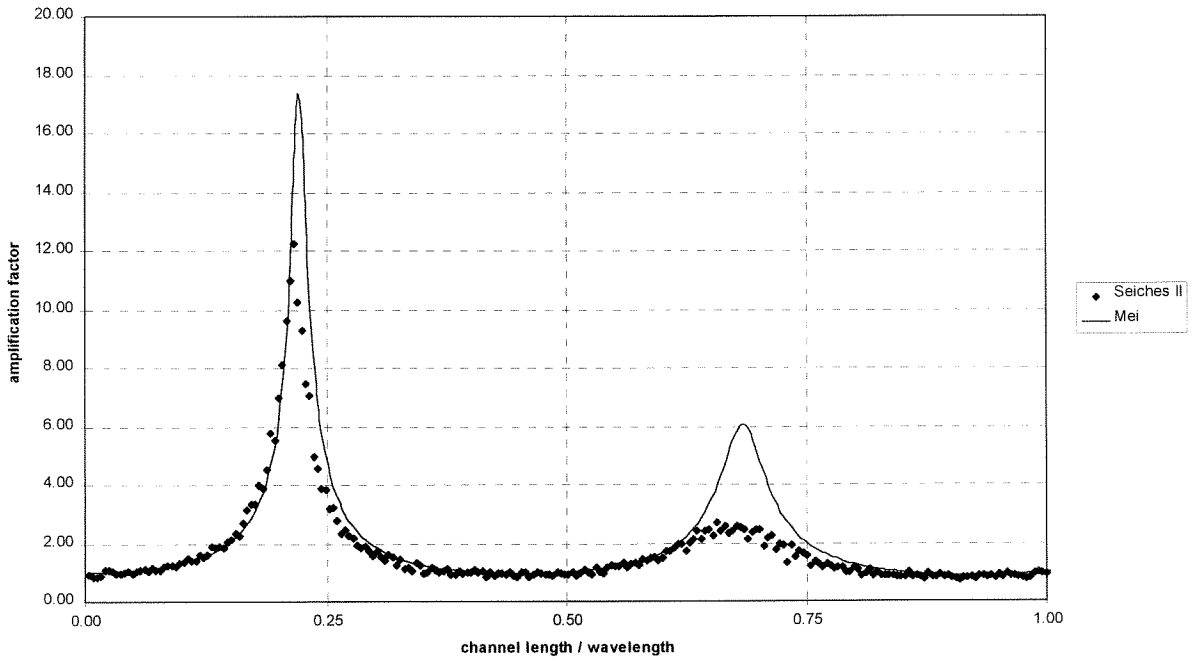

Graph 12 Amplification function Seiches II, non-linear mode. Advection and friction term activated. Epsilon tuned to the first peak.

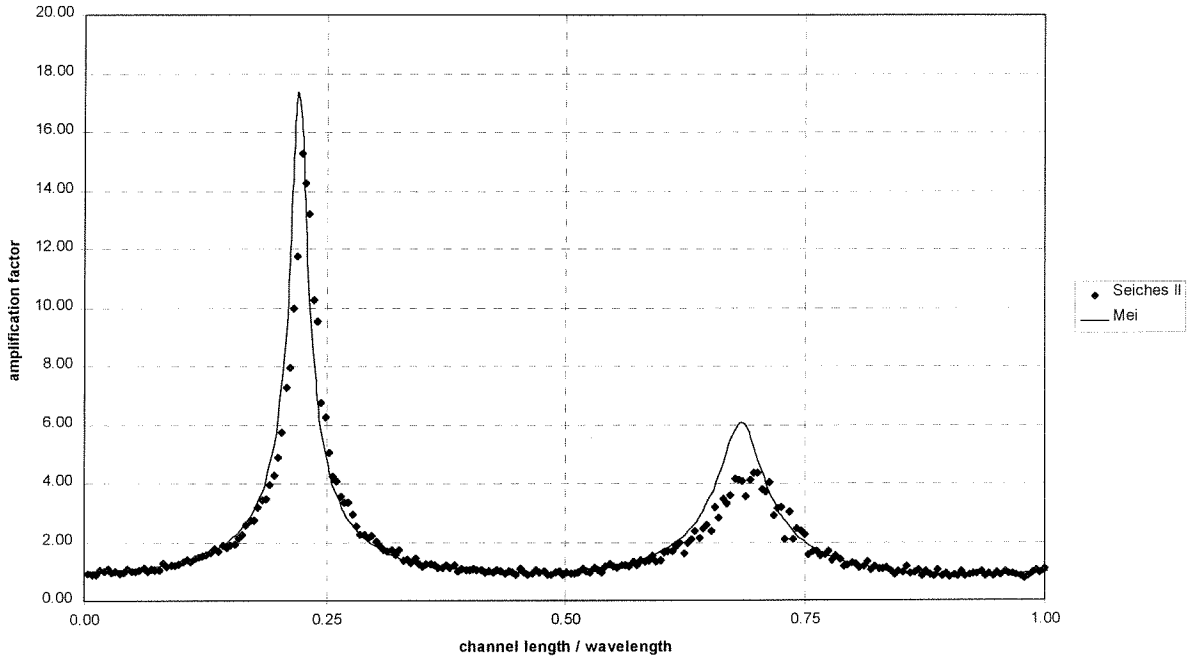

Graph 13 Amplification function Seiches II, non-linear mode. Advection and friction term activated. Epsilon tuned to the second peak.

4.6 Conclusion for the one-dimensional approach

A numerical model with an epsilon boundary condition has to be tuned. This has to be done such that the damping is reasonable for a range of frequencies. Its qualitative behavior seems to overestimate the damping of higher harmonics as compared to the fundamental harmonics. This is principally caused by the need to supply a predetermined epsilon before the calculation. This fixed epsilon causes only one of the peaks in an amplification function to be matched exactly. Other peaks will be too high or too low. For a model with simple geometry, this is not a serious problem because there are only two peaks in the spectrum of our interest. So with two runs the entire amplification function can be made to match. With a more complex geometry such as for the Europoort, this is a much more difficult task. The complex geometry results in an amplification function with many peaks. To determine the amplification function of such a complex model many runs are required with each a different epsilon. Sending in only one frequency at the time is not a solution either, considering the fact that the energy is transmitted to higher harmonics and that the entire signal plays a role in the amplification function. The addition of non-linear terms to the one-dimensional model has not improved this situation, although it could not be verified entirely due to lack of comparative material. What is needed is a boundary condition, which does not depend on part of the answer to obtain the solution. Further investigation is needed to improve the epsilon boundary condition. This option is not pursued. A different approach to the boundary condition problem will be studied further. This approach, consisting of one-dimensional and two-dimensional coupling, will be presented in the next chapter.

5. Combined one and two-dimensional approach

5.1 Introduction

Although a one-dimensional approach, as chosen in the previous chapter, can provide adequate results with respect to the amplification function, it is not a perfect solution. Especially the choice for a fixed epsilon is problematic. A less complex boundary condition can be achieved by constructing a coupled one-dimensional and two-dimensional model: a one-dimensional area (the channel) connected to a two-dimensional area (sea) as is shown in Figure 10. (This model will be referred to as the 1D2D model).

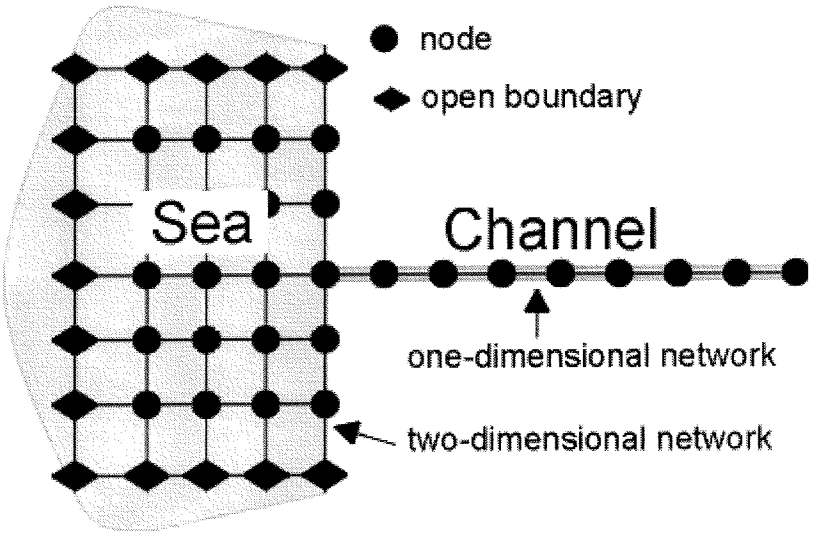

Figure 10 Connection of the one-dimensional channel to the two-dimensional sea

In this setup, both components of the model do exactly what they are best at: the two-dimensional component takes care of the radiation of energy outward into the sea, and for the channel a one-dimensional network is sufficient. This cooperation between both components has a great potential. In this thesis, this 1D2D model has been developed to evaluate its usefulness and its accuracy with respect to the one-dimensional approach as explained in the previous chapter. To be able to compare the results with the test problem all calculations with the 1D2D model will be done for the linear case. However, because the D2D model is based on the non-linear shallow water equations it is capable of doing non-linear calculations.

5.2 Numerical approximation

5.2.1 Computational grid

The continuous formulae for motion (2 & 3) and continuity (1) cannot be used by a discrete (digital) system. They therefore have to be discretized. The discretization of these formulae results in a grid. In this grid, all variables are calculated in all points, but to solve the equations not all the variables are necessary in each point. Only one is required per grid point. To remove this redundancy the grids can be shifted with respect to each other. This results in a staggered grid: A grid with only one variable per grid point. Such a grid is shown in the next figure:

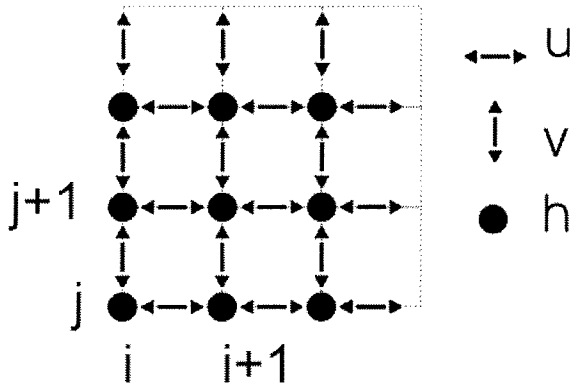

Figure 11 Staggered grid

As can be seen from the scheme in every branch the velocity either in y or x direction is calculated and the water level (h) is calculated in the nodes.

5.2.2 Discretization

The discretization is based on a completely implicit scheme with a staggered grid as shown above. The discretization in time is based on the theta method. This results in a grid of spatial points. For the linear case the following discretization is used:

Equation of continuity:

$$\frac{\zeta^{n+1}-\zeta^{n}}{\Delta t}+(1-\Theta)h\left(\frac{u^{n}_{i+1/2,j}-u^{n}_{i-1/2,j}}{\Delta x}+\frac{v^{n}_{i,j+1/2}-v^{n}_{i,j-1/2}}{\Delta y}\right)+\Theta h\left(\frac{u^{n+1}_{i+1/2,j}-u^{n+1}_{i-1/2,j}}{\Delta x}+\frac{v^{n+1}_{i,j+1/2}-v^{n+1}_{i,j-1/2}}{\Delta y}\right)=0 \qquad (46)$$

Equation of motion:

$$\frac{u^{n+1}_{i+1/2,j}-u^{n}_{i+1/2,j}}{\Delta t}+(1-\Theta)\left(g\frac{\zeta^{n}_{i+1,j}-\zeta^{n}_{i,j}}{\Delta x}\right)+\Theta\left(g\frac{\zeta^{n+1}_{i+1,j}-\zeta^{n+1}_{i,j}}{\Delta x}\right)=0 \qquad (47)$$

$$\frac{v^{n+1}_{i,j+1/2}-u^{n}_{i,j+1/2}}{\Delta t}+(1-\Theta)\left(g\frac{\zeta^{n}_{,j+1}-\zeta^{n}_{i,j}}{\Delta x}\right)+\Theta\left(g\frac{\zeta^{n+1}_{i,j+1}-\zeta^{n+1}_{i,j+1}}{\Delta x}\right)=0 \qquad (48)$$

5.2.3 Matrix inversion

Using a minimum degree method (Duff, 1986) solves the resultant array of equations. With a minimum degree method, the array is solved by eliminating the node which has the least edges connected to it. The prerequisites for using this method are a symmetrical and positive definite matrix.

5.3 Model

The numerical model is based on the sources of Sobek and a newly developed 1D2D (alpha stage) program. For efficiency reasons θ=0.55 turned out to be the best choice (See appendix VII & VIII). The schematic layout of the model is as follows:

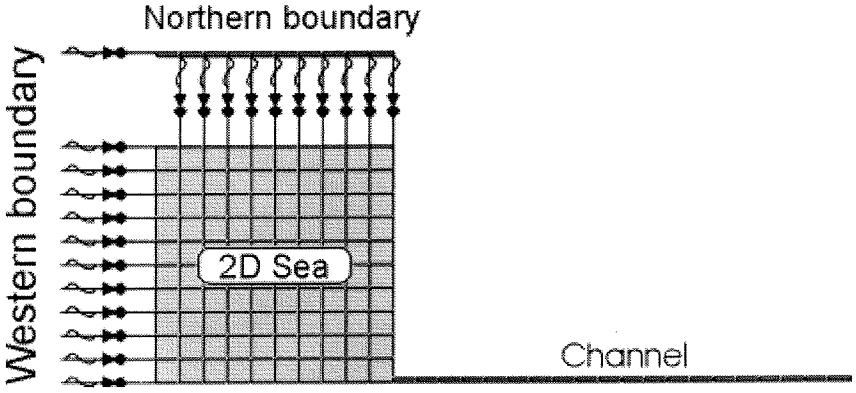

Figure 12 Schematic view of the numerical model

The different components of the model are:

5.3.1 Channel

For the situation in the channel a one-dimensional network is sufficient. At the end of the channel a discharge equal to zero is imposed.

5.3.2 Western boundary

A series of one-dimensional channels are attached to the two-dimensional sea area to impose the correct boundary condition. At the end of the one-dimensional channels, it is possible to impose a water level, discharge or Riemann boundary condition. The Riemann boundary condition is essential in this model since it allows for an approximation of the Sommerfeld condition. As stated before in chapter 4 the Riemann boundary condition is capable of handling the incoming and outgoing waves independently. This enables it to send in an incoming wave and just let the outgoing wave pass through without reflecting. By making use of the Riemann boundary condition waves can be sent into the channel without reflecting outgoing waves.

5.3.3 Northern boundary

For the open northern boundary of the model a Riemann boundary with amplitude of zero could be imposed. This would ensure that all waves in the outgoing direction can pass undisturbed. Unfortunately, the incoming wave from the western boundary is also influenced by the open boundary and will therefore leak energy through it. This results in a curved wave front. (See figure 11).

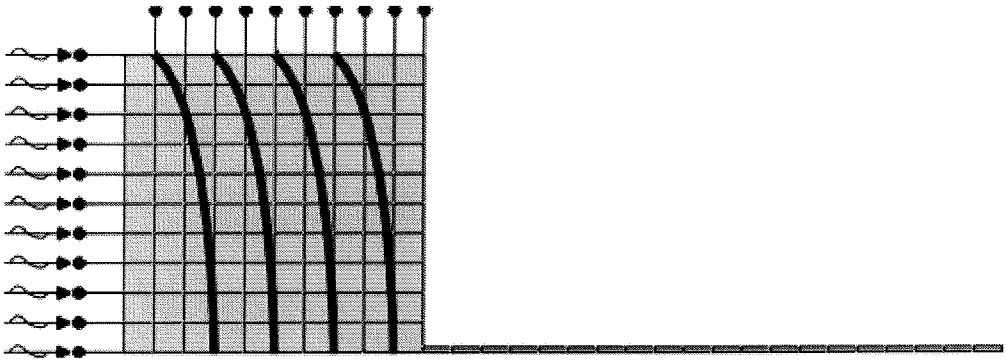

Figure 13 Incoming wave front for a Riemann boundary condition on the northern boundary of the model.

The amplitude of this wave decreases due to the leakage of energy through the northern boundary. The incoming signal into the channel is thus dependent on the open boundary condition. Increasing the width of the 2D sea will decrease the effect of the north boundary on the channel, but a larger width will also result in a longer calculation time.
To completely solve the problem a boundary condition has to be devised that will let outgoing waves pass through undisturbed but that works as a closed boundary for the incoming waves. The requirements for this boundary condition can be analyzed if one splits the waves in the 2D area into their respective components as was used in the test problem (Chapter 3). One can see that it is composed of an incoming wave, a reflected wave from the shore and the radially emitted wave from the channel entrance. To make use of the symmetry of the model the incoming waves are perpendicular to the shoreline.

$$\zeta = \zeta_i + \zeta_r + \zeta_c \qquad (49)$$

With:
ζ_i = incoming wave
ζ_r = reflected wave
ζ_c = radiated wave from the channel

The waves ζ_i and ζ_r are required to be able to pass parallel to the northern boundary. The wave emitted from the channel entrance, ζ_c, will move in a radial fashion and it should pass through the northern and western boundary without any reflections.
In the report *Seiches Europoort* (Kernkamp, 1994) a special boundary condition is used to model the open boundary. The basis for this condition is the Riemann invariant, but with a special incoming signal. The incoming signal is based on the fact that if only incoming and reflected waves are present then the velocity (u) in the direction perpendicular to the boundary is zero as is the case in a closed boundary. Recall that a Riemann boundary condition is composed of:

$$u + \zeta \sqrt{\frac{g}{h}} = f(t) \qquad (50)$$

With:
u = Velocity component in the direction perpendicular to the boundary
f(t) = Incoming Riemann Signal.

Now with the first requirement that u = 0 the boundary condition results in:

$$\zeta \sqrt{\frac{g}{h}} = f(t) \qquad (51)$$

With the proper value for f(t) the correct signal can be sent into the two-dimensional sea. This signal should only be composed of the incoming and outgoing wave, without the effect from the radiated wave. The value for ζ is found by adding an auxiliary channel to the system in which only the incoming and outgoing waves are present. This auxiliary channel can be one-dimensional because the waves are all straight and perpendicular to the coast. The auxiliary channel has the same depth and length as the 2D sea and the input signal is identical. The end of the channel is also closed. The required ζ_i and ζ_r can then be calculated for the auxiliary channel. During

calculation the values of the water levels in each cell in the auxiliary channel are then extracted and multiplied with the factor sqrt(g/h). These values are then used as input for the right hand side in the Riemann boundary condition imposed on the two-dimensional sea. This one-way communication between the two models results in a proper boundary condition that meets both aforementioned requirements. The next figure depicts the situation.

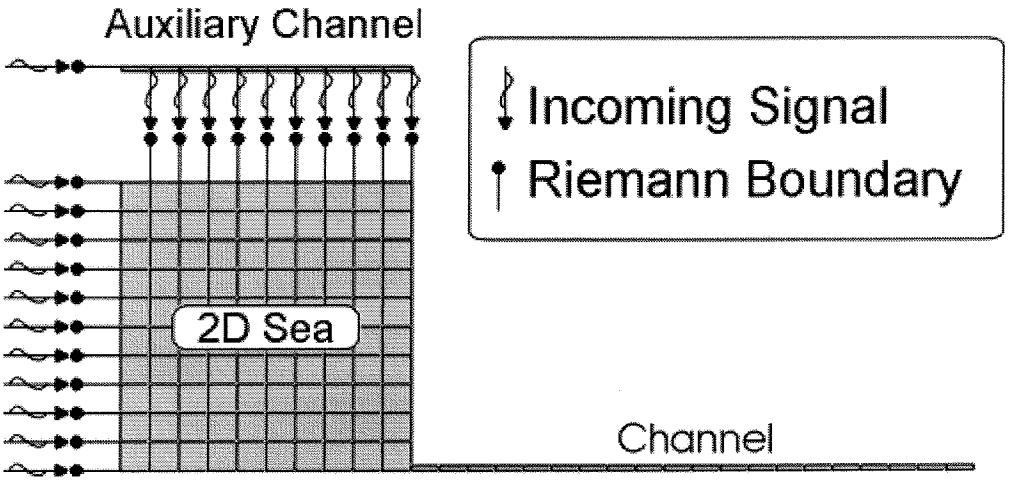

Figure 14 Layout of the model with the auxiliary channel.

The incoming wave from the western boundary will be supported by the incoming waves from the northern channel. If the phase and period is correct then the waves will travel in a straight path. This has been confirmed in test runs.

5.3.4 Sea

By making use of the symmetrical properties of the model the sea area can be halved. This results in a more efficient model and an increase in resolution for the same calculation time. Due to the radiation of energy by its boundary conditions, the area of the 2D component can be reduced considerably. It is no longer necessary to model an area sufficiently large to ensure that the amplitude of the waves approaches zero, as stated in the Sommerfeld condition. The minimum requirement for the size of the two-dimensional sea area has not been determined yet.

5.4 Results

The results from the 1D2D model are depicted in the following graphs. The results are quite satisfactory as can be seen from the graphs. It shows that this approach is not only efficient but also very useful. Although there is still a bit of deviation at the first peak, the order of error taken over the entire graph is minimal.

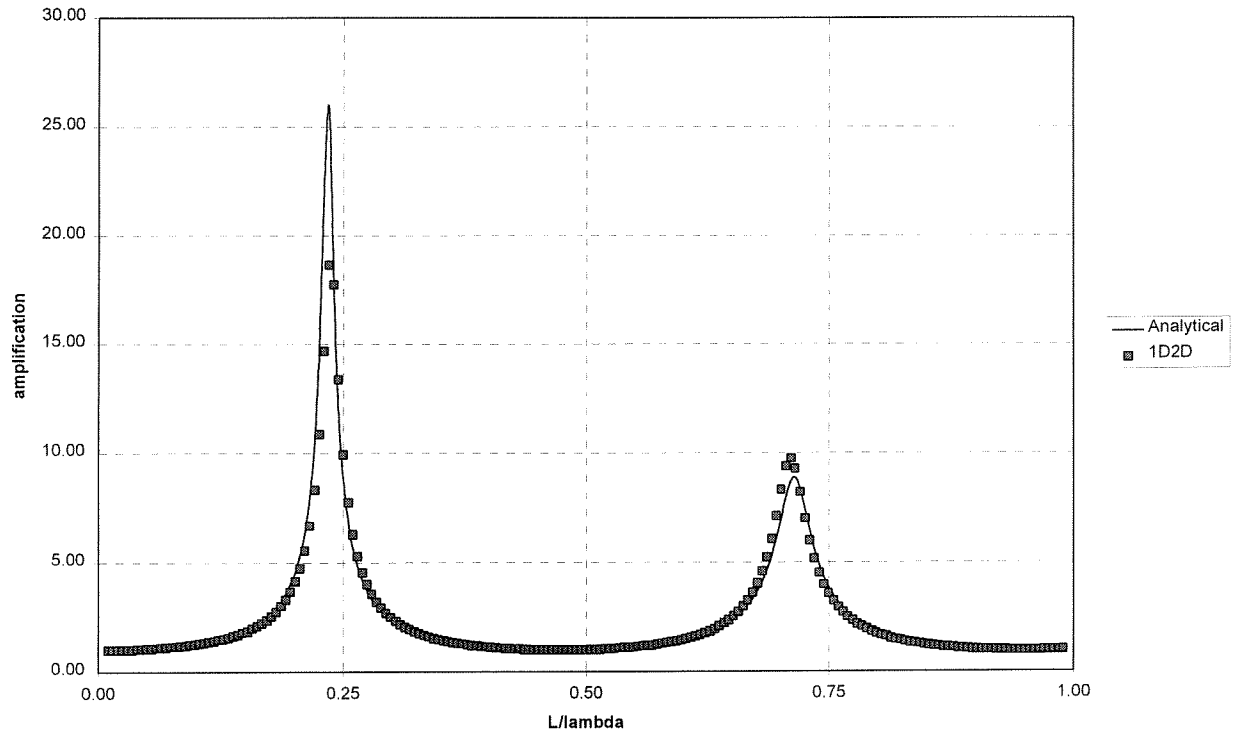

Graph 14 Amplification function for the modified 1D2D model. (200 frequencies).

The numerical results map very well on the analytical function, the position of both peaks is identical and in the regions next to the peaks, the amplification is exactly one. Only the first peak is too low, this is might be a result of the lack of resolution.
The analytical amplification function on the graph above is made with the same resolution as for the numerical model. This illustrates the narrowness of the peak very well because if the analytical function were plotted with a higher resolution the height of the first peak in the amplification function would be 28. An increase in resolution should deliver a graph, which matches the analytical function better. However, at this moment the total accuracy over the entire spectrum is already very good.

For comparative purposes, the amplification function is also made for more length/width ratios, resulting in the following graphs:

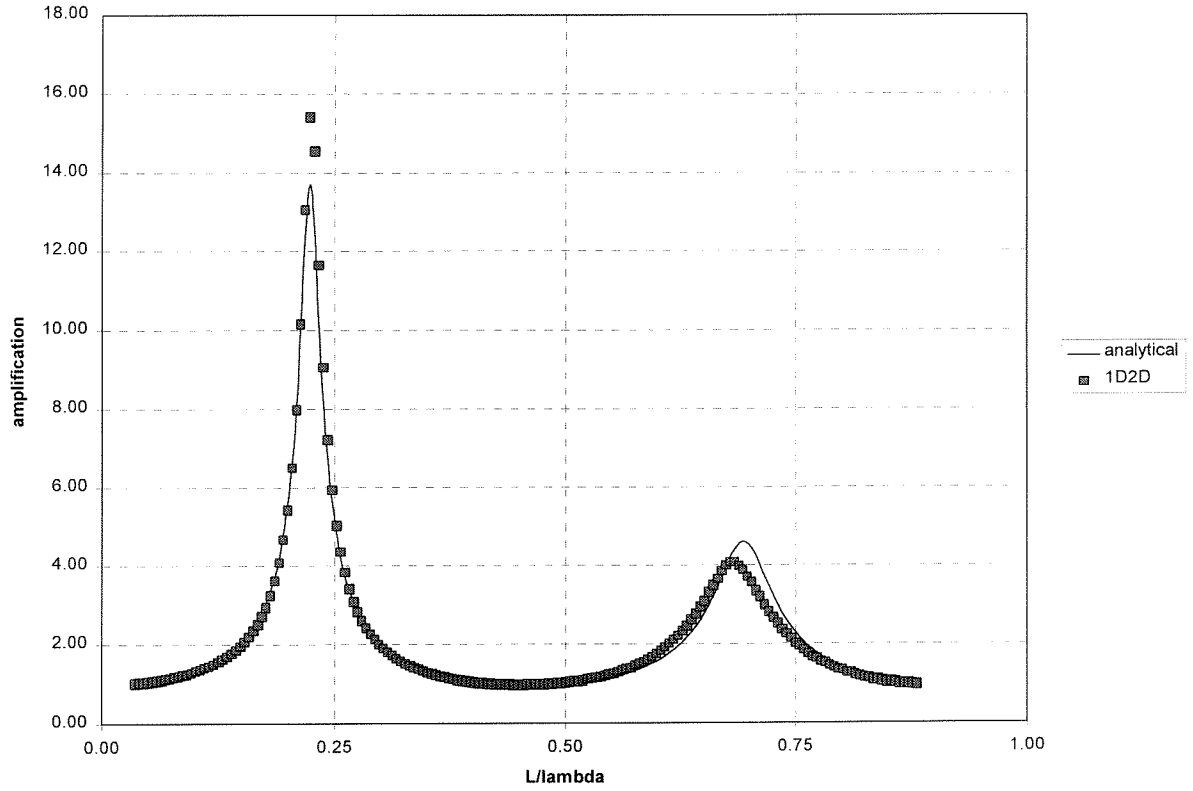

Graph 15 Amplification function for a channel with a length/width ratio of 10

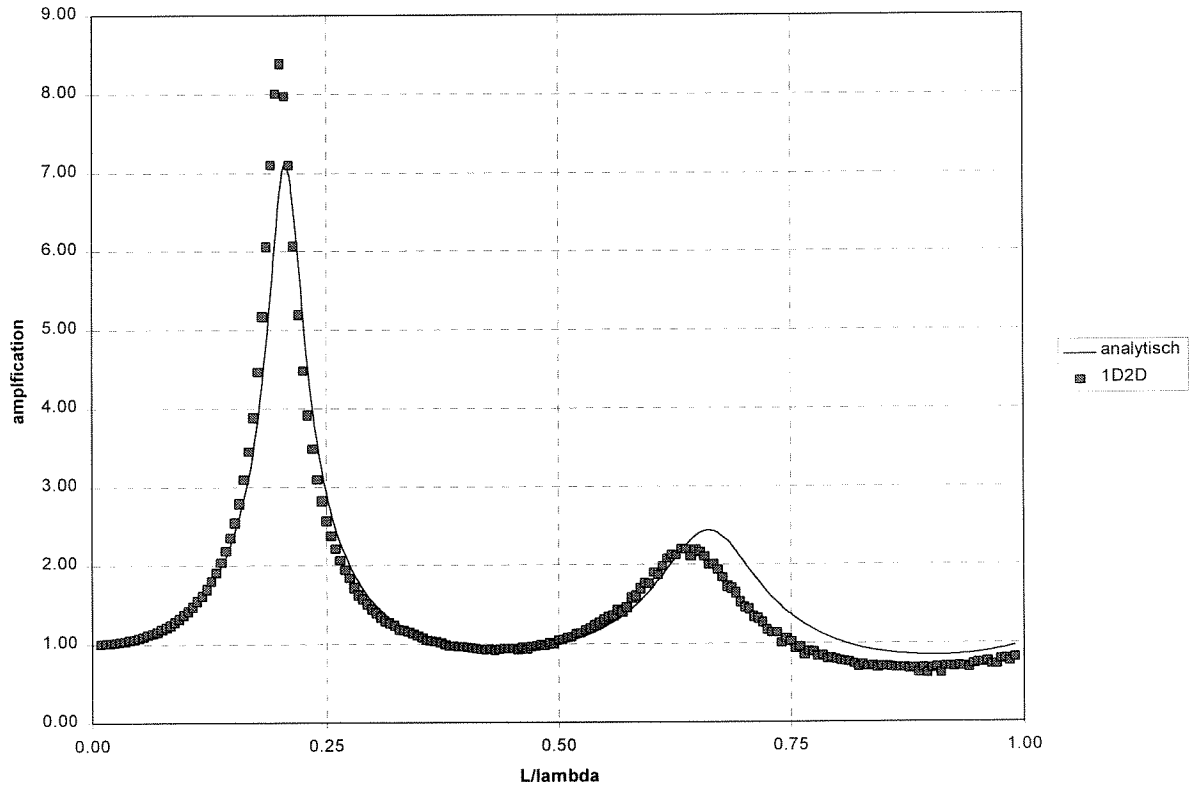

Graph 16 Amplification function for a channel with a lenght/width ratio equal to 5.

It is evident from the previous two graphs that for shorter channels the amplification factor for the first peak is overestimated. This might be attributed to the fact that a Riemann boundary is only reflectionless when a wave hits it perpendicularly. The radiating waves from the channel entrance will hit it at an angle resulting in small reflections. This bit of energy remains trapped inside the two-dimensional sea area. This means that the Sommerfeld radiation condition is not fully met. Verboom and Slob studied a modification to the Riemann boundary, which enables it to let outgoing waves at an angle pass through without reflections. The second peak appears to be shifted more to the lower frequencies. This might be caused by a decrease in spatial resolution for the higher frequencies (Stelling, 1984)

5.5 Conclusion on the 1D2D model

Due to the small size of the 2D-sea area, the calculation time is not much longer than that of a one-dimensional model. The addition of 121 grid points for the 2D-sea barely influences the calculation time. The results are quite satisfactory. In contrast to the one-dimensional approach with the epsilon boundary condition this boundary condition can be used with minimal tuning, which is a definite advantage.

6. Comparison with other models

6.1 Introduction

The linear aspects of the Seiches II program and the 1D2D model have already been verified against the test problem, but it is also good to see how well the developed models work compared to existing solutions. Furthermore, there is no analytical solution to verify the non-linear aspects. Therefore, the non-linear results have to be compared to those of another accepted computer package. This has led to a comparison with the packages Pharos and Trisula. Pharos is a two dimensional linear package with the possibility of using a Chézy type of bottom friction. Trisula is a full non-linear two-dimensional program.

6.2 Pharos

For seiche calculations, the computer package Pharos is being used. Pharos uses the Helmholtz equations (8) and solves these for the system. It does offer a possibility to include a friction like term. By enabling this term to simulate a Chézy type of bottom friction, it is possible to get an pseudo non-linear model. The model in Pharos consists of a long and narrow channel connected to a wide sea basin.
The sea boundary of the Pharos model deserves special attention. It is based on the principle that waves radiating out of the domain can be modeled as radiation sources along an open boundary, and that the energy emitted from these sources travels radially. In this manner the Sommerfeld radiation condition is modeled. Two different procedures are used to accomplish this, however only the one relevant to this thesis will be described here. For more information refer to page 3-26 *Seiches Europoort* (Kernkamp, 1994).
The procedure uses an evenly spaced number of sources at the sea boundary $\partial\Omega$ that emit waves radially. The emitted potential ϕ is described by:

$$\tilde{\phi}(\underline{p}) = \int_{\partial\Omega} \mu(\underline{s}) G(\underline{p},\underline{s}) d\underline{s} \qquad (52)$$

μ being the strength of the source, which will be calculated as part of the solution, and G(p,s) is the factor of influence in a point p resultant of a source with end strength $\underline{s}$ given by:

$$G(\underline{p},\underline{s}) = \frac{i}{2} H_0^1(kr) \qquad (53)$$

in which $r=|\underline{p}-\underline{s}|$ s.
The unknown $\mu(\underline{s})$ is found by the Fredholm integral after imposing the incoming wave on equation 54.
With this configuration, the energy loss due to radiation of wave energy can be correctly modeled.
In the linear case the results from the Pharos calculations only differ a few percent with the analytical test problem.

For the non-linear case a Chézy type of bottom friction was used, to get an indication of how well the Seiches II program compares to Pharos. For this purpose the results from an existing Pharos model were taken and compared to the results obtained from an identical model made with Seiches II
The amplification factor calculated with Pharos is 8.4 whereas with Seiches II the amplification factor is 12.6. However, this is not the only difference between both programs:

1. The peak of is shifted to a higher frequency for Pharos.
2. The amplification function in Pharos is constructed by a series of single waves. This is not a correct approach because individual waves influence each other in a non-linear case. Energy is transferred from the base frequency to the higher harmonics, hereby lowering the amplitude of the first peak and raising the amplitudes at higher peak frequencies. This can be clearly seen in paragraph 5.3.4 and in appendix III graph 4.

6.3 Trisula (Delft3D)

Trisula is a fully non-linear two-dimensional package. With Trisula a similar model was made as in figure 2, except that the channel is two-dimensional as well. The concept of handling the boundary condition as described in paragraph 7.4 with the additional channel was taken from this model. At the channel entrance a fine grid was used to be able to provide sufficient resolution to model the inflow and outflow energy losses.

To verify the non-linear results obtained with the one-dimensional approach as implemented with Seiches II a comparison should be made with Trisula. Unfortunately, no full amplification function is available for a calculation made with Trisula for the non-linear case. Only the linear results are available. Trisulas results can be compared to the results from Seiches II because the model used in Trisula is non-linear, and it is possible to send in a complete signal of multiple waves into the channel. Its only drawback for a comparison with the approaches used in this thesis is that it also models the energy loss due to advection at the entrance of the channel. Taking relatively large grid spaces in this region can compensate this (Kernkamp, 1994).
The non-linear results that are available from calculations with Trisula, are obtained from a model with similar geometry to the one used in Pharos, with a single wave sent into the channel. The resultant amplification factor is 5.5

For the linear case there is a full amplification function available as shown in the following two graphs. The results resemble those obtained with the 1D2D program (compare this to graph 15). For a long and narrow channel the amplification for the first peak is also too low compared to the analytical case:

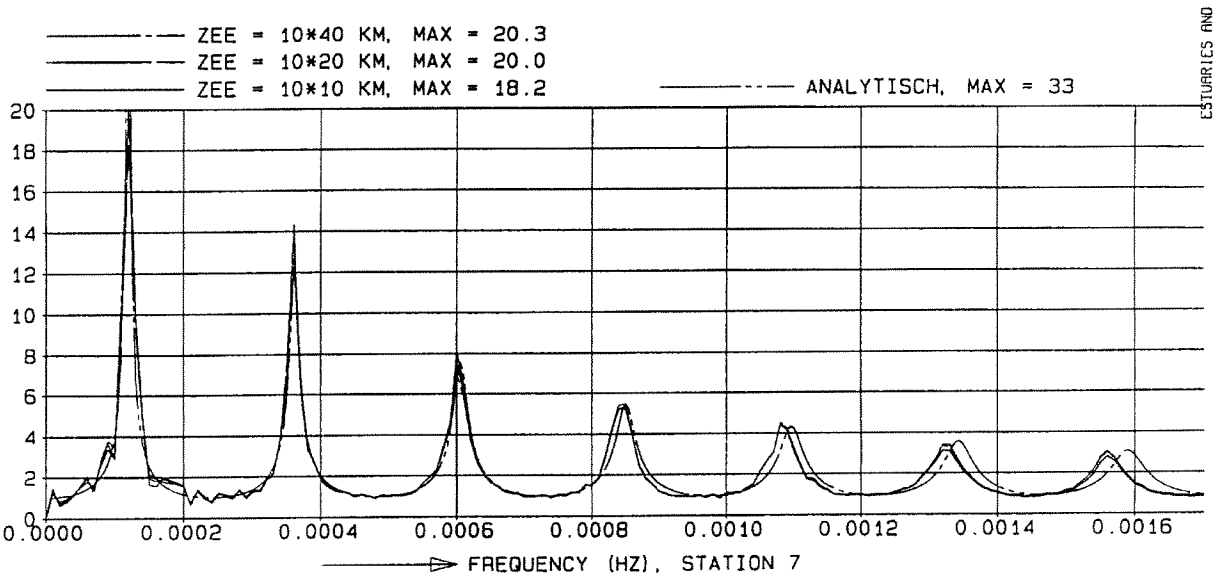

Graph 17 Results from Trisula for a channel length to width ratio 28[1]

Apparently, the solutions from the analytical model and the Trisula model match exactly. Unfortunately the graph is a bit deceptive, not the full analytical function is plotted in the WL report. The first peak is 33 but this is omitted from the graph, but it is mentioned in the legend. This shows how the results from Trisula are 33% off whereas the results from the 1D2D model are only 25% off. This can be attributed to a lack of frequency components used (Kernkamp, 1994). Due to the narrowness of the peak only a small deviation from it results in a significantly smaller amplification.

For a shorter channel the results form Trisula also resemble those obtained with the 1D2D model (graph 16).

[1] Figure 8.2.1.i, from *Seiches Europoort*, Kernkamp, 1994. Printed with permission from WL|Delft.

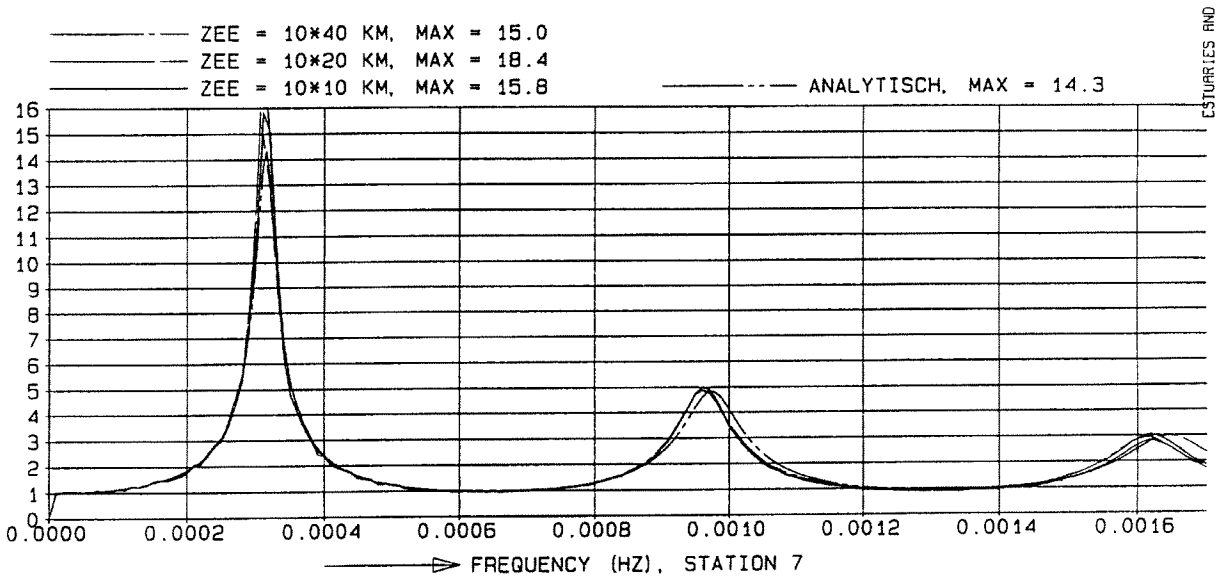

Graph 18 Results from Trisula for a channel length to width ratio 10[2]

Graph 18 shows how for a shorter channel the amplitude for the first peak is too high compared to the analytical solution. The same is the case for the 1D2D model, both models are quite similar in their results. This is surprising because the Trisula model uses a fine mesh at the channel entrance to model the flow. In the 1D2D model only a single grid point is used, proving that this is sufficient resolution to model the radiation condition at the entrance.

[2] Figure 8.2.1.g, from *Seiches Europoort*, Kernkamp, 1994. Printed with permission from WL|Delft.

7. Conclusion and recommendations

7.1 Conclusion

The aim of this thesis has been to find a practical solution for the seaward boundary condition for a numerical model that correctly describes the amplification effect of seiches in a channel. For the channel a one-dimensional network is assumed to be sufficient. To find this solution two different approaches have been studied.

For the one-dimensional approach studied there is a perfect boundary condition: the combination of a water level and Riemann invariant multiplied by a certain factor epsilon. However, at this stage, this epsilon boundary condition cannot correctly model the seiches phenomenon over the entire wave spectrum This is caused by the (numerical) approximation for epsilon, which makes it wave length dependent. This results in only one of the peaks being modeled correctly. A different approximation for epsilon (Majda & Enquist, 1977) could remove this dependency of the amplification function, which would probably lead to better results.

The solution of attaching a two-dimensional sea area to a one-dimensional channel is a much better alternative as is demonstrated in this study. The boundary is moved from the entrance of the channel to an area at sea. This simplifies the required boundary condition, because the radiation of energy is automatically modeled by the two-dimensional component. It is therefore not necessary anymore to concentrate this effect into a boundary condition at a single point. The boundary condition at the sea boundaries are relatively simple. Due to the small area needed to model the sea the calculation time is of the same order of magnitude as that for the one-dimensional channel itself. What is more important is that no special tuning is required to obtain correct results. This in contrast to the one-dimensional approach with the epsilon boundary condition, where actually part of the answer is needed to find the correct results.

The results from both the one-dimensional and the 1D2D approach do not match the analytical test problem exactly but they are quite satisfactory. The difference at the peaks is minimal, especially if compared to the large degree of uncertainty about the rest of the seiche phenomenon. No one knows what the incoming amplitudes are and very few actual measurements are available. The uncertainty of approximately 20% in the peak of the amplification function is probably negligible compared to the uncertainty of the rest of the factors that play a role in the generation of seiches.

7.2 Recommendations

For the modeling of seiches a 1D2D model is recommended. It has proven to be flexible and accurate and the calculation time is not affected significantly compared to a full one-dimensional model. What remains to be investigated are the non-linear effects on the 1D2D model. Special care should be taken at the boundaries of the two-dimensional sea area. The Riemann boundary used currently is not particularly suited for handling waves at an angle. These waves reflect a bit of their energy back into the system. A solution to this problem has been found by G.K. Verboom and A. Slob (1982). Alternatively, a radiation boundary condition could be used at the open boundaries.

What should be incorporated into the model is a method to model the energy loss due to entrance and outflow at the entrance of the channel because for larger amplitudes this is a major damping mechanism. This could be done by moving part of the 2D area into the channel and increasing the spatial resolution. The effect of the resolution in the entrance of the channel should also be evaluated to find the optimal resolution. If a higher resolution is required, this can be achieved by introducing a finer mesh at the entrance only.

There is still one other feasible alternative for the boundary that could be investigated. This is a boundary composed of a two-dimensional area but then written in polar coordinates, which reduces it back to a one-dimensional system. The one-dimensional channel in Cartesian coordinates will then have to be connected to a sea area in polar coordinates. Part of the difficulties in this project would be how to send in a straight wave front

into the system from the sea. Modeling a complex sea area might also be more difficult to do in polar coordinates than in a Cartesian grid.

Appendix

Appendix

I Derivation of the Analytical Solution according to CC Mei

I.I Introduction

The general solution can be found by a method of matched asymptotic expansions, which is very convenient for a problem with is governed by different scales. The equations and boundary conditions are approximated according to local scales with solutions valid for these regions. Then the solutions are required to smoothly match in the intermediate region. In the following figure the different regions are depicted:

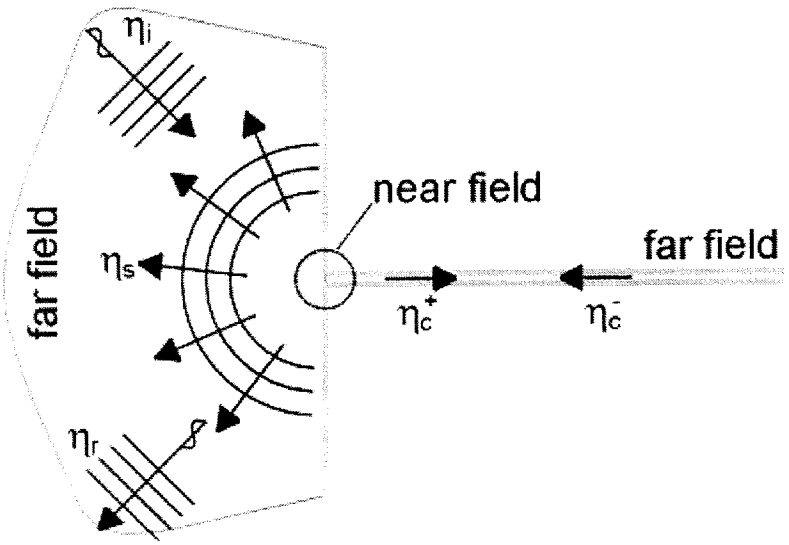

Figure 1 Definition of the far and near fields for the problem

For this problem the situation can be divided in four different regions:
1. Far field for the channel
2. Near field for the channel
3. Near field in the ocean
4. Far field in the ocean

Far field channel

In the far field section of the channel, there are only waves travelling in the +x and –x direction. These can be described by the following solution:

$$\eta_c = Be^{-ikx} + De^{ikx}$$

With the inner expansion for |kx|<<1:

$$\eta_c = (B+D) + ik(-B+D)x + \ldots O(kx)^2$$

Far field Ocean

In the ocean far away from the channel, there are two types of waves present. One is the incoming wave, which moves perpendicular to the coast. This wave is reflected on the shore, which results in a doubling of amplitude if the coast is vertical. Second is the outgoing wave, which move in a radially expanding fashion away from the origin. These waves correspond to the Sommerfeld radiation condition.

The Sommerfeld condition states that a wave emitted from a channel or narrow gap into the sea will expand radially with a decreasing wave height. Far away from the gap, the wave height will approach zero. At r = ∞ only outgoing waves will be present.

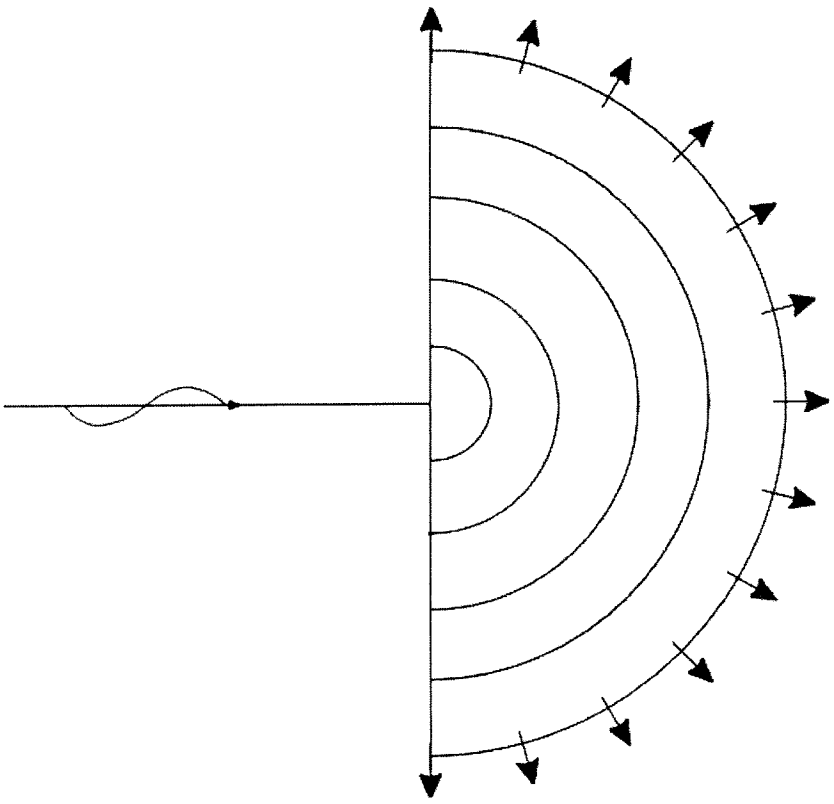

Figure 2 Sommerfeld Radiation Condition

Combining these two waves, the solution for the far field in the ocean becomes:

$$\eta_o = 2A\cos kx + \frac{\omega Q}{2g} H_o^1(kr)$$

The first term represents the incoming wave with twice the amplitude of the same wave far away on the ocean. The second term represents the radially expanding wave emitted from the channel entrance.
After the inner expansion of the Hankel function H for a kr<<1:

$$\eta_o = 2A + \frac{\omega Q}{2g}(1 + \frac{2i}{\pi}\ln\frac{\gamma kr}{2}) + O(kr)$$

Near field Ocean

The near field is a problem of potential flow past a right-angled estuary. For this purpose the near field must be divided in two sections one for the ocean side x>0 and one for the channel x<0. For the ocean side the solution is reduced to the following formula after several operations:

$$\eta \cong M \ln \frac{\pi r}{2a} + C$$

Near field Channel

For the near field in the channel the solution is reduced to:

$$\eta \cong M \frac{\pi x}{2a} - M \ln \frac{e}{2} + C$$

Now matching the solution from the channels near field and far field gives:

$$B + D = C - M \ln \frac{e}{2}$$

$$ik(-B + D) = \frac{\pi M}{2a}$$

Doing the same for the ocean:

$$2A + \frac{\omega}{2g} Q(1 + \frac{2i}{\pi} \ln \frac{\gamma k}{2}) = C + M \ln \frac{\pi}{2a}$$

$$\frac{iQ\omega}{\pi g} = M$$

Now only the boundary conditions are needed. For the end of the channel, this is a fixed highly reflective wall. Therefore at x=-L the flow is zero this results in this boundary condition:

$$\frac{\partial \eta_c}{\partial x} = 0 \qquad \text{(at x=-L)}$$

This leads to the outer solution:

$$\eta_c = E \cos k(x + L)$$

With the corresponding variables:

$$B = \frac{1}{2} E e^{-ikL}$$

$$D = \frac{1}{2} E e^{ikL}$$

Combining these with the previous formulae for matching the near and far field the response of the bay can be found:

$$\eta_c = \frac{2A\cos k(x+L)}{\cos(kL) + \frac{2ka}{\pi}\sin(kL)\ln\left(\frac{2\gamma ka}{\pi e}\right) - ika\sin(kL)}$$

The amplification factor is defined as being the response of the bay to the incoming wave. Recall that the incoming wave for the channel is:

$$\eta_c = 2A\cos k(x+L)$$

This results in the amplification factor, R is defined as:

$$\Re = \frac{1}{\cos(kL) + \frac{2ka}{\pi}\sin(kL)\ln\left(\frac{2\gamma ka}{\pi e}\right) - ika\sin(kL)}$$

With:
k: Wave number
L: length of the channel
a: Half the width of the channel
γ: Euler's constant 0.577215

II Program

II.I Introduction

In this chapter only a brief description of the basics of the program Seiches II will be given. The user manual can be found in the help function when running the program.

II.II Overview

The program follows this path during execution:

1. Collect input
The input variables can be collected from the screen or from a pre-formatted file. To simplify use there are already a set of default values inserted at start up. A hint box pops up to give additional help at the input stage. Specifications on how to change the default values and the pre-formatted file can be found in user guide.

2. Generate random phase
The random phase is generated by using the standard random generator with a pre determined random seed value. The seed value ensures that the data set will be the same every run.

3. Generate appropriate equations
Depending on the choice of boundary condition and wave type the equations are generated. For multiple waves the signal is composed of a orthogonal wave spectrum.

4. Solve equations
The equations solved by using a double sweep method.

5. Fourier analysis
The incoming and outgoing water levels are analyzed with a Fourier analysis. The Fourier analysis results can be imported into a spreadsheet program such as excel to plot the amplification function.

6. Output
The Fourier analysis, water level and velocity is saved to disk in two separate files. The water level can be animated on screen.

7. End

II.III Limitations

Although the program has been subjected to extensive tests, it cannot be a guarantee for a 100% bug-free program due to the intrinsic nature of software development. Several limitations of the program were discovered in the testing phase, for a detailed description of the tests please refer to appendix VI.

If one looks at the amplification function, the first peak stands out as being very sharp, in contrast to the second peak, which is much gentler. This sharpness of the first peak is what makes it so difficult to obtain the accurate results. A bit left or right of the peak the values are much lower than exactly on the peak. This means that to obtain the correct amplification function one has to 'hit' the peak exactly on its correct frequency. A small deviation results in a much lower peak. This is exactly where the limitations of this program can be found. There are four main factors that

contribute to this apparent erratic behavior, but actually it can all be reduced to one thing: the number of calculations is too short. After numerous test runs the following limitations of the program were discovered.

II.III.I Random generator.

The set of incoming waves must all have a different phase in order for the Fourier analysis to work correctly. If they are too much in phase, the resultant amplification function will be too high. The random generator is used to produce a set of numbers, which is used for the phase of the incoming waves. This data set will be different every time and consequently the resultant maximum peak of the amplification function can vary as well. Most likely because the amount of time steps calculated is not sufficient to reach an equilibrium state.
Several runs with exactly the same parameters have resulted in peaks varying between 18 and 26. Using a random seed variable the data set will be random, but the sequence of random numbers will be the same every time, thus creating a reproducible phase and a amplification function that is the same every time. This is important if one wants to evaluate the effects of the non-linear terms on the amplification function. If a greater number of time steps is used the effect of this random generator is smaller because the situation in the channel will have had enough time to come to a stable solution.

II.III.II Amplitude

In theory, the amplitude of the imposed wave does not have any effect on the amplification function. This is valid for our program as well as long as the amplitude is greater than 0.0001 meters. Working with lower values for the imposed amplitude will give less accurate results because the Fourier analysis cannot discern the signal correctly anymore.

II.III.III Depth

The depth of the channel is of no influence on the amplification function, that is in theory, in this program the depth can influence the amplification factor. At first sight it is not obvious how this can affect the outcome, if one takes a closer look at how the amplification function is constructed it becomes clearer. The graph shown is a function of L/λ on the x-axis and the amplification factor on the y-axis. The Fourier analysis is based on a orthogonal set of waves it starts with the lowest possible frequency (1/dt*maxtime), every next frequency is n times this base frequency up to the Nyquist frequency (maxtijd/2). From this it is clear that the Fourier analysis provides us with maxtijd/2 frequencies. This is a fixed number, however the frequency for the shortest wavelength one is interested in (λ=L) depends on the water depth:

$$\lambda = \frac{gH}{frequency} \text{ or } frequency = \frac{\sqrt{gH}}{\lambda}$$

This means that with a greater depth H the frequency at which L=λ is also higher. Therefore the number of frequencies below L=λ is higher. With more frequencies in the amplification the resolution for this graph increases, consequently the peak can be modeled with a higher accuracy resulting in a higher peak. A higher resolution can also be obtained by taking more time steps in our calculation.

Single Waves

Imposing a single wave on the boundary and then finding the amplification function without the Fourier analysis is not a solution either. In simple cases without second order effects the amplification factor of a single wave can be calculated by finding the amplitudes at the end of the canal. Graph A-1 shows the water level at the end of the channel. In this case no Fourier analysis is needed to determine the amplitude of the wave: 2.65 m, dividing this by the amplitude of the signal imposed on it 0.18 m an amplification factor of 14.7 is found which corresponds exactly to the amplification factor found by the Fourier analysis in.

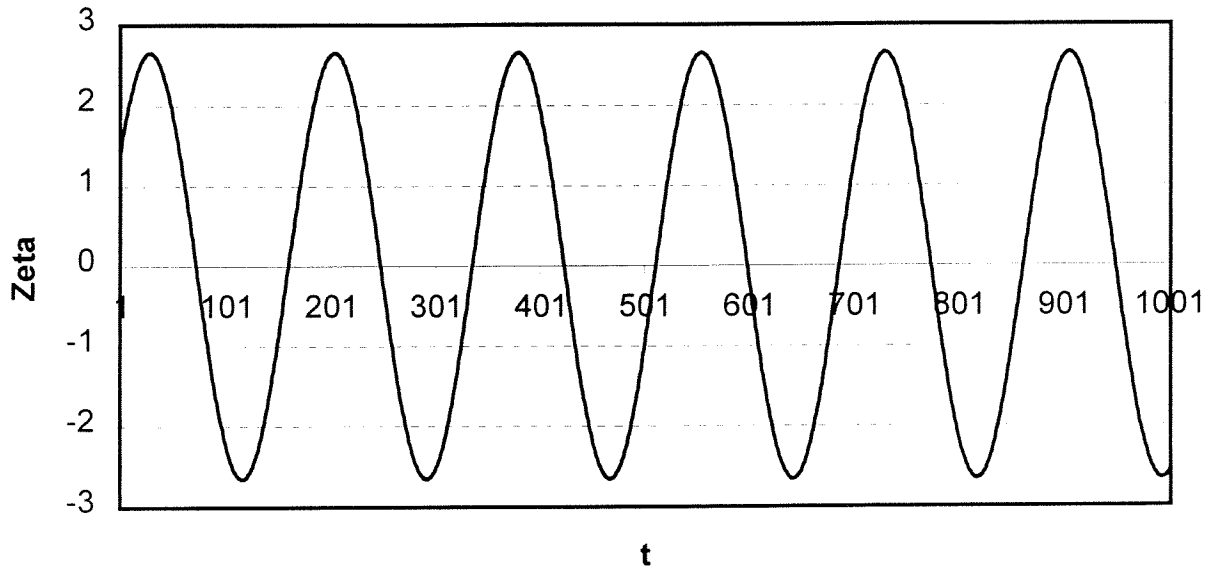

Graph 1 Water level at the end of the channel for a linear model. (Single wave)

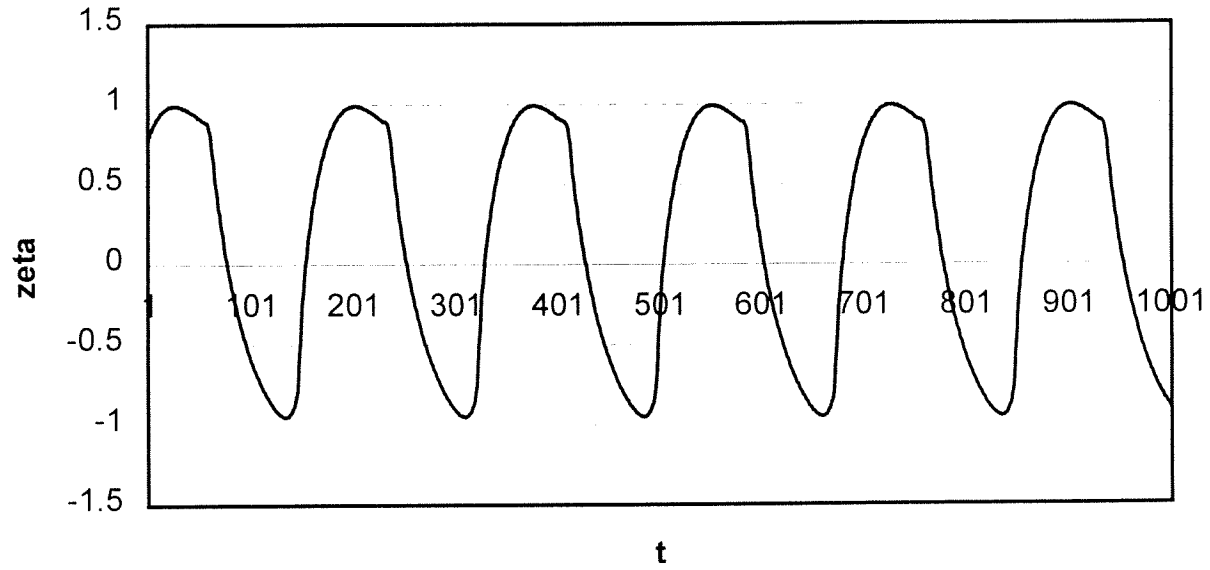

Graph 2 Water level at the end of the channel for a non-linear model. (Single wave, different scale)

However with second order effects the waves are distorted and it is impossible to visually determine the amplitude. Graph 2 shows such a distorted signal.

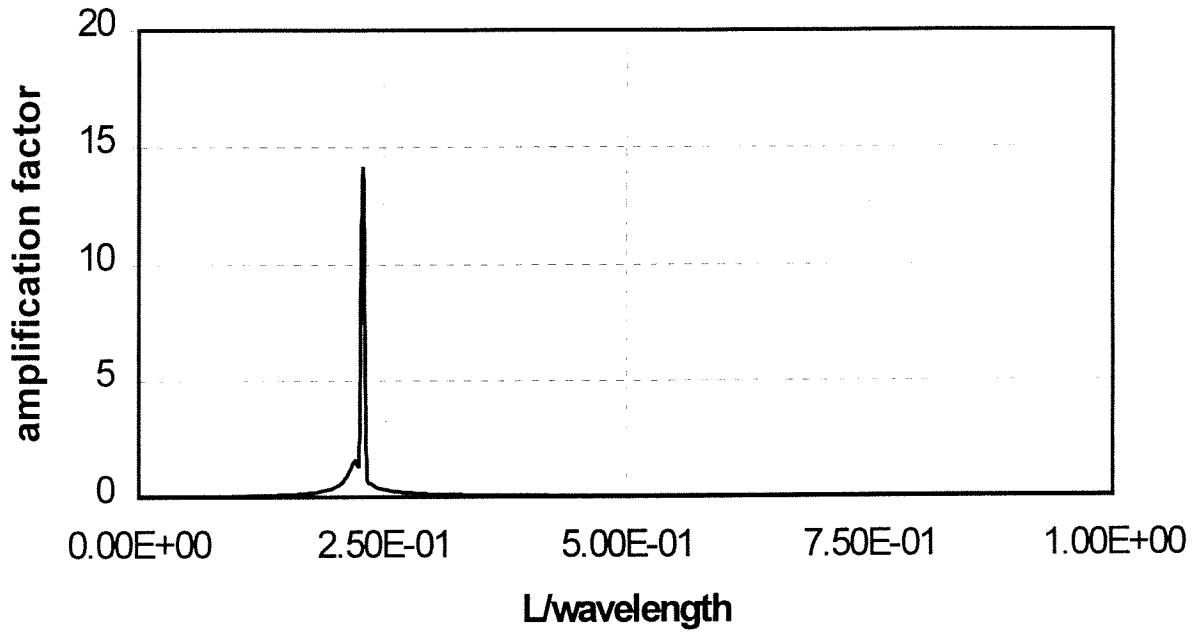

Graph 3 Amplification function for a single wave: 699m (L/wavelength=0.229) amplitude 0.18

Applying a Fourier analysis to this signal shows why: not only is there a peak at the imposed frequency but also at the second and higher harmonics! (Graph 4) This means that the model is also taking into account the effects of energy shifting to higher order harmonics.

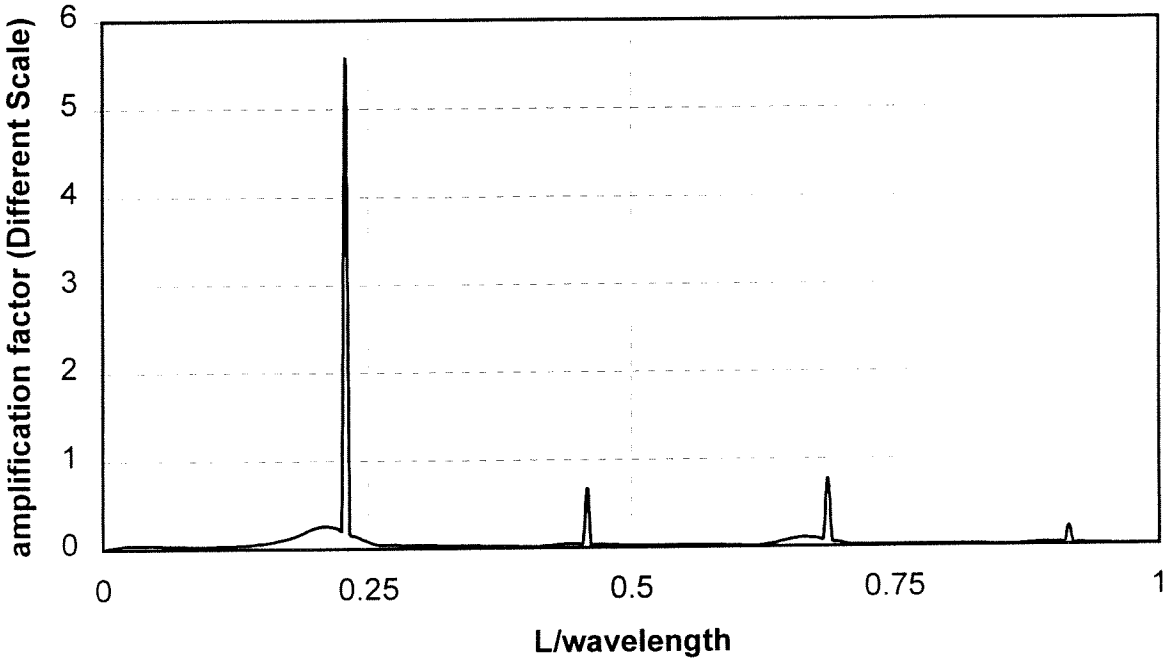

Graph 4 Amplification function for a single wave: 699m (L/wavelength=0.229) amplitude 0.18. Non-Linear mode: Advection and Friction activated. (Different Scale!)

The interaction between waves in a non-linear case is evident from this. Waves from lower frequencies contribute to the amplitude of their higher harmonics, running the model with single waves will therefore not give accurate results. The amplitude is also much lower than for the linear case, this is due to the energy loss from advective and friction terms in the calculation. To illustrate the effect 16 runs were made each with a single wave in the channel and these are compared to a run with multiple waves. The results can be seen in

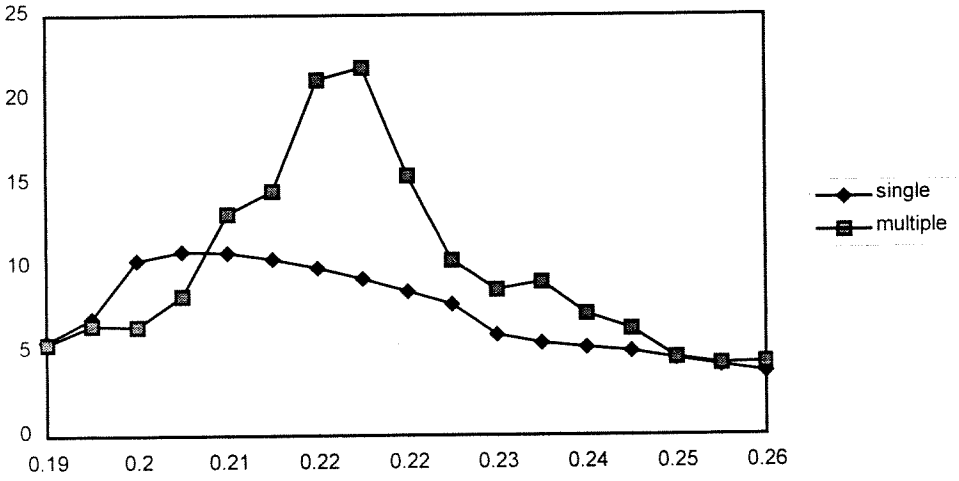

Graph 5. The peak of the single waves run is shifted to a lower frequency and much lower than the peak with obtained by using the full spectrum. The interaction between waves of different frequency is evident from this and cannot be neglected. Fortunately, it is also more efficient to run the program with multiple waves because it does not take more time to run the model with the full spectrum than to run it with a single wave.

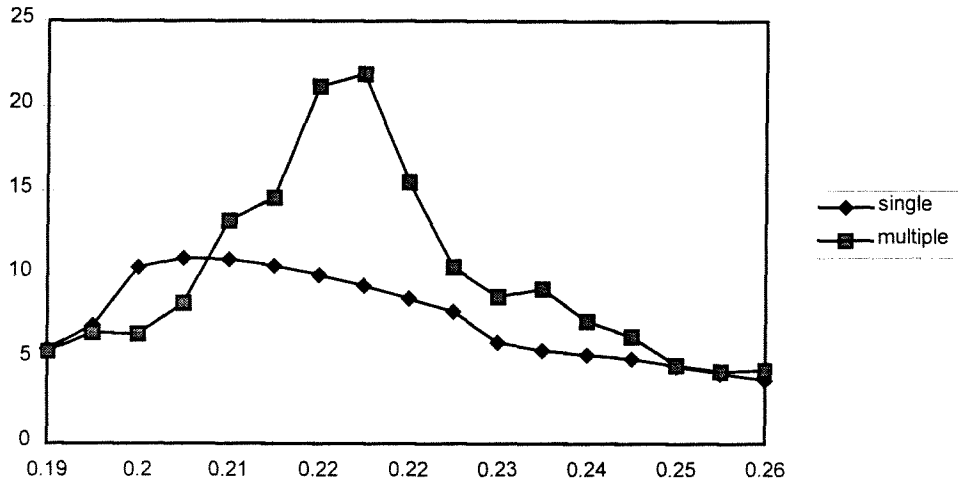

Graph 5 Amplification function of single vs. multiple wave approach.

II.III.IV Initialization

Every model needs to be initialized at the start. The simplest way of doing this is by setting all the levels at zero at the beginning of the calculation. When the program starts running it takes some time before the effect initial situation is not noticeable anymore. On graph 7 it can be seen that the effect from the initial disturbance of the model is still noticeable after 4000+ time steps. The exact time it takes before this effect is gone depends on the disturbance and the type of boundary condition.

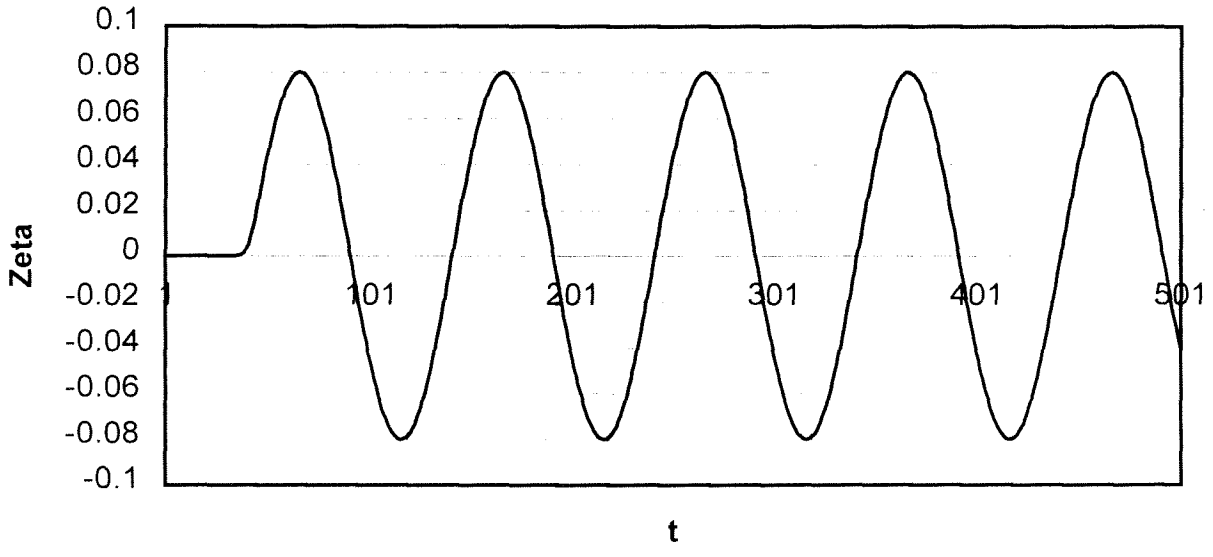

Graph 6 Water level at the end of the channel for a Riemann boundary

In the case of a Riemann boundary, all waves are transmitted and none reflected. This means that the initial effects are not noticeable anymore after the first wave has exited the channel.

With water level boundary the waves are all reflected back and forth in the channel so the disturbance is also contained in the channel this results in a very long time before this effect is damped out if it happens at all. Without any second order effect, there is no mechanism for the waves energy to dissipate, the initial wave will therefore stay in the channel forever, this results in an always present initial effect. This can be clearly seen in Graph 6. There is a beat in the wave. Increase the θ, a form of numerical dissipation is introduced. The beat effect is less but it does not disappear completely.

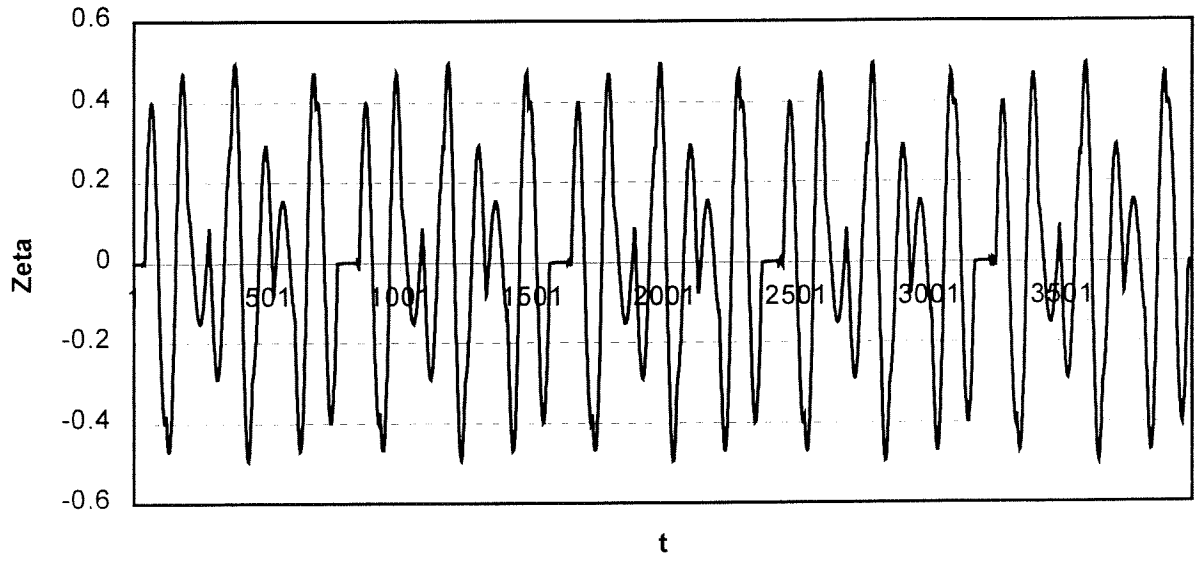

Graph 6 Water level at the end of the channel for a Water level boundary.

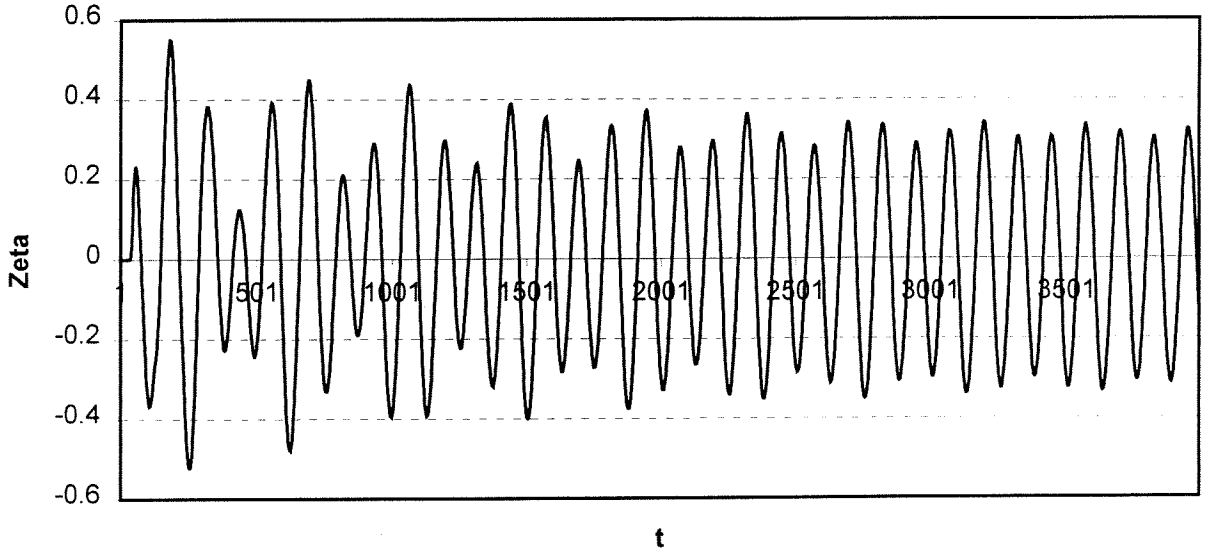

Graph 7 Water level at the end of the channel for an Epsilon boundary. (Theta=0.5)

The epsilon boundary, being a combination of the two takes quite some time to damp out the effects of an initial disturbance. In the linear case, this is achieved through radiation energy loss.

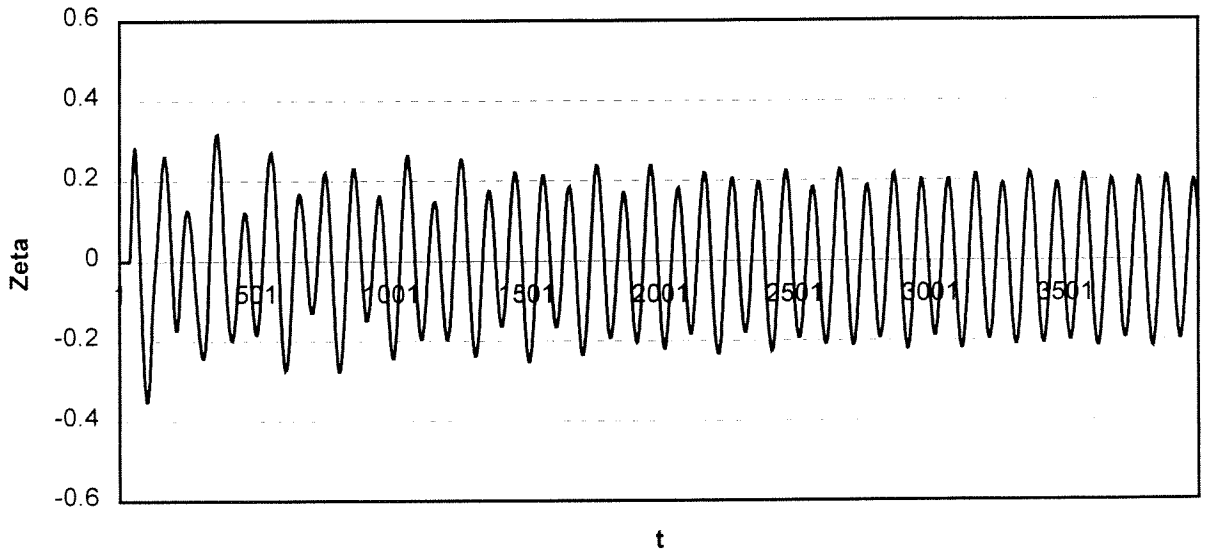

Graph 8 Water level at the end of the channel for an Epsilon boundary. (Theta=0.6)

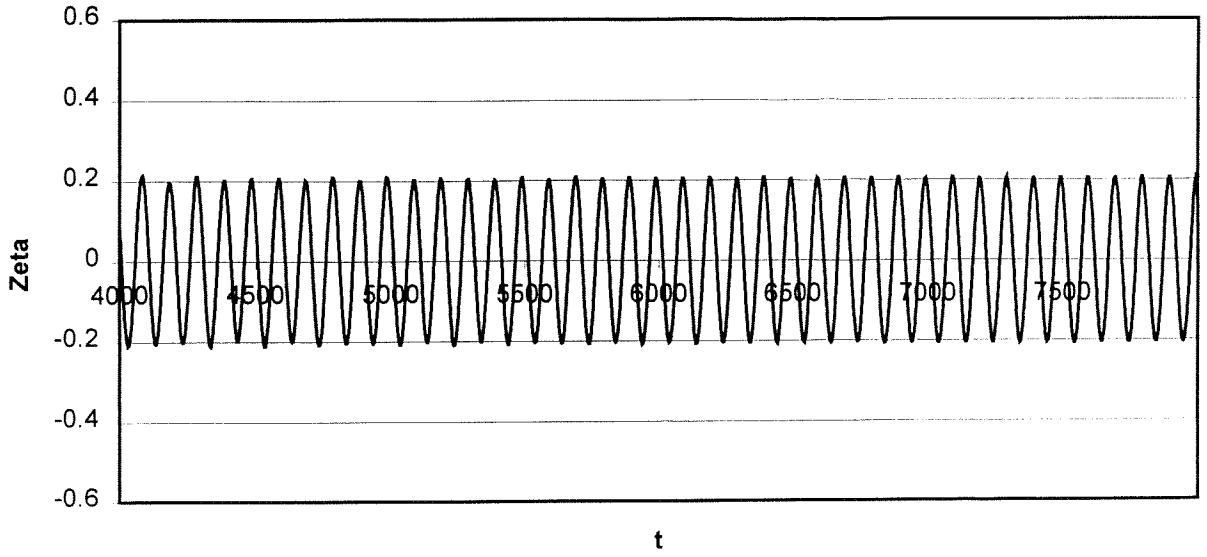

Graph 9 Water level at the end of the channel for an Epsilon boundary Continued from previous graph. (Theta=0.6)

III Equations and discretizations used in Seiches II

The non-linear equations and their discretization as used in Seiches II are stated in this appendix. In the model three versions of the Non-Linear equations are used:

1. Non-Linear Equations with Friction
2. Non-Linear Equations with Advection
3. Non-Linear Equations with Friction and Advection

III.I Non-Linear Equations with Friction:

III.I.I Motion:

$$\frac{\partial u}{\partial t} + g\frac{\partial \zeta}{\partial x} + u\frac{\partial u}{\partial x} + \frac{g \cdot u\,u}{C^2 H} = 0$$

Discretization

$$\frac{u_j^{n+1} - u_j^n}{2\Delta t} + \frac{u_{j+1}^{n+1} - u_{j+1}^n}{2\Delta t} + g\left\{(1-\theta)\frac{\zeta_{j+1}^n - \zeta_j^n}{\Delta x} + \theta\frac{\zeta_{j+1}^{n+1} - \zeta_j^{n+1}}{\Delta x}\right\} + \left\{\frac{\frac{1}{2}u_{j+1}^n \cdot u_{j+1}^{n+1} - \frac{1}{2}u_j^n \cdot u_j^{n+1}}{\Delta x}\right\} + \frac{u_{j+1}^{n+1} + u_j^{n+1}}{2} \cdot \frac{g\,u_{gem}}{C^2 \cdot H_{gem}} = 0$$

III.I.II Continuity:

$$\frac{\partial \zeta}{\partial t} + \frac{\partial uH}{\partial x} = 0$$

Discretization:

$$\frac{\zeta_j^{n+1} - \zeta_j^n}{2\Delta t} + \frac{\zeta_{j+1}^{n+1} - \zeta_{j+1}^n}{2\Delta t} + \left\{\frac{u_{j+1}^{n+1} \cdot H_{j+1}^n - u_j^{n+1} \cdot H_j^n}{2\Delta x} + \frac{u_{j+1}^n \cdot H_{j+1}^{n+1} - u_j^n \cdot H_j^{n+1}}{2\Delta x}\right\} = 0$$

With H = (depth + ξ):

$$\frac{\zeta_j^{n+1} - \zeta_j^n}{2\Delta t} + \frac{\zeta_{j+1}^{n+1} - \zeta_{j+1}^n}{2\Delta t} + \left\{\frac{u_{j+1}^{n+1} \cdot (diepte + \zeta_{j+1}^n) - u_j^{n+1} \cdot (diepte + \zeta_j^n)}{2\Delta x} + \frac{u_{j+1}^n \cdot (diepte + \zeta_{j+1}^{n+1}) - u_j^n \cdot (diepte + \zeta_j^{n+1})}{2\Delta x}\right\} = 0$$

Expand:

$$\frac{\zeta_j^{n+1}-\zeta_j^n}{2\Delta t}+\frac{\zeta_{j+1}^{n+1}-\zeta_{j+1}^n}{2\Delta t}+\left\{\frac{u_{j+1}^{n+1}\cdot(diepte+\zeta_{j+1}^n)-u_j^{n+1}\cdot(diepte+\zeta_j^n)}{2\Delta x}+\frac{u_{j+1}^n\cdot diepte+u_{j+1}^n\cdot\zeta_{j+1}^{n+1}-u_j^n\cdot diepte-u_j^n\cdot\zeta_j^{n+1}}{2\Delta x}\right\}=0$$

III.II Non-Linear Equations with advection

III.II.I Motion:

$$\frac{\partial u}{\partial t}+g\frac{\partial \zeta}{\partial x}+u\frac{\partial u}{\partial x}+\frac{g\cdot u\,u}{C^2H}=0$$

Discretization

$$\frac{u_j^{n+1}-u_j^n}{2\Delta t}+\frac{u_{j+1}^{n+1}-u_{j+1}^n}{2\Delta t}+g\left\{(1-\theta)\frac{\zeta_{j+1}^n-\zeta_j^n}{\Delta x}+\theta\frac{\zeta_{j+1}^{n+1}-\zeta_j^{n+1}}{\Delta x}\right\}+\left\{\frac{\frac{1}{2}u_{j+1}^n\cdot u_{j+1}^{n+1}-\frac{1}{2}u_j^n\cdot u_j^{n+1}}{\Delta x}\right\}+\frac{u_{j+1}^{n+1}+u_j^{n+1}}{2}\cdot\frac{g u_{gem}}{C^2\cdot H_{gem}}=$$

III.II.II Continuity:

$$\frac{\partial \zeta}{\partial t}+\frac{\partial uH}{\partial x}=0$$

Discretization:

$$\frac{\zeta_j^{n+1}-\zeta_j^n}{2\Delta t}+\frac{\zeta_{j+1}^{n+1}-\zeta_{j+1}^n}{2\Delta t}+\left\{\frac{u_{j+1}^{n+1}\cdot H_{j+1}^n-u_j^{n+1}\cdot H_j^n}{2\Delta x}+\frac{u_{j+1}^n\cdot H_{j+1}^{n+1}-u_j^n\cdot H_j^{n+1}}{2\Delta x}\right\}=0$$

With H = (depth + ξ);

$$\frac{\zeta_j^{n+1}-\zeta_j^n}{2\Delta t}+\frac{\zeta_{j+1}^{n+1}-\zeta_{j+1}^n}{2\Delta t}+\left\{\frac{u_{j+1}^{n+1}\cdot(diepte+\zeta_{j+1}^n)-u_j^{n+1}\cdot(diepte+\zeta_j^n)}{2\Delta x}+\frac{u_{j+1}^n\cdot(diepte+\zeta_{j+1}^{n+1})-u_j^n\cdot(diepte+\zeta_j^{n+1})}{2\Delta x}\right\}=0$$

Expand:

$$\frac{\zeta_j^{n+1}-\zeta_j^n}{2\Delta t}+\frac{\zeta_{j+1}^{n+1}-\zeta_{j+1}^n}{2\Delta t}+\left\{\frac{u_{j+1}^{n+1}\cdot(diepte+\zeta_{j+1}^n)-u_j^{n+1}\cdot(diepte+\zeta_j^n)}{2\Delta x}+\frac{u_{j+1}^n\cdot diepte+u_{j+1}^n\cdot\zeta_{j+1}^{n+1}-u_j^n\cdot diepte-u_j^n\cdot\zeta_j^{n+1}}{2\Delta x}\right\}=0$$

III.III Non-Linear Equations with advection and friction

III.III.I motion:

$$\frac{\partial u}{\partial t} + g\frac{\partial \zeta}{\partial x} + u\frac{\partial u}{\partial x} + \frac{g \cdot u\,u}{C^2 H} = 0$$

Discretization

$$\frac{u_j^{n+1} - u_j^n}{2\Delta t} + \frac{u_{j+1}^{n+1} - u_{j+1}^n}{2\Delta t} + g\left\{(1-\theta)\frac{\zeta_{j+1}^n - \zeta_j^n}{\Delta x} + \theta\frac{\zeta_{j+1}^{n+1} - \zeta_j^{n+1}}{\Delta x}\right\} + \left\{\frac{\frac{1}{2}u_{j+1}^n \cdot u_{j+1}^{n+1} - \frac{1}{2}u_j^n \cdot u_j^{n+1}}{\Delta x}\right\} + \frac{u_{j+1}^{n+1} + u_j^{n+1}}{2} \cdot \frac{g\,u_{gem}}{C^2 \cdot H_{gem}} = 0$$

III.III.II Continuity:

$$\frac{\partial \zeta}{\partial t} + \frac{\partial uH}{\partial x} = 0$$

Discretization:

$$\frac{\zeta_j^{n+1} - \zeta_j^n}{2\Delta t} + \frac{\zeta_{j+1}^{n+1} - \zeta_{j+1}^n}{2\Delta t} + \left\{\frac{u_{j+1}^{n+1} \cdot H_{j+1}^n - u_j^{n+1} \cdot H_j^n}{2\Delta x} + \frac{u_{j+1}^n \cdot H_{j+1}^{n+1} - u_j^n \cdot H_j^{n+1}}{2\Delta x}\right\} = 0$$

With H = (depth + ξ);

$$\frac{\zeta_j^{n+1} - \zeta_j^n}{2\Delta t} + \frac{\zeta_{j+1}^{n+1} - \zeta_{j+1}^n}{2\Delta t} + \left\{\frac{u_{j+1}^{n+1} \cdot (diepte + \zeta_{j+1}^n) - u_j^{n+1} \cdot (diepte + \zeta_j^n)}{2\Delta x} + \frac{u_{j+1}^n \cdot (diepte + \zeta_{j+1}^{n+1}) - u_j^n \cdot (diepte + \zeta_j^{n+1})}{2\Delta x}\right\} = 0$$

Expand:

$$\frac{\zeta_j^{n+1} - \zeta_j^n}{2\Delta t} + \frac{\zeta_{j+1}^{n+1} - \zeta_{j+1}^n}{2\Delta t} + \left\{\frac{u_{j+1}^{n+1} \cdot (diepte + \cdot\zeta_{j+1}^n) - u_j^{n+1} \cdot (diepte + \cdot\zeta_j^n)}{2\Delta x} + \frac{u_{j+1}^n \cdot diepte + u_{j+1}^n \cdot \zeta_{j+1}^{n+1} - u_j^n \cdot diepte - u_j^n \cdot \zeta_j^{n+1}}{2\Delta x}\right\} = 0$$

IV Testing

IV.I Introduction

Several tests were run to verify the results of the program. Due to the complexity of the program, the program cannot be guaranteed to be 100% error free regardless of how many tests are done.

IV.II Test 1. 0=0 Test

The program was initiated without any disturbances. All water levels must remain the same in this condition. Instead of using 0 the program was initialized with 1, because 0 is often not a good number to test with. This test was passed successfully with all three boundary conditions and in the linear and non-linear modes.

IV.III Test 2. Verification with previous program

The results of the program were compared to the results obtained by previous Fortran versions of Seiches I program. These obviously matched exactly, as can be seen from the following graphs:

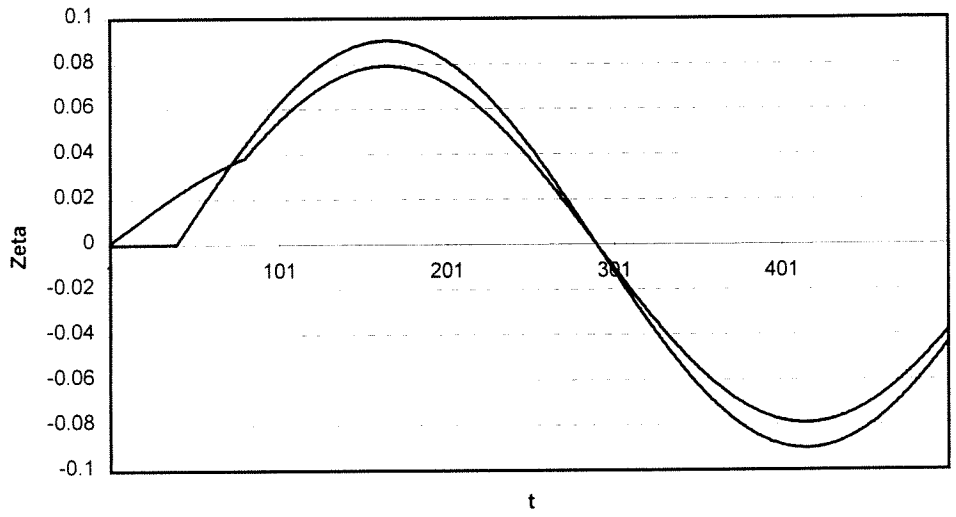

Graph 10 Original Seiches I program.

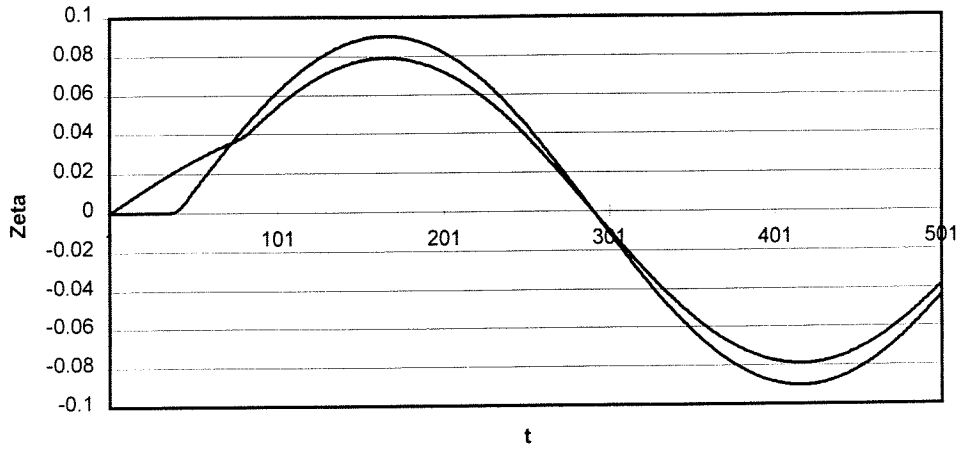

Graph 11 Seiches II program.

IV.IV Test 3. Fourier Analysis

The Fourier analysis was tested thoroughly by letting it analyze a set of known waves and comparing the results with the expected output. The Fourier analysis passed the test successfully. As mentioned before in the limitations section, the random phase of the incoming signal is extremely important to obtain accurate results. Waves that coincide in phase produce unpredictable results.

This graph shows the results of one of the runs. The signal consists of an orthogonal set of 25 superimposed waves each with amplitude of 0.2 meters. The set starts with a base frequency. From the Graph IV-13 it can be seen that the Fourier analysis is correctly identifying the amplitude and frequency of each wavelength.

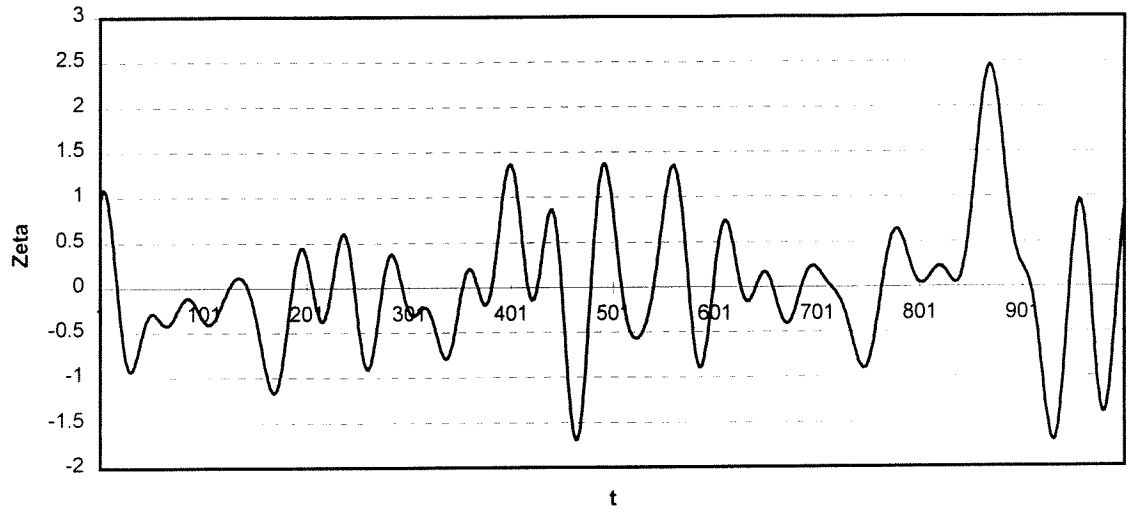

Graph IV-3Signal composed of 25 waves each with amplitude of 0.2, out of phase. Every wave is n times the base tone.

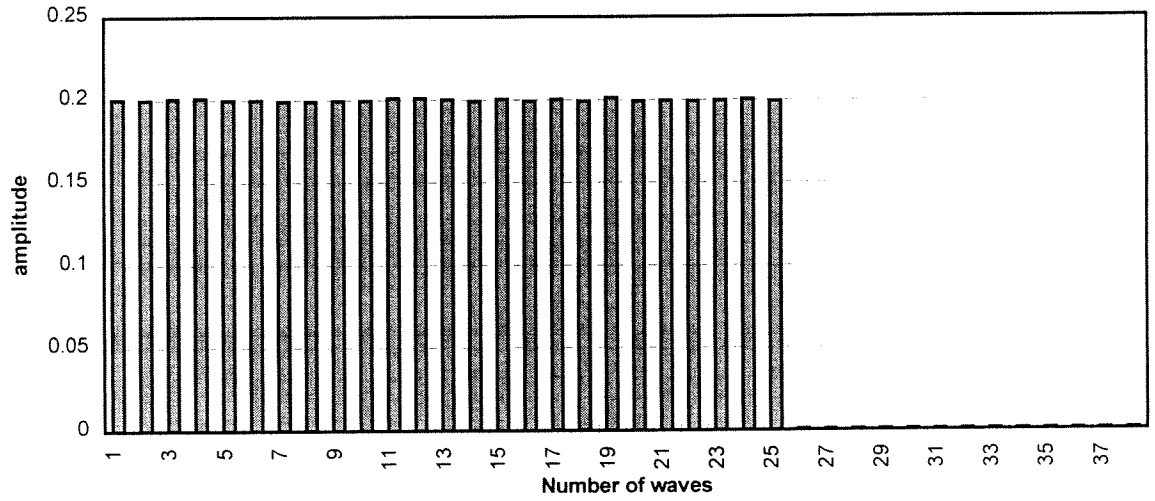

Graph IV-13 Results of the Fourier analysis.

IV.V Test 4. Small amplitudes test

With small amplitudes the effect of the non-linear terms is negligible the results therefore should be exactly the same in the linear case. The following graph shows that this is the case for the program:

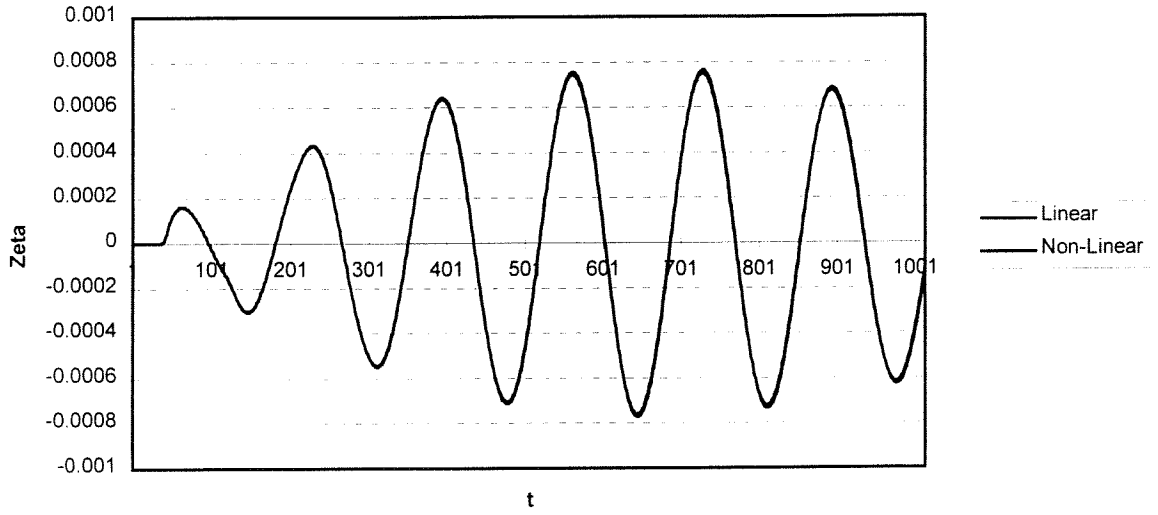

Graph IV-5 Comparison linear to non-linear mode with very small amplitudes.

V Amplitudes for stable calculations

V.I Introduction

Due to their long period and small amplitudes, seiches are not easy to measure. Mainly due to the lack of interest in this region of the wave spectrum very few measurements are available and not much is know about the origin and behavior of seiches at sea. Recently the seiche phenomenon has been getting more and more attention. especially because of the problems caused by seiches in the Storm Surge Barrier New Waterway. New measurement projects are being set up to finally obtain accurate data.

V.II Assumptions

This lack of data forces this project to make an assumption on the incoming amplitude of seiches at sea. Most estimates of this amplitude state that it should be around a few decimeters amplitude. Other model studies on seiches such as the ones done by Delft Hydraulics. Work with a H_i of 0.3 meters. This is the incoming wave height at sea. The amplitude is one half of the wave height. Therefore, the amplitude at sea is 0.15 meters. When the wave reflects at the shore boundary the amplitude is doubled. Therefore, the amplitude at the open boundary of the model is twice the amplitude at sea: 0.3 meters.
To obtain reasonable results one should use the incoming amplitude at the sea boundary of the same order of magnitude as 0.3 meters. The following index is used:

$$\frac{depth}{amplitude} \geq\approx 50$$ ***Equation V-1***

V.III Multiple waves

With a single frequency, the imposed amplitude is straightforward. If a combination of frequencies is used the amplitude is not so easy to determine, especially if they are all out of phase as in this case. The root mean square method can be used in this case to determine the overall amplitude.
Example:

- 245 different frequencies (As used with 10,000 time steps)
- 20 meters depth. (width=1km length=28km)
- amp (of a single frequency) = 0.02

$$\sum_{1}^{245}(0.02^2) = 0.313m$$

$$\frac{20m}{0.313m} = 63.9$$

Amplitude of 0.02 m per frequency is therefore a valid entry for multiple waves.

V.IV Stability

Instability of the program occurs when the slope of the wave front becomes infinite. This occurs only in the non-linear case due to the celerity difference between the trough and the crest. The celerity is a function of the depth (c=sqrt(gh)) and is higher for the crest than for the trough.

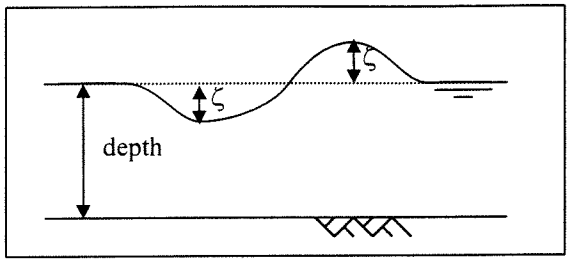

Test with the program have shown that it remains stable with multiple frequencies with an amplitude of 0.16m and a depth of 20 m this gives a index of 8, with a smaller model, depth is 2m, the lowest index that still is stable is 14. With a single frequency, the max amplitude for a depth of 20 meters is 6 meters. This gives an index of 3.33. This shows that the stability of the program is sufficient for the region of interest.

VI Restrictions for using the 1D2D model

VI.I Introduction

To obtain accurate and stable results the following suggestions and restrictions should be followed. They are however no guarantee for correct results, they only serve as guidelines for a stable model.

VI.I.I Grid size

Frequency spectrum

The input signal is composed of an orthogonal series of waves all added. It is formed by taking a wave with a base frequency and adding n times to this a wave with a frequency on step shorter. All waves have the same amplitude just their frequency is different. This signal is composed as follows:

$$Signal = \sum_{n=1}^{n=\#freq} amp \cdot n \cdot f_{base}$$

With:

$$f_{base} = \frac{1}{\Delta t \cdot T_{\max}}$$

The base frequency is the longest wave this Fourier analysis will distinguish:

$$\#freq = \max freq$$

This is the maximum number of frequencies. The shortest wavelength in the signal is then restricted to the wavelength of the channel.

The shortest wavelength used equals the length of the channel. If the grid size of the 2d sea is bigger than that of the 1d channel anti-aliasing occurs in the 2d sea and the high frequency part of the spectrum is erroneously mapped onto

the low frequency part resulting in a very strange signal for the 1d channel.

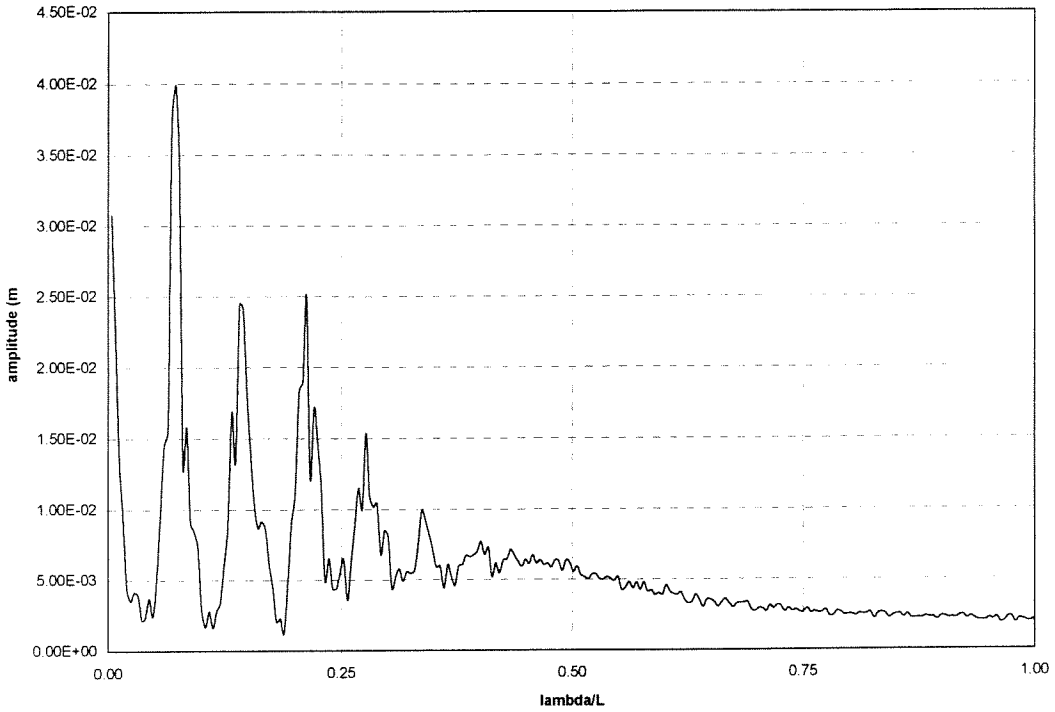

Graph 6 Fourier analysis of the signal at N116.

Graph 6 Fourier analysis of the signal at N116. depicts the results from a Fourier analysis of the signal at node 116, which is on the sea boundary of the 2d model. Although a clean signal was imposed on this boundary, which should have resulted in a straight line for all the frequencies. The lower frequencies show spikes in the signal. This effect can be attributed to the anti-aliasing of the signal. By reducing the grid size and the time step to the same value as used in the 1d component this effect can be reduced until a clean signal is obtained at the sea boundary.

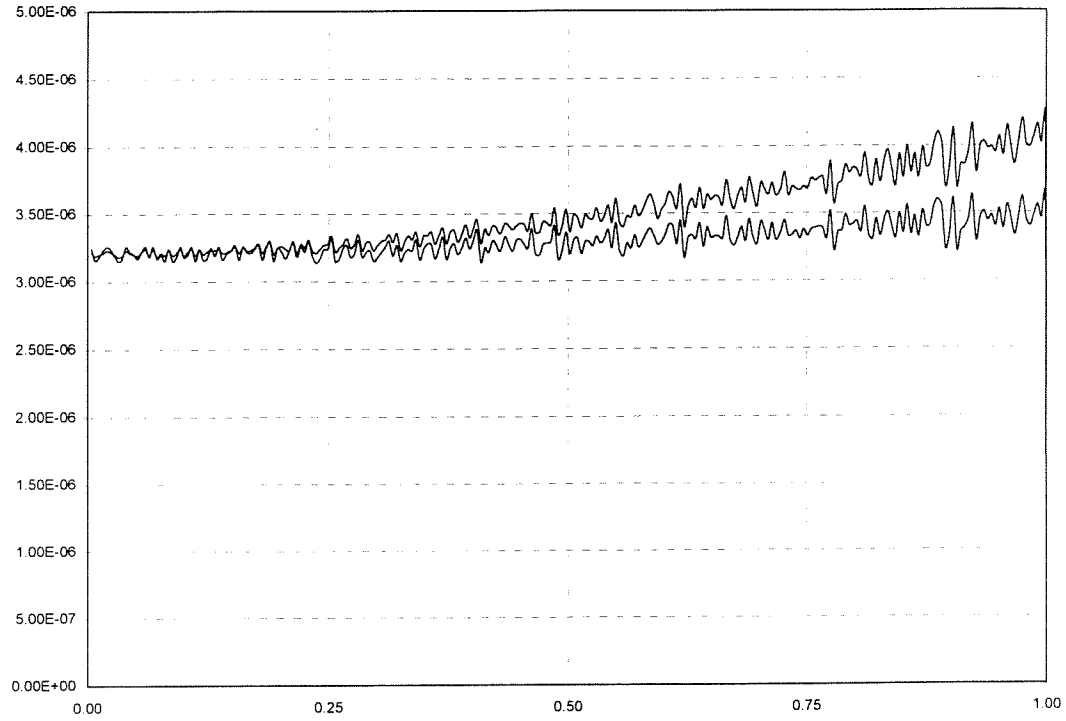

Graph 7 Fourier analysis of the signal at the sea boundary of the 2d model. Node 116 and n823

Graph 7 shows the clear signal obtained now at both the beginning and end of the 2D component. The amplification of the amplitudes for the higher region of the spectrum is due to the fact that this signal was obtained from closed model[1], more information on the models used can be found in the appendix III: testing of the 1D2D model.

This closed model acts as a closed sea basin. When waves hit the shores, they are reflected. With a vertical shore, which is the case in this model, the wave will double in amplitude during the reflection. Although this also happens in this model, it cannot be distinguished clearly due to size of the model. The 2D area is only 40 meters long and the shortest wave in the signal is 160 meters. This means that the signal imposed on the boundary is not the same as the original signal on the ocean far away. If this could be compared to the signal on the boundary, the doubling would be evident. In this case, in the short wavelengths one is able to distinguish a certain degree of amplification. The signal on the boundary is also influenced by this effect and will therefore increase in amplitude as well.

VI.I.II Time Step

Due to its highly dissipative behavior of the model it is necessary to choose a small time step in order to compensate this effect. Normally the courant number serves as a good indicator for what would be a good choice for the time step / spatial step. This number should have a value of approximately one for an ADI method. In this case, with a depth of 2m and a spatial step of 4 m a time step of 0.9 s would result in a courant value of: 0.99. Test runs with a value of 0.9 for a time step reveal a significant amount of dissipation especially in the higher frequencies. A wave height decrease of 30% or more is not acceptable especially with very small amplitudes. The test was done on a similar model as the original, with the exception of the boundary on the end of the channel. Instead of a discharge=zero boundary this was changed into a Riemann=zero boundary. The effect of this is that for a wave the channel will seem to have an infinite length. No waves are reflected and the signal can be analyzed without any amplification or other effects.

[1] A closed model is similar to the standard model but with the 1D component closed.

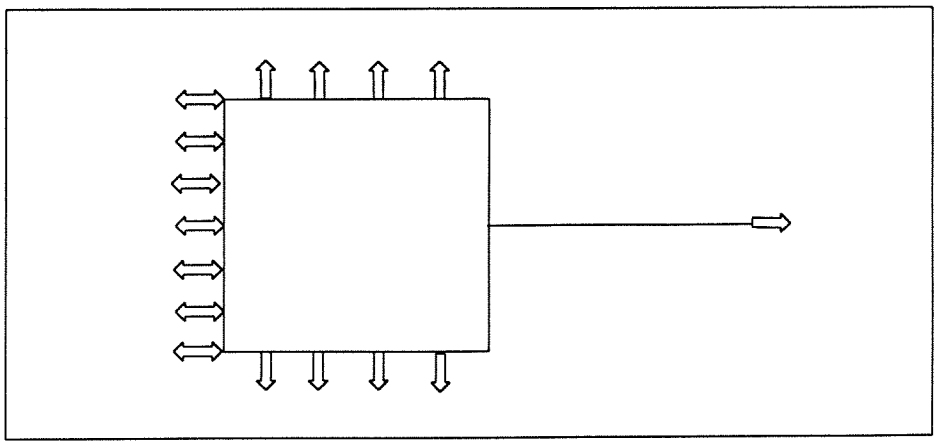

Figure 3. Riemann model

In Graph 8, the Fourier analysis of the water levels at both the beginning and the end of the channel are shown. The amplitude of the signal is very small 3x10-6 on a depth of 2 meters this should result in a linear case. This means that the amplitudes at the beginning of the channel are equal to those at the end of the channel. This clearly not the case, the very long wavelengths stay around their original amplitude but the shorter frequencies tend to decrease approaching zero. With a larger time step, this effect is even bigger; wavelengths shorter than one half the length of the channel just disappear. In this manner, part of the signal is lost.

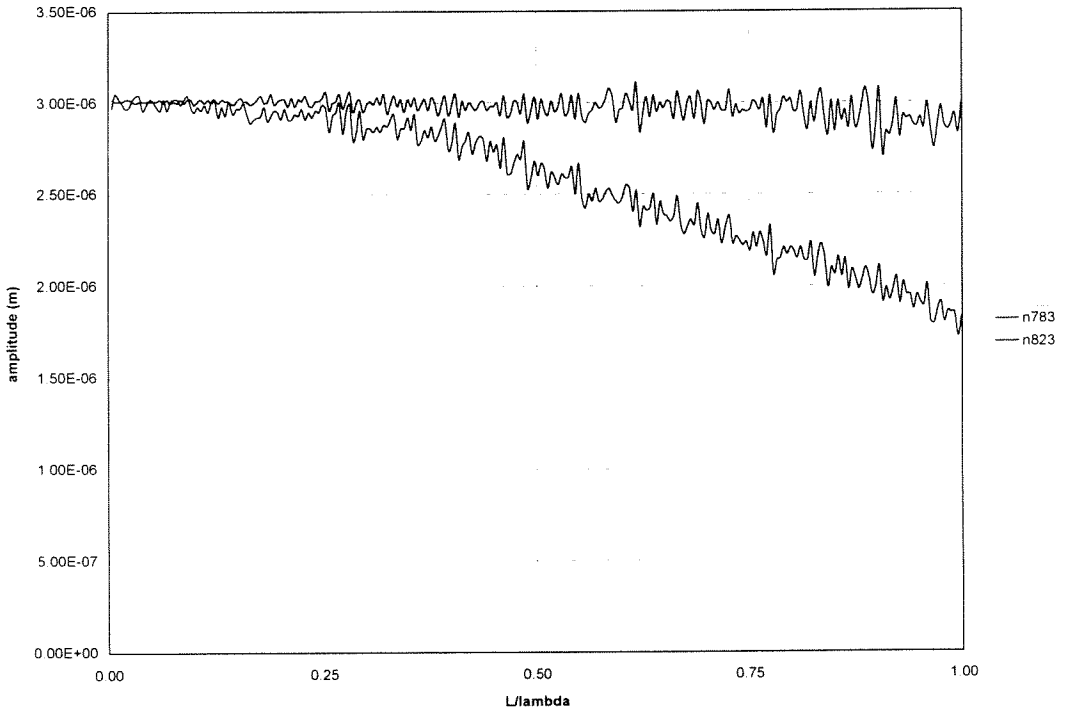

Graph 8 Fourier analysis of the signal at both beginning and end of the channel in a Riemann model.

Decreasing the time step can alleviate this problem. Graph 9 represents the results of a Fourier analysis of the signal but now with a time step of 0.1 s. The line has only 30 points in contrast to the 250 obtained by the 0.9 s time step

but it serves as a good indicator of the effect the time step has on the dissipative behavior of the model. It can be seen that up to a L/lambda ratio of 0.25 both lines are equal. For higher frequencies, the differences are greater but not as extreme as for a 0.9 s time step. A graph of the signal with a higher resolution can be found in the appendix III testing of the 2D model.

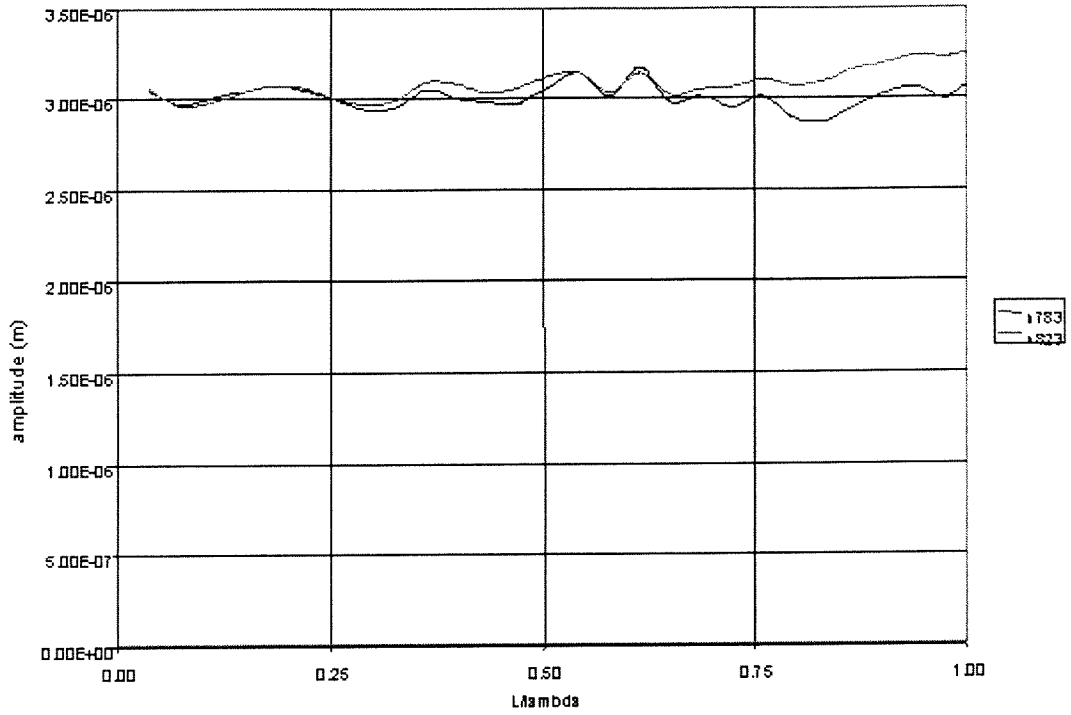

Graph 9 Fourier analysis of the signal at nodes 783 and 823 for a Riemann model. Time step equal to 0.2 s.

The effect of a dissipation of energy can also be illustrated by analysis of a wave with a single frequency travelling through the system. For this purposes the same Riemann model was used as for the previous result except for the input frequency. This provides a clear signal that can be analyzed visually without any post processing. In this case the signal was constructed by taking a single wave with a L/lambda ratio of 0.75 this is one of the waves in the higher region of the spectrum the amplitude is extremely small: just a fraction of a millimeter. This wavelength is the most influenced by the dissipative effects as can be seen from graphs 3 and 4.

The following graphs represent this signal at 6 different point in the model through time. The points at which the measurements were taken are:

N116 : a point at the western boundary. This is were the signal is imposed on the model
N17 : one node just before the connection between the 2D sea and the 1D channel.
N823 : node at the joint between the two models
N822 : one node further into the channel
N803 : node half way in the channel
N783 : node at the end of the channel at the outgoing Riemann boundary

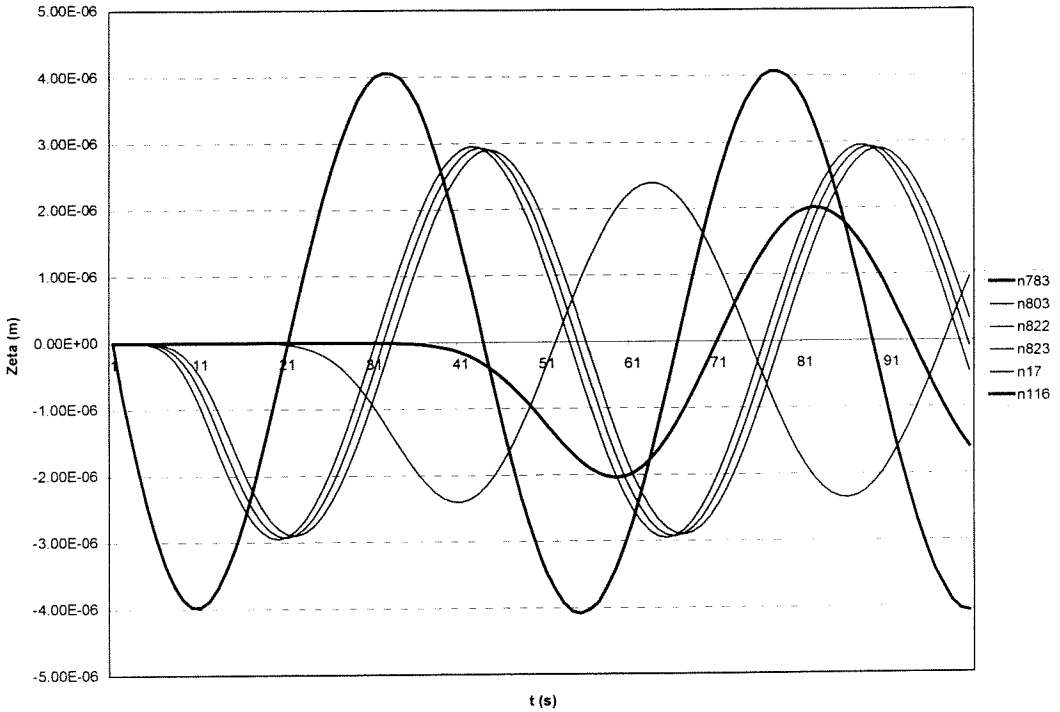

Graph 10 Single wave travelling through the model. Dt=0.9 s

In Graph 10 one can see how the wave decreases in amplitude by 25% and this over a distance of just 44 m. The decrease in amplitude for the 2D component cannot be attributed entirely to the dissipation of energy. A great deal of energy is also sent out through radiation at the open sides of the 2D region. More about this radiation can be found in the next paragraph. Once the wave enters the 1D channel, it continues to decrease in amplitude eventually losing another 33% of its amplitude in just 160 meters. With a large amplitude this could be attributed to friction, but with an amplitude in the order of a fraction of a millimeter this is a negligible factor.

The effect of radiation of energy through the boundaries can be clearly seen in a top view of the 2D area:

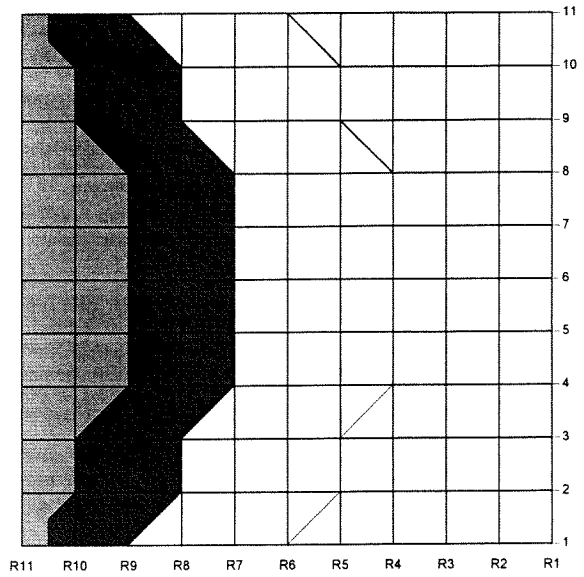

Graph 11 Top view of the 2D component of the model. Arc shaped wave pattern approaching the shore and channel.

The wave front is at the boundary a straight line because it is imposed equally on all boundary points. As soon as it enters the model, the points at the sides let the wave pass through. In this fashion energy leaks out of the model. The wave front adapts to this situation and propagates in an arc shaped way. The 2D area only serves to provide a correct boundary condition for the 1D channel. The actual information in this area is not measured or analyzed. For this thesis all this information is irrelevant. If one would be interested in this aspect of the model as well then it would be necessary to widen the model or find another trick to ensure a straight wave front.

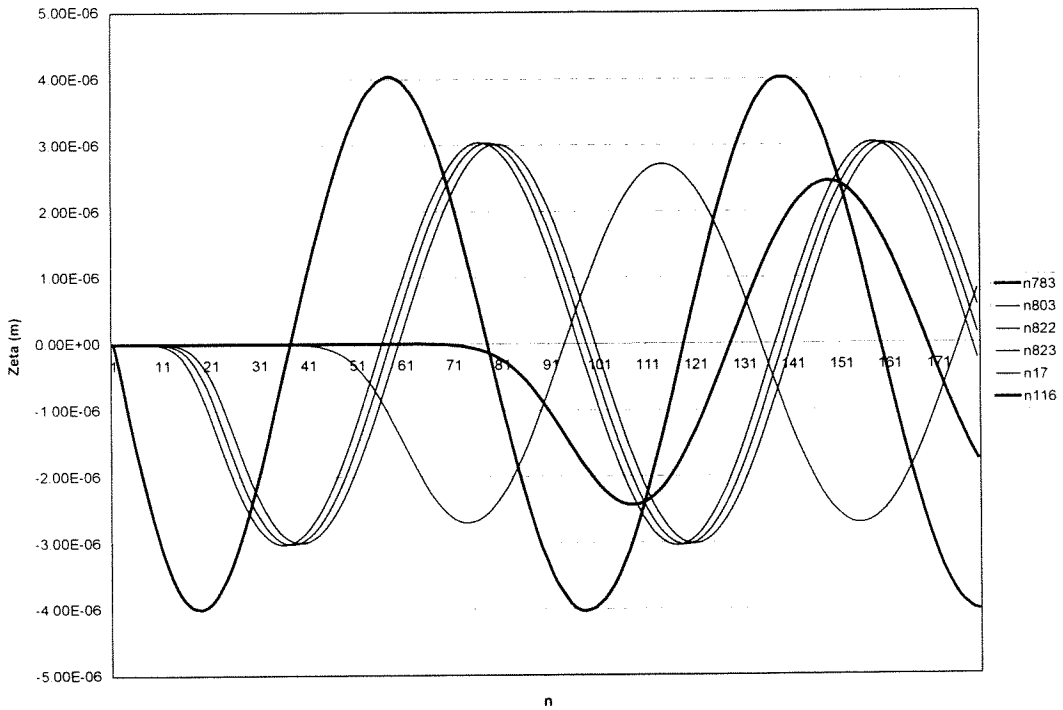

Graph 12 Single wave travelling through the model. Dt=0.5

This arc shaped pattern actually confirms the proper working of the boundary conditions on the 2D model.

A reduction of the time step from 0.9 to 0.5 seconds barely influences the decrease in amplitude in the 2D component. The amplitude in this area still decreases about 25%, this means that the majority of the energy loss in the 2D component can be attributed to the previously mentioned radiation. Entering the channel the wave still decreases significantly: 20%. This shows how the time step choice influences the dissipation of energy in the channel.

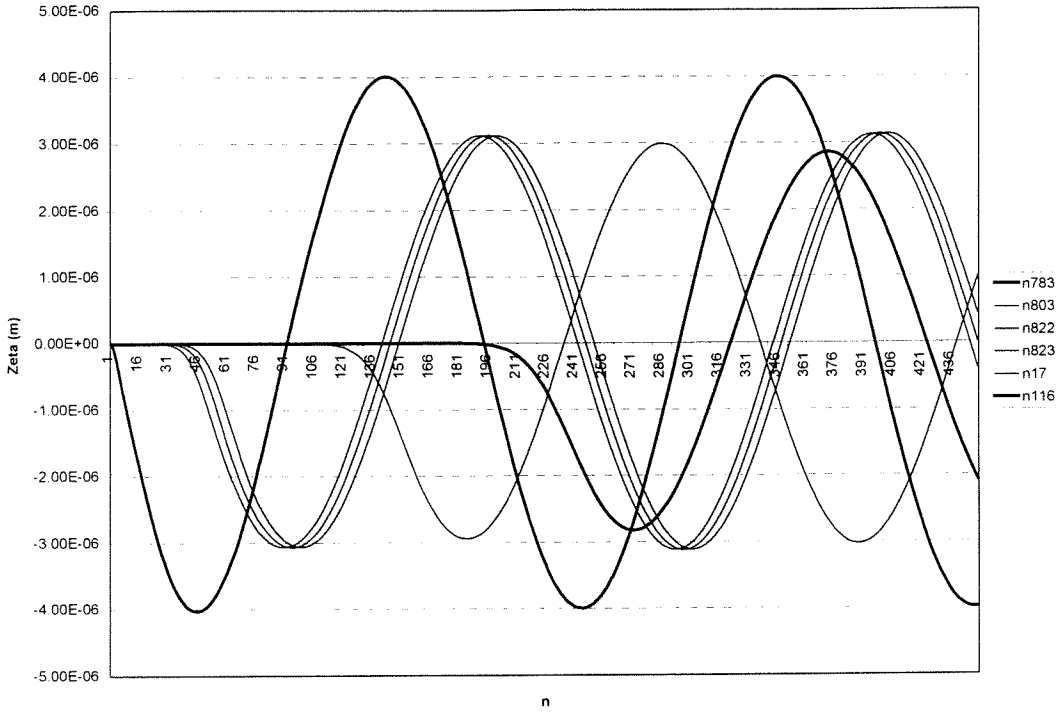

Graph 13 Single wave travelling through the model. Dt=0.2

In Graph 13 the relation between timestep and dissipation is confirmed. For the 2D component the amplitude is diminished mostly by the radiation. Decreasing the timestep barely has an effect on this. In the 1D component is the effect is more evident. A decrease in amplitude of just a few percent is now achieved. But even a reduction of the timestep to 0.1 seconds cannot remove the effect from energy dissipation altogether.

VI.I.III Number of timesteps

Although the high dissipative effect can be solved by decreasing the timestep this creates a significant side effect: a smaller time step results in less points in the Fourier analysis. Less points in the Fourier analysis not only makes the chart look rougher but since the first peak is so sharp it also diminshes the chance of actually hitting the exact frequency of amplification. A small deviation can already result in a significantly lower peak. To obtain an equal resolution with smaller timesteps the number of timesteps have to be increased. In other words the total calculated time must remain equal. Althought the effect of increasing the total time on the calculation time is directly proportional it is not so on the Fourier analysis calculation time. A Fourier analysis of a signal of 10000 timesteps takes about 10 minutes a Fourier analysis of 60000 timesteps exceeds 6 hours sometimes even leading to a system crash. The typical Fourier analysis consist of 250 frequencies for a timestep of 0.9 s and 10000 timesteps. Decreasing the timestep to 0.2 s and doubling the number of timesteps to 20000 results in a analysis of approximately 110 samples. Eventhough this is far less than that of the other graphs it serves as a good indicator of the amplitude.

VI.II Results

The results from the initial 1D2D model are not what were expected from this model. The model did not match the analytical solution perfectly. Several tests were done to determine the cause for this behavior, from this the recommendations and restrictions on the model followed. (For a precise description of the tests run and their results refer to appendix III.) Even with these restrictions and suggestions the model did not succeed in producing an amplification function that matched the analytical solution. If the dissipation can be fixed by decreasing the time step even further it is not a useful model for such small time steps require an enormous amount of calculation time. This would then just result in a working but impractical model. A better solution for this had to be found.

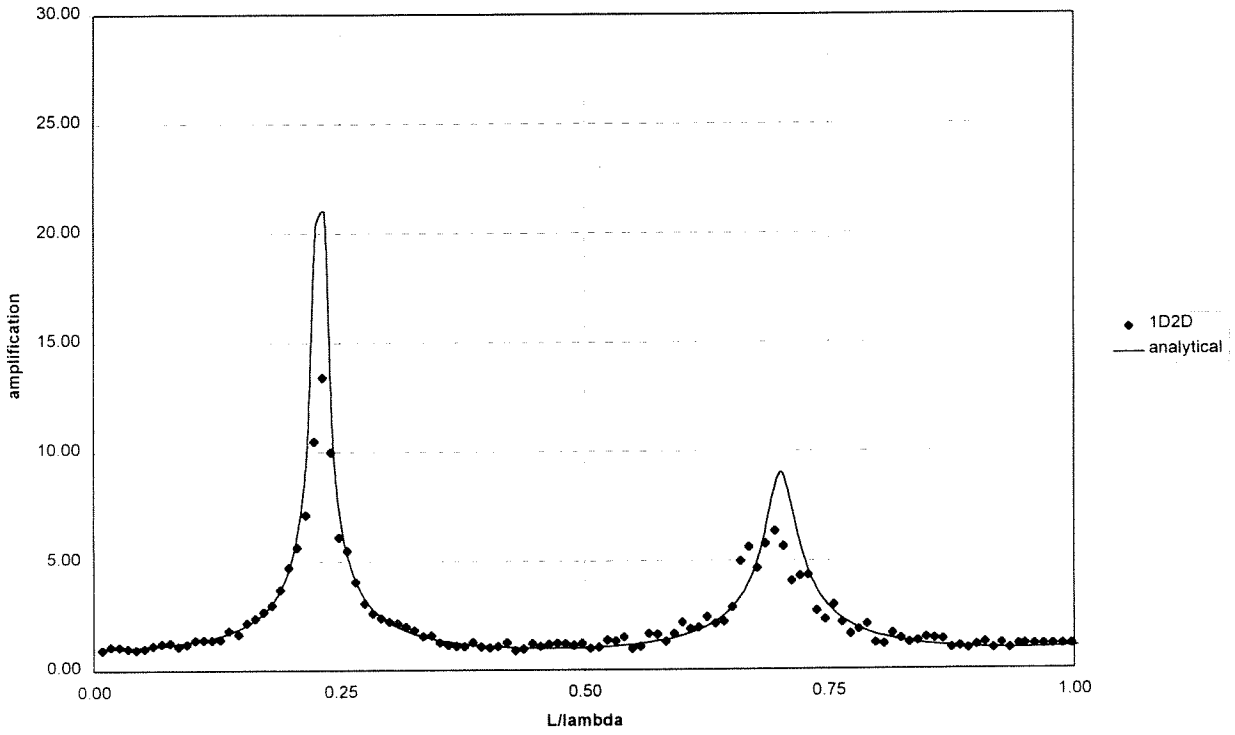

Graph 14 Amplification function for a time step of 0.2 and 20000 time steps.

In Graph 14 the amplification function is shown obtained by a small time step. In the areas outside of the peaks, the amplification function correctly provides a factor 1. Nevertheless, in the peaks the value of 14 for the first peak is well below the analytical solution of 28. The second peak with a value of 7 is remarkably closer to the analytical solution 9. This shows that it is not only dissipation that causes the low results. A brief look at the spectrum for a Riemann boundary reveals that the dissipation for the higher frequencies is noticeable but for the lower frequencies both lines are identical.

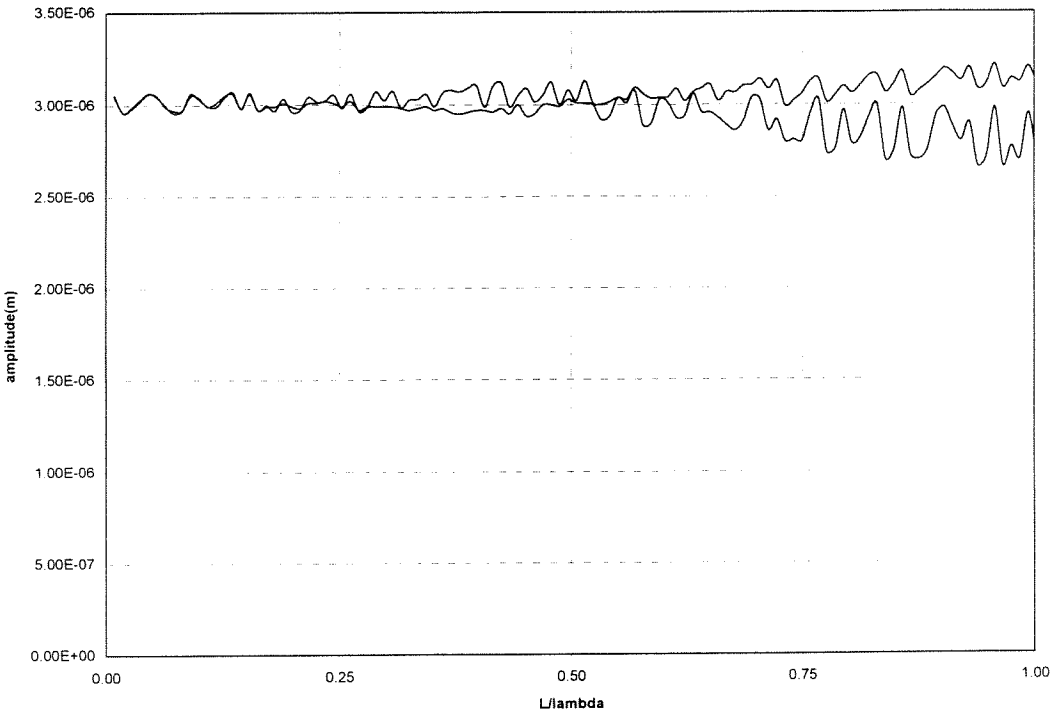

Graph 15 Fourier analysis of the signal at the entrance and at the end of the channel, with an open boundary on the end of the channel.

One would therefore expect the higher frequencies to be further away from the analytical solution and the lower frequencies closer to it. Nevertheless, the opposite is the case. This means that the high degree of dissipation is not the cause for the difference between the analytical and 1D2D model. The source of this discrepancy has to be investigated before further calculations are made with this model. After thorough investigation and several modifications the 1D2D model proved to work correctly as can be seen in chapter 8.

VII Testing of the 1D2D model

VII.I Introduction

The original 1D2D engine developed by Stelling has been adapted to model the seiche problem. To validate the results of this new model several test runs were made. Initially there were some problems with the choice grid spacing and time step. (See chapter 7 for more details) After some trail and error runs, an acceptable choice was made about these settings. Quick run with the Europort model provided promising results. To verify the validity of the model several other test are necessary. The results do not match the analytical solution exactly. In this appendix synopsis will be given on the test done to with the initial 1D2D model.

VII.II Models

To verify the results of the 1D2D method four models were used: the standard model closed model, the Riemann model and the Europort model. Every one of them has a specific testing purpose.

VII.II.I Standard Model

The standard model consists of a square two-dimensional area attached to a one-dimensional channel. The 2D area represents the sea. The water depth is equal to 2 meters in the whole model. The North, South and West boundaries are Riemann boundaries. The amplitude of the imposed Riemann boundary equal to zero characterizes the North and South boundaries. This results in only outgoing waves and no incoming waves. The Western boundary, also a Riemann boundary, is responsible for sending in the desired signal. For waves travelling in an outward direction, this boundary is completely transparent. The eastern boundary at the end of the channel is a discharge boundary set on zero. This type of boundary is a pure reflective one and will reflect all incoming waves.

With this setup of boundaries on the two dimensional component the outgoing radiation of waves can be modeled correctly. Incoming waves are send into the channel by the western boundary. Waves reflecting from the shore and radiating from the channel pass the boundaries unobstructed without any undesired reflections.

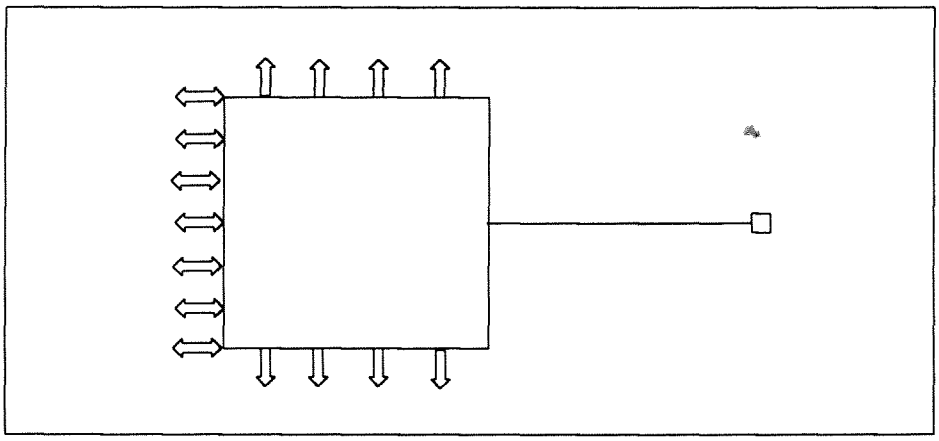

Figure 4. Standard model.

The dimensions of the model are not set to model real world dimensions but at this stage; it is only necessary to evaluate the validity of the results. The dimensions are set to give a width/length of the channel ratio of 20:

Dx, Dy =4 m
Dt = 0.9 s
Depth = 2 m
Chezy =60
Width of the channel = 8m
Lenght of the channel = 160

VII.II.II Closed Model

The closed model is used to evaluate the amplitude of the waves at the shore. For a correct calculation of the amplification function it is necessary that a clear signal be obtained without of the disturbing effect of the radiating waves emitted from the channel. For this purpose, the channel is removed from the system.

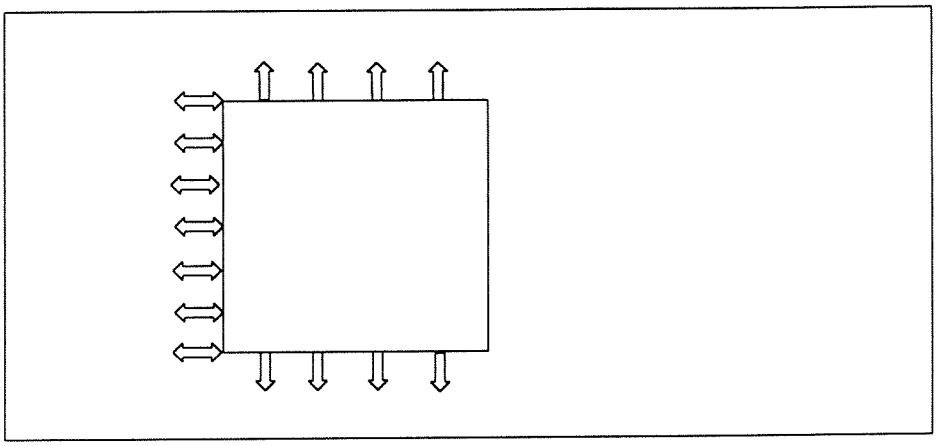

Figure 5. Closed Model

VII.II.III Riemann Model

As stated before the 1D2D engine suffers from a high degree of energy dissipation. To evaluate it magnitude and the effect of it on the model it's necessary to remove the other variables that also influence the amplitude. A clear signal

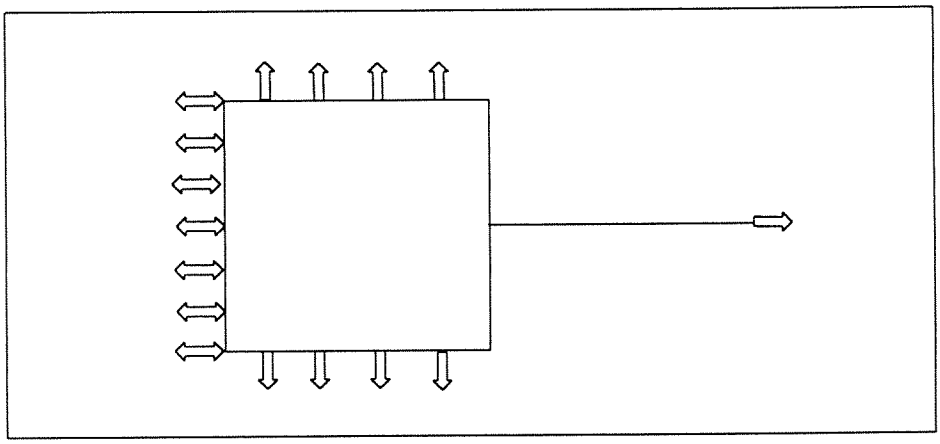

Figure 6. Riemann Model

without the effects of reflections or radiation is required for this. This can be accomplished by making the channel infinitely long so that no reflections can influence the waves in the rest of the channel. Creating a signal originating at the western boundary will send a pure signal into the system. This signal will propagate through the model undisturbed.
Imposing a Riemann boundary with amplitude equal to zero on the end of the channel will make this boundary completely transparent for outgoing waves. In this case waves will travel through the channel into the Riemann boundary and disappear. The resultant effect is the same as for an infinitely long channel. All waves can pass through.

VII.II.IV Europort Model

This model is almost identical to the standard model. The difference lies in the dimensions. The dimensions in the Europort Model are equal to those as used for the modeling the Europort in the Trisula and Pharos calculations. This permits a comparison between the four models, namely: Seiches II, Trisula, Pharos and 1D2D.

The dimensions are:
Width = 1000m
Length = 28000m
Chezy = 60
Δt = 50 s
Δx= 700 m

VII.III Analytical Solution

The analytical solution, explained in detail in chapter3, is derived from the Sommerfeld boundary condition and the linear shallow water equations. The validity of the model can be verified by comparing the results to those obtained by an analytical model. This comparison is valid because with small amplitudes and flow velocities the effect of friction and advective terms is negligible compared to the linear terms.

VII.III.I Test 1

The standard model was used in this test. A signal consisting of multiple frequencies is sent into the model, with a spatial step of 4m and a time step of 0.9 seconds.

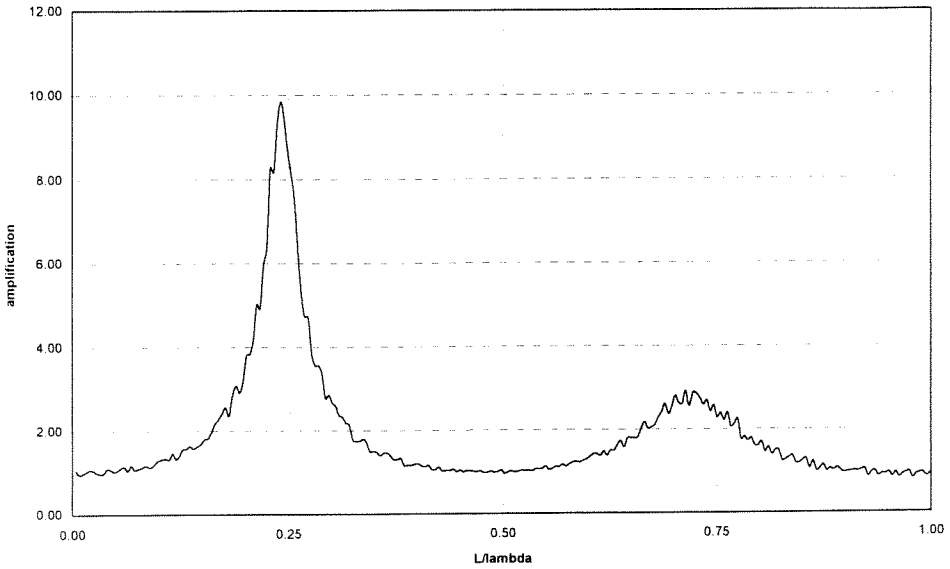

Graph 16 Amplification function (c11)

At first sight, this graph appears to give correct results. The peaks are on the right position: one fourth and three-fourths. The amplification factor on the regions next to the peaks is 1. However, the peaks height is not correct. According to the analytical solution, the first peak should give a value of 28 and the second a peak of 9. Both peaks are about 3 times less!
This low amplification factor cannot be attributed to friction because the amplitudes are in the order of a few millimeters on a water depth of 2 meters. Friction is negligible on this scale.

VII.IV Numerical dissipation

Depending on the way a numerical model is implemented and what schemes and discretization are used, a type of numerical dissipation can be introduced into the system. Numerical dissipation is similar to ordinary dissipation of energy due to turbulence or friction, but it is not caused by natural phenomena but rather their translation into a digital system. Numerical dissipation can also 'leak' energy. To verify the order of magnitude of this numerical dissipation the Riemann model was used. With this model a clear signal can be obtained without any amplification or other disturbances in the signal. In theory, the incoming signal should be equal to the outgoing signal. A combined signal was sent into the Riemann model and the signal at the begin and end of the channel were analyzed.

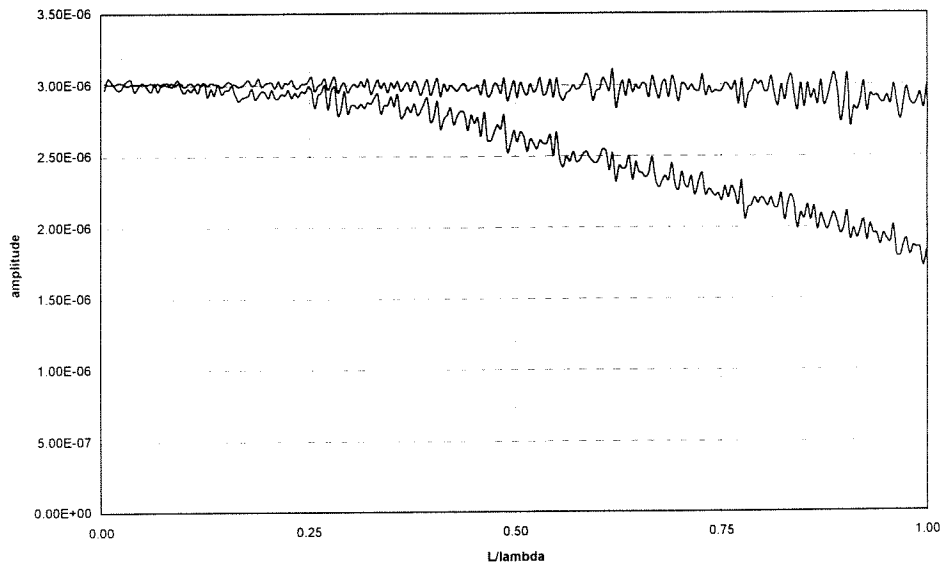

Graph 17. Fourier analysis for a Riemann model

The line at the top shows the amplitudes per frequency at the begin of the channel, node 823. The line sloping down is the spectrum at the end of the channel. The input signal is uniform over the entire spectrum. At node 823 the signal is still uniform, just a bit lower than the imposed signal. This confirms the hypothesis that the majority of the energy, which is lost in the 2D part, can be attributed to radiation through the boundaries. This radiation lowers all amplitudes regardless of their frequency; it does not work as a filter. Therefore, the entire signals amplitude is decreased instead of only the higher frequencies. The signal in the 1D channel is distorted. The waves at the lower end of the spectrum retain their amplitude; this in contrast to the significant reduction in amplitude of 40% by waves in the higher region of the spectrum. It should also be noted that since there is no radiation through the boundaries the entire signal is not lowered. It is as if some sort of filter acts on the signal. The short waves are influenced much more by a large time step than the longer waves. This is due to the numerical dissipation in the model. The shortest wave in the spectrum has a wavelength of 160 m, at a water depth of 2 m this is a period of: 36 seconds. With a time step of 0.9 seconds this is more than 40 points per wave: sufficient to correctly model it. Therefore, this cannot be the cause either.

To verify the hypothesis that the amplitude reduction is caused by a too large time step, the time step is reduced to 0.2 seconds, resulting in the following graph:

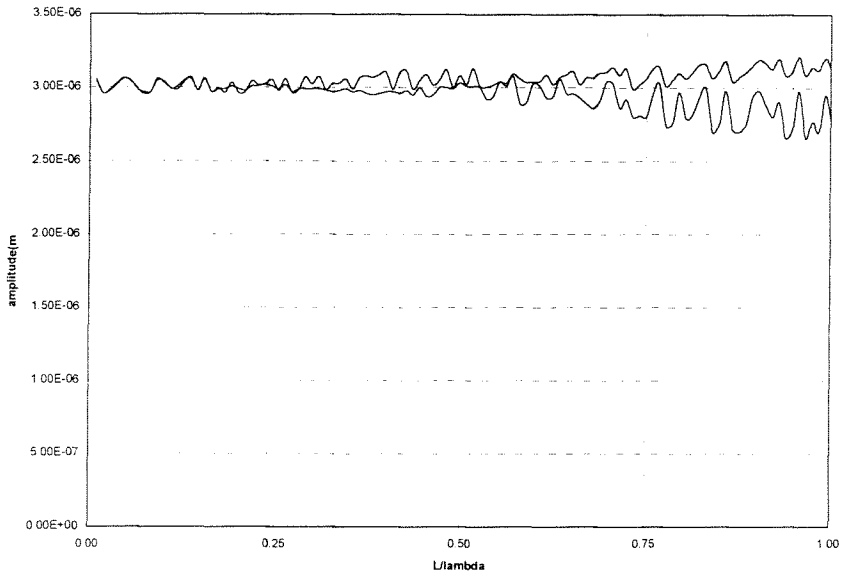

Graph 18 Spectrum of the signal at node 783 and 823 for a Riemann model. Time step = 0.2 seconds

In graph 3, it can be clearly seen that now the amplitude of the higher spectrum does not decrease as much as with a large time step. For the lower region and especially near 0.25, for the factor L/lambda, both signals are identical. This is an important part of the signal because this is where the first peak occurs. The first peak now should have reached the analytical solution and the second peak should be close to it. Due to some numerical dissipation, it can be lower though. Another test run was made with the standard model to verify this, but now with a time step of 0.2 seconds. Since the resolution of the spectrum is directly proportional to the time step and number of time steps, a smaller time step results in a decreased resolution. To compensate for this the number of time steps was doubled. This should be enough to provide an indication of the amplification and confirm the theory.

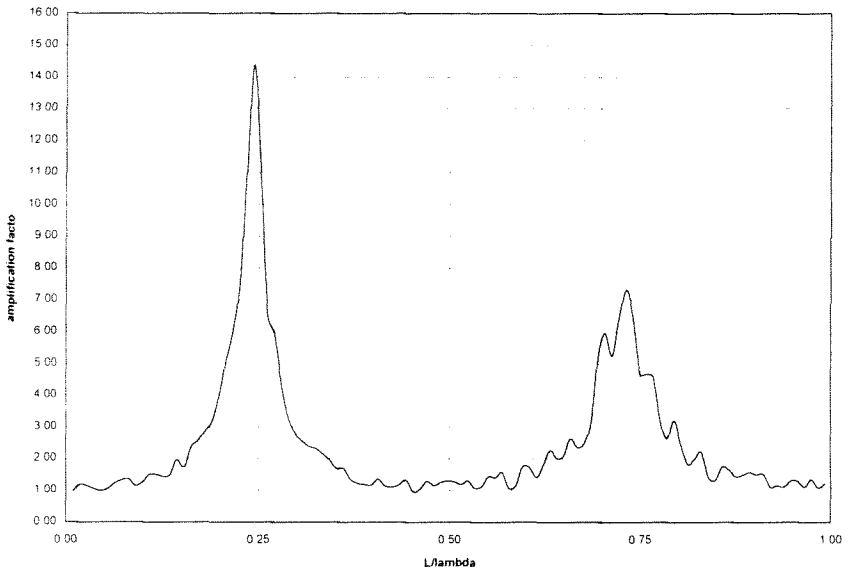

Graph 19. Amplification function for a Standard model. Time step = 0.2 seconds.

Although the first peak shows an increase up to 14, it is still a factor 2 away from the analytical solution for the first peak of 28. The second peak, with 7, is much closer to the analytical solution of 9 for the second peak. If one now compares the spectra from both signals one with a time step of 0.9 and one with 0.2 seconds, it can be seen that the difference for the lower frequency region is small. The amplitude decrease for waves with a L/lambda factor of 0.25

is minimal. However, this minimal difference accounts for an increase in amplification factor of 40%. This shows how sensitive the peak is for numerical dissipation an even smaller time step could be taken to circumvent this but this would result in an impractical model.

VII.V Resolution

Due to smaller time steps the resolution of the signal decreases. A typical graph of the amplification function is composed of 250 points/frequencies. Decreasing the time step from 0.9 to 0.2 decreases the number of samples to 55. This results in a very rough chart. By doubling the total number of time steps one can obtain a graph with a resolution of 110 points. This is still not as accurate as the one with 250 points but it may serve as an indication. The number of samples is so important because of the narrowness of the peak itself.
It could be that the model is actually behaving correctly with a time step of 0.2 but that the peak, because of its narrowness, has not been sampled on the exact frequency. With such a narrow peak, a small deviation from the exact frequency results in a much lower amplification factor. To circumvent this the resolution of the graph could be increased. This requires more samples and therefore longer total time. Because the other programs used to perform the Fourier analysis cannot cope with more than 20000 time steps, another method was used. Using a single frequency wave it is not necessary to employ a Fourier analysis to determine its amplitude. This is of course only possible as long as the wave does not deform. Due to the extremely small amplitude bottom friction has no significant effect on the wave. The wave will remain sinusoidal in the linear region. Therefore, various runs were made with single frequencies each to verify the results:

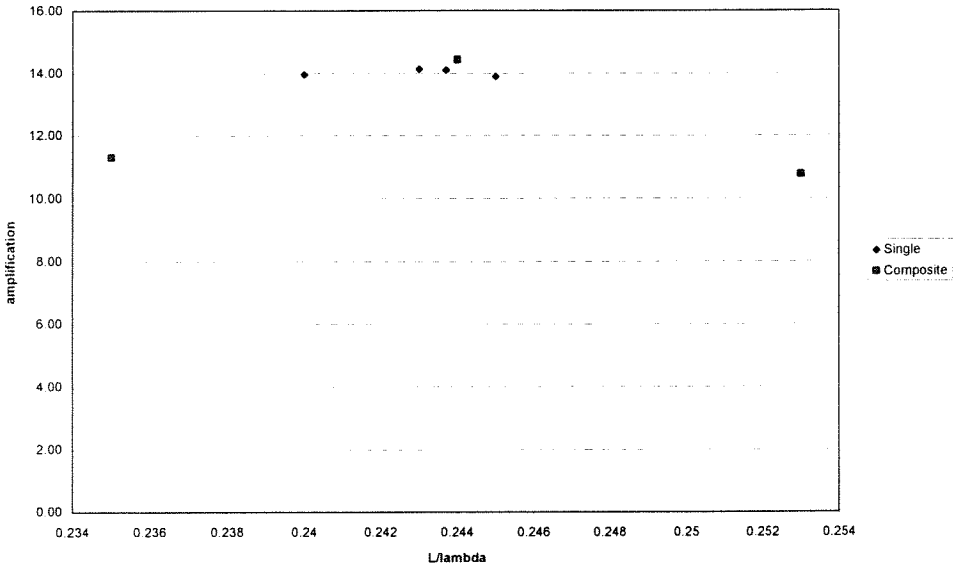

Graph 20. Sensitivity analysis for the first peak.

The squares on graph 5 are the 3 points surrounding the first peak on the Fourier analysis graph 4. The diamond shaped points show the results from the various single frequency runs. Although it appears that the actual peak has been hit correctly, it must be noted that due to the narrowness of the peak it may still lie in between the investigated points. Only an increase in resolution can prove this.
It should be noted that this is actually not a truly correct manner of obtaining the amplification factor. In a signal composed of many frequencies, all frequencies influence each other. Sending in a single frequency this effect is not present. However, this effect only occurs as soon as the non-linear terms in the equation of motion start kick in. The order of magnitude of the used frequencies is still in the linear region. Therefore, this is a legitimate way of verifying the amplification factor.

VII.VI Conclusion

The model failed in reproducing the exact results of an analytical model. Without this important requirement further testing and use of this model is not advised. Unless the cause and solution to the discrepancy in the peak height can be found and implemented this model should not be used to calculate the amplification function for a seiches problem. It may be that comparing this model to an analytical model is not valid. The analytical model has of course only one boundary condition, the Sommerfeld radiation condition. This model is implicitly fitted with this boundary and perhaps more. What is surprising is that the results resemble those of the true 2D model such as TRISULA and PHAROS. Those models do not match the peak of the analytical amplification function exactly either.